12-1995

# Mafic volcanism in the Colorado Plateau: basin and range transition zone, Hurricane, Utah

Alexander Sanchez
*University of Nevada, Las Vegas*

# MAFIC VOLCANISM IN THE COLORADO PLATEAU / BASIN-AND-RANGE TRANSITION ZONE, HURRICANE, UTAH

by

Alexander Sánchez

A thesis submitted in partial fulfillment
of the requirements for the degree of

Master of Science
in
Geoscience

Department of Geoscience
University of Nevada, Las Vegas
December, 1995

The thesis of Alexander Sánchez for the degree of Master of Science in Geoscience is approved.

[redacted]

Chair, Eugene I. Smith, Ph.D.

[redacted]

Examining Committee Member, Wanda J. Taylor, Ph.D.

[redacted]

Examining Committee Member, David L. Weide, Ph.D.

[redacted]

Graduate Faculty Representative, Stephen H. Lepp, Ph.D.

Interim Dean of the Graduate College, Cheryl L. Bowles, Ed.D.

University of Nevada, Las Vegas
December, 1995

## ABSTRACT

The Hurricane volcanic field (HVF) is a small-volume (0.48 $km^{3)}$ mafic volcanic field in the Colorado Plateau / Basin & Range Transition Zone located in the eastern part of the St. George basin in southwestern Utah. Strombolian-Hawaiian style eruptions produced thin (10 m) a'a lava flows and cinder (scoria) cones composed of vesicular basalt, bombs and agglutinate. Radiometric dating and geologic relationships demonstrate that the HVF formed over a period of at least 100,000 years. In the upper crust, magma probably rose along joints in sedimentary rocks because chains of volcanic vents follow joint orientation maxima in sedimentary rocks.

Three rock groups, low-silica basanite (<42% $SiO_2$), basanite (43-46% $SiO_2$) and alkali basalt (>46% $SiO_2$), originated from the partial melting of four isotopically distinct garnet-free mantle sources. Limited mixing between two of the four types of magmas may explain intra-element variation of basanites and some alkali basalts. HVF mafic lavas have relatively high La/Ba, La/Nb and $^{87}Sr/^{86}Sr$ and lower $\varepsilon_{Nd}$ values compared to Basin-and-Range basalts less than 5 m.y. old indicating that HVF magmas originated in the lithospheric mantle and interacted with lower crustal component(s) in one or two steps. With distance from the Colorado Plateau and time HVF magmas, like those in other areas of the Transition Zone, become more like ocean island basalt (OIB). The contamination by a lower crustal component of the Transition Zone basalts reflects the thick lithosphere beneath the Transition Zone and Colorado Plateau when compared with the Basin-and-Range basalts which lack this component. The transition of HVF lavas toward an OIB composition with time may reflect the thinning of the lithosphere during extension.

Differences in chemical and isotopic features of volcanic rocks erupted from the Volcano Mountain vent complex indicate that the complex is polygenetic. Geochronological data indicate that the complex erupted over a period of at least 100,000 years and is also polycyclic.

## TABLE OF CONTENTS

## LIST OF FIGURES

## ACKNOWLEDGMENTS

Financial support for this thesis was provided by the Nevada Nuclear Waste Project Office through the Center for Volcanic and Tectonic Studies (CVTS) at UNLV, and by a research grant from Graduate Student Association of UNLV.

I would like to thank my advisor, Dr. Gene Smith for his patience and generosity and the members of my graduate committee: Dr. Wanda Taylor, Dr. David Weide, and Dr. Stephen Lepp for their guidance and support. I would like to acknowledge Meg Schramm (UNLV) and Dr. David Nealey (USGS, Denver) who provided me with early results of their work from southwestern Utah. Dr. Doug Walker (University of Kansas) completed isotope analyses, Dr. Phillip Simpson (Phoenix Memorial Lab, University of Michigan) completed other trace and rare-earth element analyses, and Dr. Larry Snee (USGS, Denver) did the $^{40}Ar/^{39}Ar$ analysis. The research staff of CVTS; Dr. Tim Bradshaw, Dr. Gene Yogodzinski, and Shirley Morikawa provided helpful discussions and insight.

For logistical support, my thanks go to the Department of Geoscience staff: Vicki DeWitt, Deborah Jones-Selk, Jo Beth Stockstill, and to Carole Hofle (UNLV Graduate College).

Also, my personal thanks goes to all the students, faculty, and staff of the Department of Geoscience at UNLV, especially: Gary Gin (whom I followed to Las Vegas from Sonoma State University), Joe Blaylock (for greatly appreciated lunch-time transportation and lunches), KellyAnn Boland, Kelly Rash, and Holly Langrock.

And finally but most importantly, I would especially like to express my love and gratitude to my wife Donna, my sons Sam and Andrew, and my parents, Jess and Victoria Sánchez, for their support, encouragement and interest in my studies.

# CHAPTER 1

## INTRODUCTION

Alkali basalt volcanoes near Hurricane, Utah make up a small-volume, Pleistocene, mafic volcanic field in the transition zone between the Colorado Plateau and the Basin-and-Range province. The volcanic field is situated in the eastern part of the St. George basin in southwestern Utah, approximately 25 km east-northeast of St. George, Utah near the small town of Hurricane (Figure 1). The volcanic field is bounded on the west and north by the Virgin River and it straddles the north-striking Hurricane fault. Volcanoes in this study are located immediately to the west and north of Hurricane and about 12 km south of the town (Figure 1 and Plate 1).

Small-volume mafic systems are traditionally thought to be chemically simple, monogenetic and monocyclic, although some studies have shown that they can be very complex (Foshag and González-Reyna, 1956; Hasenaka and Carmichael, 1985). Petrologic and chemical studies, and the identification of the structural controls of vent areas, are important for understanding small-volume volcanic centers and their magmatic evolution. Renewed interest in small volume mafic volcanic fields has been stimulated by volcanic hazard studies related to the evaluation of a high-level nuclear waste repository at Yucca Mountain, Nevada. Seven Pleistocene or younger mafic volcanoes are found within 40 km of the proposed repository site. Accordingly, volcanic hazard studies are an important part of the site characterization process. Studies of cinder cones near Yucca Mountain show that some are polygenetic and many are controlled by regional structures

(Crowe et al., 1989; Wells et al., 1990, 1992; Bradshaw and Smith, 1994). An important question then is whether or not volcanism at Yucca Mountain is typical of volcanism in the region. To answer the question, field and geochemical studies in analog areas are important. Smith et al. (1990) suggested that a good analog site should consist of volcanoes that are: (1) Plio-Pleistocene or Quaternary in age, (2) eroded or quarried so that vents are exposed, (3) extinct, (4) located in a tectonic environment controlled by normal faulting, and (5) similar in volume to both individual cones and the entire volcanic field at Crater Flat, Nevada. The volcanoes of the Hurricane field satisfy all of these criteria and therefore are an excellent analog to volcanoes near Yucca Mountain.

The purpose of this thesis is to: (1) determine the petrogenesis and magma source of the Pleistocene volcanic system near Hurricane, Utah, (2) determine whether the cinder cones are polycyclic and/or polygenetic, (3) identify the structures that are most important in controlling the location of volcanic vents, (4) provide data on the physical properties of the mantle beneath the Basin-and-Range / Colorado Plateau transition zone, and (5) provide an analog for volcanic hazard assessment studies related to the proposed high-level nuclear waste repository at Yucca Mountain, Nevada.

## Geologic Background

In the western United States, tectonic and magmatic patterns changed dramatically at about 30 Ma at the time when the East Pacific Rise collided with the North American plate (Atwater, 1970). Before 30 Ma, subduction of the Farallon plate resulted in a broad belt of calc-alkaline magmatism as far inland as the margin of the Great Plains (Snyder et al., 1976). Plate convergence led to Mesozoic crustal shortening and thickening across parts of the western United States and resulted in east-directed thrusting (Burchfiel and Davis, 1975). After 30 Ma, calc-alkaline volcanism remained the most common type of magmatism. Bimodal or fundamentally mafic volcanism dominated only during the waning phase or after extension (McMillan and Dungan, 1986; Thompson et al., 1986). Mafic

volcanism occurred in the southern Basin-and Range Province mainly after 17 Ma and migrated from south to north. In the northern Basin-and-Range, fundamentally mafic volcanism occurred after 12 Ma. Small-volume Pliocene to Quaternary volcanic centers (<1.0 $km^3$) are preferentially located on the east margin, west margin, and in the center of the northern Basin-and-Range province (Fitton et al., 1991). One of these young, small-volume fields is the Hurricane volcanic field (HVF) in the transition zone between the Basin-and-Range and Colorado Plateau tectonic provinces in southwestern Utah (Figure 1).

The change from relatively undeformed Paleozoic and Mesozoic sedimentary rocks of the Colorado Plateau to the faulted blocks of the Basin-and-Range Province in Utah and Arizona occurs in the "Transition Zone", an area marked by a series of north-striking, widely spaced normal faults (Hamblin, 1970a). On the western edge of the Colorado Plateau, three major normal fault systems from east to west are the Toroweap, Hurricane and Grand Wash faults. The faults are down-to-the-west and, at some locations, have displacements of up to 2700 m. These faults are continuous for nearly 500 km from southern Utah to northern Arizona. In Arizona, the Paleozoic and Mesozoic strata in the Transition Zone is relatively undeformed, while in Utah, sedimentary rocks are generally folded into north-northeast trending anticlines and synclines. The crust in the Transition Zone thins (40 to 30 km) from east to west and the seismic low-velocity zone thickens so that in the west the top of this zone is nearly coincident with the base of the crust (Allmendinger et al., 1987). The Basin-and-Range region to the west of the Transition Zone exhibits recent uplift, extensional tectonism and high heat flow.

Volcanism occurred in the Transition Zone concurrently with normal faulting and regional uplift. Late Cenozoic volcanism in the Transition Zone in northwestern Arizona and southwestern Utah produced alkalic basalts like those found on the western margin of the Basin-and-Range Province (Leeman and Rodgers, 1970).

Previous geologic and chemical studies of the volcanoes near Hurricane by Hamblin (1970b), and Best and Brimhall (1970, 1974) did not address the physical volcanology of the volcanoes in any detail. These studies were regional and/or chemically classified the volcanoes as part of a survey of volcanism in the greater western Grand Canyon region including the St. George basin in Utah. Best and Brimhall (1974) focused on the regional chemical composition of the mafic volcanic rocks in the western Grand Canyon region and classified them as alkali basalt, hawaiites and basanites. They suggested that the mafic volcanic rocks were derived by partially melting the mantle at depths ranging from ~ 60 to ~95 km. Hausel and Nash (1977) suggested that the mafic rocks were produced by "partial fusion" of quartz eclogite of the subducted Farallon plate and spinel peridotite in the mantle wedge. Reid and Ramos (1993) proposed an enriched mantle source for these volcanic rocks based on Th isotopic studies. Additional geochronological work by Best et al. (1980) and Wenrich et al. (1995) show that hawaiite volcanism migrated to the northeast or east at a rate of 1.2 cm/yr in the western Grand Canyon region. This migration corresponds with an eastward shift of normal faulting. Vents, however, do not coincide with traces of exposed faults (Best and Brimhall, 1974; Anderson, 1988).

Three K-Ar dates, on basalt lavas in or near the Hurricane field were published by Best et al. (1980) (locations shown on Figure 1). The Washington flow, 10 km west of the HVF, was dated at 1.7 ± 0.1 Ma and a flow 25 km to the north of the HVF on the Black Ridge of the Hurricane Cliffs was dated at 1.0 ± 0.1 Ma. A flow that underlies the town of Hurricane and is offset by the Hurricane fault was dated at 289 ± 86 ka. This same flow was re-dated by the $^{40}Ar/^{39}Ar$ technique for this study (see chapter 2, geochronology section).

## Instrumental Techniques

Chemical analyses were completed on whole rock samples. A volume of approximately 250-350 ml of fresh, unweathered rock chips was collected for each sample. Samples chips were initially crushed to "pea" size using a Braun jaw crusher fitted with tungsten carbide jaws. The sample was then powdered for 2 minutes to about 200 mesh in a Bico shatterbox with tungsten carbide rings and bowl. The practice of leaching powdered rock samples in a dilute hydrochloric acid (HCl) solution or distilled water to remove carbonate contaminates was found by Morikawa (unpublished study, 1992) to significantly affect retention of major and trace elements. For this reason, leaching was not done in this study for preparation of samples for any chemical analysis. Sixty samples were collected and analyzed for major oxides and trace elements. Rare-earth element (REE) and other selected trace element analyses were completed for 38 samples at the Phoenix Memorial Laboratory at the University of Michigan. Radiogenic isotope analyses (Sm/Nd, Rb/Sr, and Pb systems) were completed on 31 samples at the Isotope Geochemistry Laboratory at the University of Kansas. Radiometric dating ($^{40}Ar/^{39}Ar$ incremental release analysis) was completed on three samples at the United States Geologic Survey's geochronology laboratory in Denver, Colorado.

Samples were processed into fused glass disks for major oxide analysis by heating 1.0 g sample, 9.0 g lithium tetraborate ($Li_2B_4O_7$), and 0.16 g ammonium nitrate ($NH_4NO_3$) to 1100°C in a muffle furnace for 30 minutes in gold-platinum alloy crucibles and pouring the resulting melt into heated Au-Pt molds (Noorish and Hutton, 1969; Mills, 1991). Samples for trace element analysis were prepared by mixing 3 g of sample with 0.6 g of methyl cellulose. The sample/binder mixture was placed on top of additional methyl cellulose backing (Hutchison, 1974) in a 1 3/8" diameter stainless steel die, and compressed to 20,200 psi for 90 seconds in an Angstrom hydraulic press to form a pellet. All samples

and reagents were weighed to ± 0.0005 g. All prepared samples were stored in desiccators prior to analysis. Chemical analyses are presented in Appendix I.

X-ray fluorescence analysis of major oxides and trace elements (Ba, Rb, Sr, Nb, Y, Zr, Cr and Ni) was done using the Rigaku 3030 X-ray Spectrometer at the University of Nevada, Las Vegas. Calibration of this spectrometer was based on the internal standards listed in Appendix II. Average of several analyses of United States Geologic Survey multi-element standards BIR-1, MAG-1 and the French Centre de Recherches Pétrographiques et Géochimiques (CRPG) multi-element standard GH were compared to published values (Govindaraju, 1994). REE and Cr, Ni, Sc, Co, Ta, Hf and Th were analyzed by instrumental neutron activation analysis (INAA) at the Phoenix Memorial Laboratory, University of Michigan. Analytical uncertainty and accuracy values for XRF analyses and INAA are reported in Appendix II.

Rb/Sr, Sm/Nd and Pb isotopes were analyzed using a VG Sector 54 mass spectrometer at the Isotope Geochemistry Laboratory, University of Kansas, Lawrence. A complete discussion of the isotope analytical methods used here is presented by Feuerbach et al. (1993). Isotope dilution data for Nd, Sm and Pb are reported in Appendix I.

Incremental release $^{40}Ar/^{39}Ar$ analysis of three whole rock samples was done at the United States Geological Survey's geochronology laboratory in Denver, Colorado. Samples were initially ground to about 60 mesh. Olivine phenocrysts were separated using a Frantz magnetic separator to concentrate the potassium in the sample. The sample minus the olivine was then ground to about 80 mesh and sent to Denver for analysis. At Denver each sample was washed in 10% HCl, acetone, alcohol and deionized water. All three samples were irradiated in a single package in the TRIGA reactor at Denver for five hours at 1 Mwatt using Fish Canyon tuff sanidine as the standard. The age used for the Fish Canyon tuff sanidine is 27.84 Ma. Geochronologic data are reported in Appendix III.

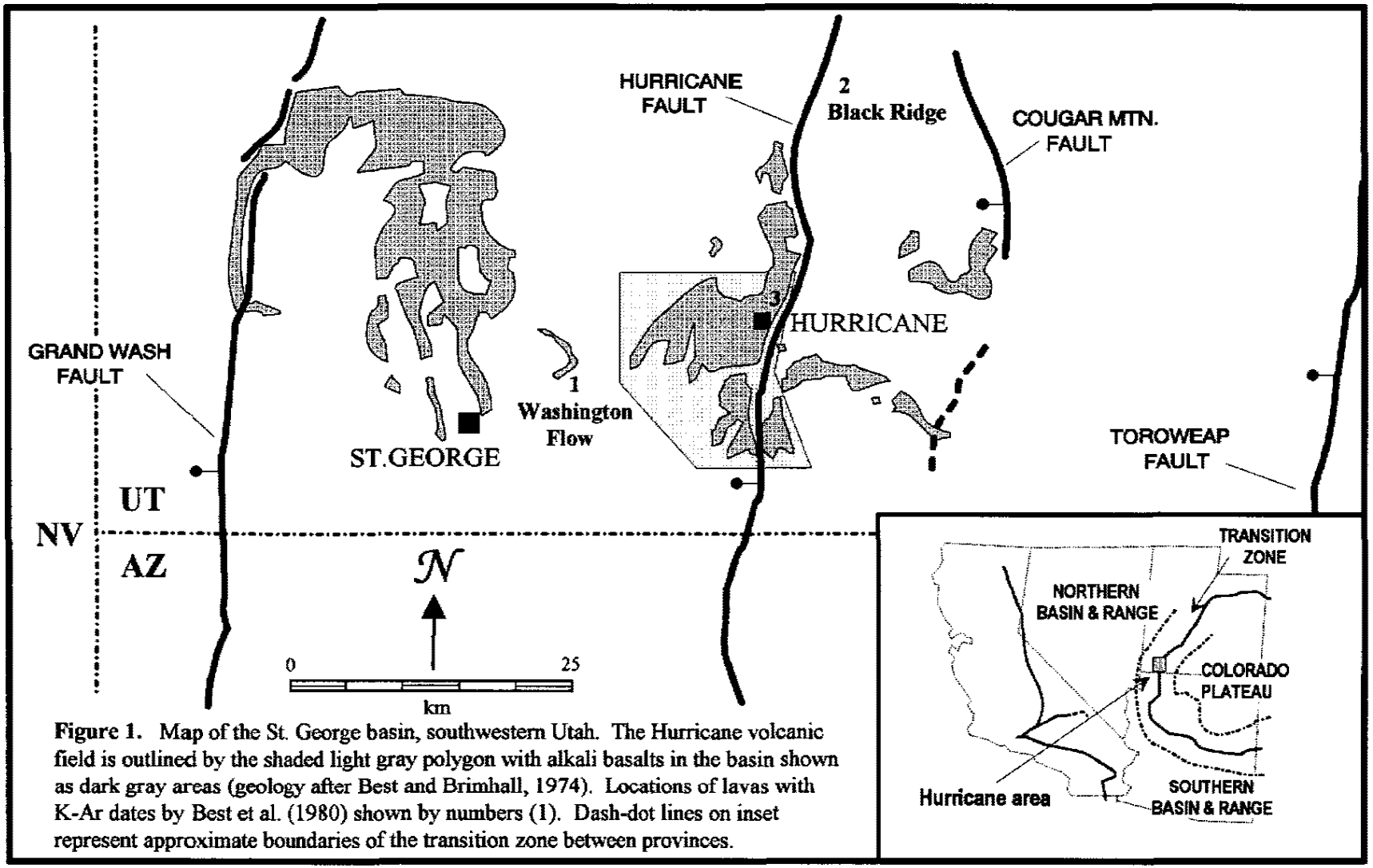


**Figure 1.** Map of the St. George basin, southwestern Utah. The Hurricane volcanic field is outlined by the shaded light gray polygon with alkali basalts in the basin shown as dark gray areas (geology after Best and Brimhall, 1974). Locations of lavas with K-Ar dates by Best et al. (1980) shown by numbers (1). Dash-dot lines on inset represent approximate boundaries of the transition zone between provinces.

# CHAPTER 2

# PHYSICAL VOLCANOLOGY, GEOCHRONOLOGY AND STRUCTURAL CONTROL

## Physical Volcanology

### Number and Volume of Centers

Five cinder (scoria) cone complexes near Hurricane consist of ten individual cinder cones (Figure 2). Nine of the ten cinder cones are breached by lava flows, eroded and/or quarried to varying degrees. The cones consist of pyroclasts of scoria and vesicular basalt that range in size from lapilli to bombs or blocks. Within eroded or quarried cones, crude bedding is exposed and defined by clast sorting. Aerodynamically shaped bombs and welded spatter (agglutinate) are commonly found on the flanks and summits of the cones. Cinder cones range in size from 200 m x 1 km (height x base diameter) at Volcano Mountain to 75 m x 300 m (height x base diameter) at Ivan's Knoll, an old eroded cone 700 m south of Volcano Mountain (Figure 2). A rough estimate of the volume of material erupted from each center was calculated by estimating the area covered by scoria and lava from air photos and field maps and then by multiplying that figure by 10 meters; an estimate of the average thickness of the flows. Volumes of the cinder cone complexes range from 0.05 to 0.30 $km^3$. The total volume for all five complexes is about 0.48 $km^3$.

### Lava Flows

Lava flows in the Hurricane volcanic field are typically 6 to 12 meters thick but are up to 60 m thick where they fill channels. The flows generally have a'a surface texture and

maintain a relatively constant thickness with distance from the vent except where they occupy channels. On Volcano Mountain and the Radio Towers cones, thin finger-like flows less than 10 cm thick crop out on the lower third of the flanks of the cones. These flows are not rootless (agglutinate deposits) but instead represent thin low-viscosity flows.

## Bombs and Agglutinate

Many large bombs (up to 2 m size) and agglutinate crop out at or near the summit of the younger cones (The Divide and Radio Towers). Agglutinate consists of ribbon bombs and rootless flows that were welded together during eruption. These deposits record a change in the style of eruption from volatile rich Strombolian to volatile poor Hawaiian eruptions. The gas content of the magma often decreases near the end of an eruption (Fisher and Schmincke, 1984) causing the ejection of larger masses of lava which often weld together on landing forming spatter and agglutinate. At the southern cone at The Divide location (Figure 2), many bombs litter the summit on its eastern and southern sides. The bombs are stretched in a manner that suggests that lava flowed downslope after impact. The east flank of this cone is being eroded at its base by intermittent flow in a large northward draining wash. Erosion exposed deposits of agglutinate just below the summit. The deposits of agglutinate extend no more than ten meters from the rim of the summit crater and are about two meters thick.

## Lava Lakes

Lava lakes are found near or at the summit of Ivan's Knoll, a satellite cone on the south side of the Cinder Pits cone, and at the Grass Valley cone (Figure 2). At Grass Valley, the lava lake is 3 m thick and consists of lava flows and agglutinate layers each two to five centimeters thick. Slickenlines on bedding planes suggest that partially solidified lava may have slipped into the summit crater during cycles of filling and draining of the crater. Another lava lake is located at Ivan's Knoll. This small cone is highly eroded and

most of its scoria is missing. The lava lake deposit is three to four meters thick and acted as a cap rock protecting the cone from erosion.

## Dikes

A north-south striking dike crops out on the steep northern flank of the Radio Towers cones. The dike is approximately 3 m wide and has an exposure length of about 20 m. This dike cuts breccia and scoria of the cone and contains xenoliths (up to 20 x 20 cm in size) of the Jurassic Navajo Sandstone. A smaller finger (2 m long x 0.5 m wide) of the dike extends at right angles to the main intrusion and cuts the breccia unit. At The Divide, a pair of north-south striking dikes about one-half kilometer in exposed length may be conduits for the two cones in this area. The northern dike crops out about one kilometer south of the southern cone and is five meters wide and at least 400 meters long. Twenty meters from the southern tip of this dike and 10 meters to the east, another dike, one-half meter wide, extends for another 200 meters before terminating in a hook. The northern dike contains abundant xenoliths of the Triassic Moenkopi Formation up to 3 x 6 cm in size. Dikes also crop out on the flanks of the Grass Valley cone and at Ivan's Knoll and project away from the lava lakes at the summit of these cones. Two dikes, about three meters wide, radiate from the center of the Grass Valley cone. At Ivan's Knoll, a dike 12 to 15 cm wide and 40 meters long extends to the southeast from a lava lake.

## Cone Stratigraphy: An Example

The Radio Towers center is composed of three coalescing north-south trending cones (Figure 2). The Virgin River has eroded a steep canyon about 100 m deep exposing a section of the northernmost cone and the underlying Navajo Sandstone (Figure 3). Overlying the Navajo Sandstone is a 1.5 m thick deposit of coarse ash and lapilli. A lava flow 8 to 10 m thick lies depositionally on the ash. Heat from the lava oxidized the upper two-thirds of the ash layer to a red color. A breccia unit 15 to 20 m thick unconformably

overlies the lava flow and makes up the interior of the volcano. This deposit contains blocks (up to 0.5 m in diameter) of Navajo Sandstone (host rock for the volcano) and vesicular basalt in a matrix of finer, poorly sorted pyroclastic material. The large size of the clasts in the breccia suggest that the initial stage of the eruption was explosive, possibly hydromagmatic. Scoria, agglutinate and bombs lie above the breccia and form the flanks of the cone. Many aerodynamically shaped bombs up to 0.5 m in size are found on this cone and larger bombs are more numerous near the summit. A dike (described above) intrudes the breccia and scoria of the cone (Figure 3).

## Eruption Dynamics

Basaltic magma has a low volatile content (< 0.5 wt. % $H_2O$), low viscosity, high diffusivity ($10^{-5}$ to $10^{-6}$ cm / sec), and high temperature (>750° C) upon eruption (Fisher and Schmincke, 1984) resulting in a relatively low ejection velocity (~ 150 m/sec) and low column height (10 - 1000 meters). Basaltic magmas are able to support large bubbles due to the lower magma (liquid) strength. The large size of bombs on the Hurricane cones reflects the fragmentation of these large bubbles. Volcanic bombs are formed from the walls of fragmented bubbles. Larger bubbles spend a shorter time in the transport system of the volcano than smaller bubbles and are produced by low velocity, high temperature eruption columns (Fisher and Schmincke, 1984). Ballistic transport of the bubble walls (i.e., the bombs) is the dominant mechanism of deposition. Eruption columns may have varied from relatively low lava fountains (tens of meters high) to more volatile rich columns, perhaps hundreds of meters high. The size of blocks in the pyroclastic deposit at the Radio Towers location suggests that early stages of some eruptions were quite explosive. Agglutinated deposits and thin rootless flows suggest that the eruptions were marked by pulses of activity rather than by continuous eruption. Lava flows and lava lakes are a typical features of volcanoes with high eruption rates and low gas content.

Hawaiian eruptions produce gentle eruptions of fluid mafic lavas. Gas escapes in lava fountains and/or spatter cones. Typical Strombolian eruptions are episodic and occur from an open vent. Lavas are mafic and are more volatile-rich than Hawaiian eruptions, resulting in the production of a cinder cone composed of cinder, spatter, bombs, and thin rootless flows. The physical features (cinder cones and relatively thin lava flows) of the volcanoes near Hurricane and their deposits (scoria, bombs, agglutinate, and thin rootless flows) indicate that they were produced by Strombolian and Hawaiian type eruptions. Most volcanic eruptions cycle through more than one eruptive type.

## Geochronology

Hamblin (1970b), in a study of Plio-Pleistocene volcanoes in the western Grand Canyon region, identified four periods of extrusion based not only on the degree of weathering and erosion, but also on the nature of the surface on which the lava flows were erupted. The present land surface is the product of erosion, the dominant process in the region during Late Cenozoic time. Lavas flows extruded at any period of time during the erosion cycle will preserve the surface that they cover from further destruction. Hamblin used the relation between the preserved surface and the present drainage to provide a reasonably objective technique for determining relative ages of the lava flows. Four major periods or "stages" of extrusion were recognized by Hamblin (1970b) in the western Grand Canyon region. They are: (1) Stage I flows deposited on an erosional surface up to 300 m above the present surface. (2) Stage II flows erupted on a surface related to the present drainage in that the flows slope in the same direction and have a similar gradient and pattern to the present drainage. This surface is 60 to 150 m above the present drainage. Volcanoes can usually be found "upstream" from flows but surface features of the volcanoes are now eroded. (3) Stage III flows deposited on surfaces 6 to 30 m above the modern drainage. These flows form inverted topography with ridges parallel to modern drainage. Volcanoes related to stage III flows are well preserved. (4) Stage IV

flows are those deposited in the present drainage system. Surface and marginal features are only slightly modified and associated cinder cones are well preserved. Where possible, stages were subdivided into substages (designated Stage IIa, IIb etc.). Substage assignments were based on local geomorphic relations. For example, two flows in one area that are the same stage may be further subdivided based on local stratigraphy (one flow may lie on another). In this case, each flow would be classified as a separate substage (i.e., Stage IIa and Stage IIb). However, the subdivisions cannot be correlated from one area in the western Grand Canyon to another and therefore represent only relative ages. In other words, Stage IIa near Hurricane may not be time equivalent to Stage IIa in other areas in the region. Stage II, III and IV surfaces are present in the Hurricane area (Plate 1).

For this work, three samples from the Hurricane volcanic field were dated using $^{40}Ar/^{39}Ar$ incremental heating techniques. Age spectra for samples 6-15 and 7-21 are concave upward and show excess argon (Figures 4A and B). In spectra that show excess argon, the lowest apparent age suggests a maximum age of the sample. Sample 6-15 is a flow that underlies the town of Hurricane and is offset by the Hurricane fault. The lowest intermediate temperature step (step 4) has an apparent age of $370 \pm 30$ ka and the isochron for the collinear array of steps 3-6 produces a date of $353 \pm 45$ ka (Figure 5A). The $^{40}Ar/^{36}Ar$ for this isochron is $300.5 \pm 6.6$ ($2\sigma$) which is acceptably close to the assumed value of 295.5. This flow was previously dated by Damon (cited by Best et al., 1980) at $289 \pm 86$ ka (K/Ar). The age spectrum for the lowest temperature step for sample 7-21 provides an apparent age of is $230 \pm 3$ ka and the first eight steps give an isochron date of $258 \pm 24$ ka (Figure 5B). The isochron $^{40}Ar/^{36}Ar$ is $296.1 \pm 2.9$ ($2\sigma$). Sample 7-21 is the second flow of a series of five thin flows from the north flank of Volcano Mountain. The age spectrum for sample 7-22, a bomb from the summit of Volcano Mountain, has a saddle shape (Figure 4C). The saddle spectrum shape indicates

that data for sample 7-22 do not produce a usable date. The lowest step has an apparent age of 270 ± 50 ka; the isochron date for steps 1-8 is 129 ± 60 ka with a $^{40}Ar/^{36}Ar$ of 301.5 ± 2.4 (2σ) (Figure 5C). All that can be concluded from this data is that the maximum age of this sample is 270 ± 50 ka.

Geochronologic data and cinder cone morphology were used to refine the age of cones in the Hurricane area (Table 1). The oldest flows are located 7 km south of Hurricane and are referred to here as the "Remnants" flows. These flows are cut and displaced by the Hurricane fault. The flow margins are eroded and the original shape of these flows is unknown. No cone is associated with Remnants flows on the footwall of the Hurricane fault or with flows directly across the fault on the hanging wall. These flows are classified as Hamblin's Stage IIa. Ivan's Knoll is the oldest cone in the Hurricane field because it is associated with flows of Stage IIb and has been stripped of most of its scoria by erosion. A Stage IIb flow from Ivan's Knoll that underlies the town of Hurricane yielded an $^{40}Ar/^{39}Ar$ isochron date of 353 ka ± 45 ka. A highly eroded cone 10 km south of Hurricane, just south of Grass Valley, is covered with soil but scoria is locally preserved. The cone and its associated flows are classified as Stage III based on the cinder cone morphology. Stage IVa cones at the Cinder Pits location, Radio Towers and Volcano Mountain have well developed vertical rilling in their scoria. Flows associated with these cones are also classified Stage IVa except for the youngest flows from Volcano Mountain. The eruption of the youngest flows breached the northeast flank of Volcano Mountain. A sample collected from one of these flows yielded an $^{40}Ar/^{39}Ar$ isochron date of 258 ka ± 24 ka. The youngest flows from Volcano Mountain and cinder cones located on the footwall of the Hurricane fault at The Divide are classified Stage IVb. One flow from The Divide has a very fresh surface morphology and cascaded over the Hurricane fault scarp. Post-basalt throw on the Hurricane fault would appear to have occurred between the two dates obtained by this work. However, the Stage IVb flow dated at 258

ka ± 24 ka does not reach the fault and the Stage IVb flow from The Divide only cascades about halfway down the fault scarp. Although the two Stage IVb flows belong to the same time stage, there still could be tens of thousands of years difference in their absolute ages. Consequently, the best age constraint that can be placed on post-basalt throw of the Hurricane fault is that it occurred in the last 353 ± 45 thousand years (t.y.) and perhaps took place in as short a time as 100 t.y.

Table 1. Summary of geochronology and cinder cone morphology in the Hurricane area.

| Stage | Location | geomorphic features | age |
|---|---|---|---|
| Stage IIa | Remnants | vent eroded away, flows eroded into segments | |
| Stage IIb | Ivan's Knoll; flow that underlies Hurricane Valley | scoria eroded away, flow margins eroded | 353 ka ± 45 ka (flow) |
| Stage III | Volcano Mtn./Ivan's Knoll | flows are not segmented by erosion | |
| Stage IIIa, b | Grass Valley | flows are not segmented by erosion | |
| Stage IVa | Volcano Mtn.; Cinder Pits; Radio Towers | cones have vertical rills; flows close to original shape | |
| Stage IVb | last Volcano Mtn. flow; The Divide | very fresh surface morphology, flow margins intact | 258 ka ± 24 ka (Volcano Mtn. flow) |

## Structural Control of Volcanism

Previous studies in the western Grand Canyon region noted that major regional structures do not appear to control the location of the eruptive vents in the western Grand Canyon region. Cook (1960) suggested that those volcanoes west of the Hurricane fault in Utah were related to faults, although he presented no evidence other than the fact that cone alignments appear to be parallel to fault traces. On the Uinkaret Plateau, Hamblin (1970b) reported that although vents show a prominent north-south alignment parallel to the major faults in the area, few vents are along the faults. Best and Brimhall (1974) also noted that vents are parallel to major faults but do not coincide with exposed fault traces. Anderson (1988) indicated that basalt flows tend to erupt on the footwall and flow across the major faults onto the hanging wall. However, he proposed that the vent locations themselves were controlled by joints. The first connection between vent locations and

joints appears to have been made by Gregory (1950). Gregory noted collinearity of the strike of the dike at The Divide and a linear trend of volcanic vents farther to the east on Little Creek Mountain. These alignments of volcanoes are coincident with the strike of joints in the immediate area (Figure 2). Threet (1958), in a study of Crater Hill in the Zion National Park region, observed that cones and vents "appear to be located along master joints or intersections of joints." Lefebvre (1961) showed that the linear trend of vents observed by Gregory (1950) is parallel to a peak in the joint distribution in the area about the Hurricane fault near Hurricane. Lefebvre's work on joint patterns in the Hurricane area showed that joint orientation data contains three nodes; N20-30°W, due north, and N20-30°E. Lefebvre divided the Hurricane area into 12 equal sections and constructed a histogram for each section showing joint orientation maxima.

The volcanoes in this study are within the boundaries of Lefebvre's area. Linear trends formed by volcanic vents match the joint orientation maxima of Lefebvre (Figure 6). West of the Hurricane fault, Volcano Mountain/Ivan's Knoll and Cinder Pits form a chain 1 km wide x 3 km long trending N27°E. The Grass Valley cone sits on an array faults that strike an average of N35°E. Strikes of individual faults were measured in the field. Lefebvre's joint orientation data in this area have a maximum at N30°E. Lefebvre's data also show a minor node at due north in the area where the Radio Towers cones form a chain 0.5 wide x 2.5 km long that trends due north. On the footwall block of the Hurricane fault, chains of vents at The Divide (0.5 x 3.5 km, N25°W) and at Gray Knoll (2 x 8.5 km, N37°W) on Little Creek Mountain just east of the study area, come close to matching the N30°W joint orientation maxima determined by Lefebvre for that area.

Delaney et al. (1986) showed that magma can invade existing joints if the magmatic pressure exceeds the horizontal stress acting across the joint plane. They also showed that the regional principal stress direction acting at the time of intrusion, need not be normal to the older joints. In other words, magmatic pressure needs to overcome only

the horizontal stress acting across the joint which can be as little as the normal component of the principal regional stress. Other recent studies have suggested that faults may not always be the pathway for magma ascent through the uppermost crust (Condit et al., 1989; Conner, 1990; Conner and Condit, 1994; and Draper et al., 1994). It appears that, in the Hurricane area, magma was transmitted along faults or produced its own path at depth but, near the surface, followed joints which are a dominant structural feature.

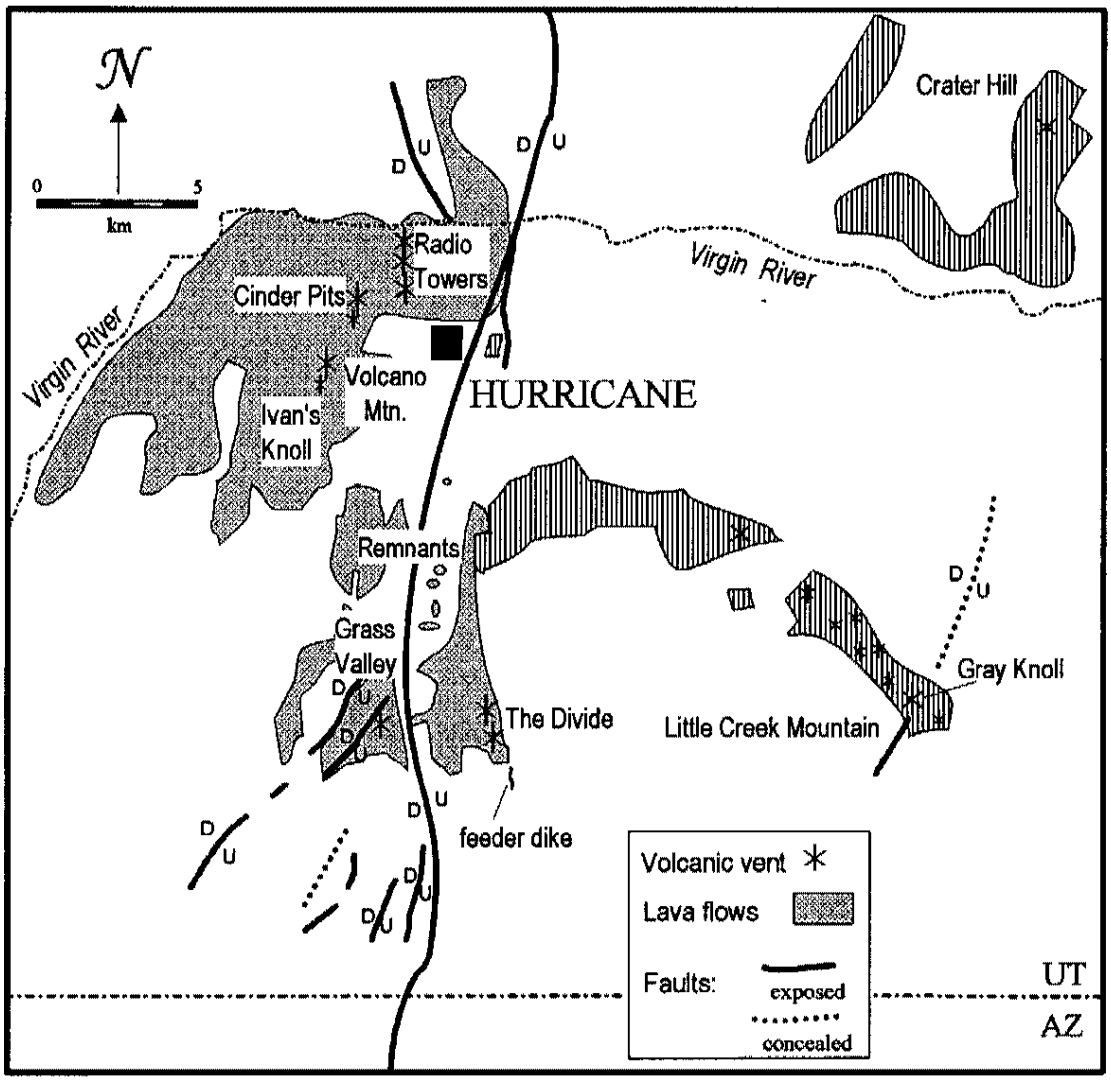


Figure 2. Map of the Hurricane volcanic field. Names and locations of cinder cones are shown. Other nearby lava flows outside the Hurricane volcanic field are shown by the vertical ruled pattern.

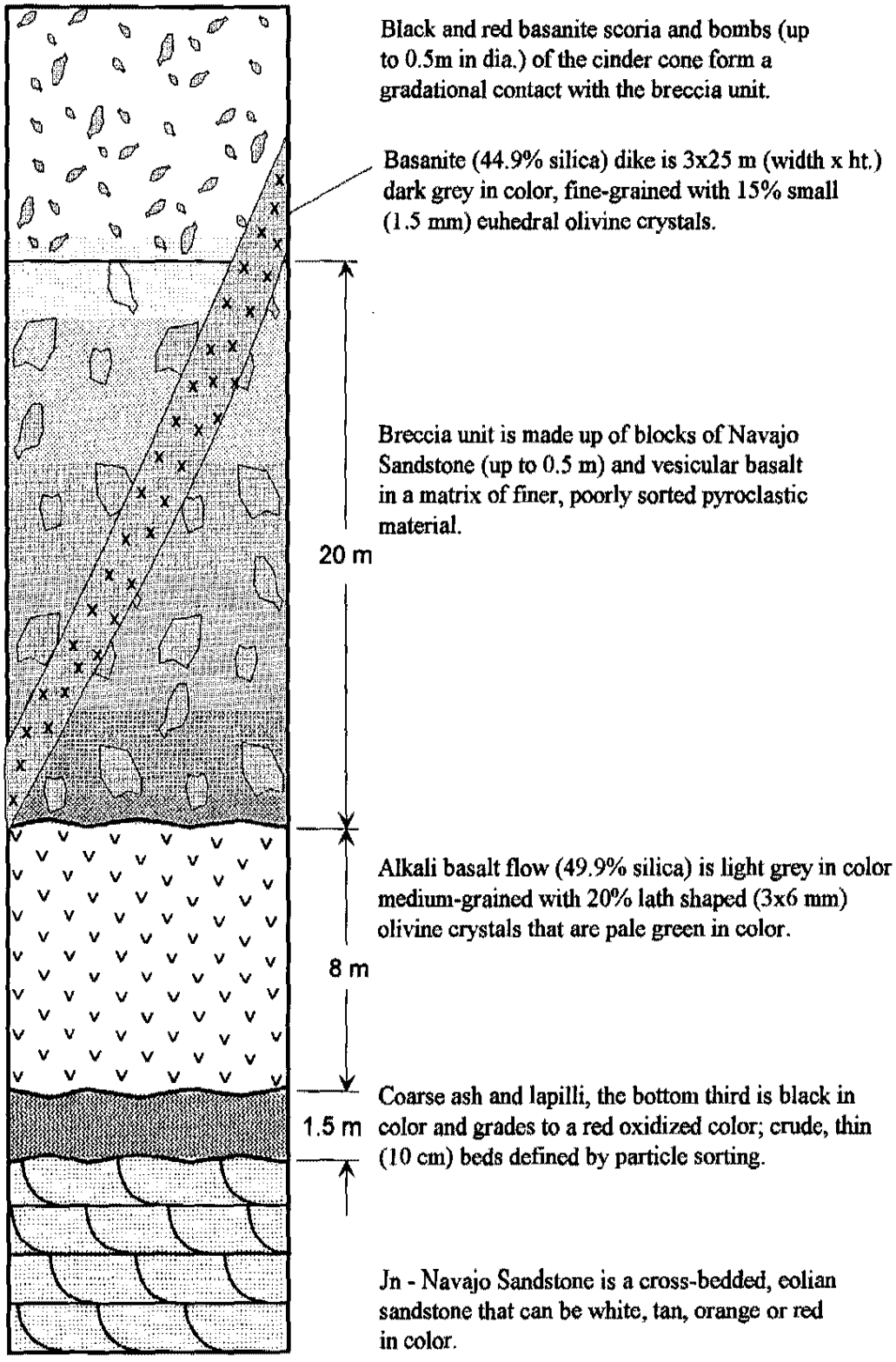


Figure 3. Stratigraphy of the Radio Towers northern cone (not to scale).

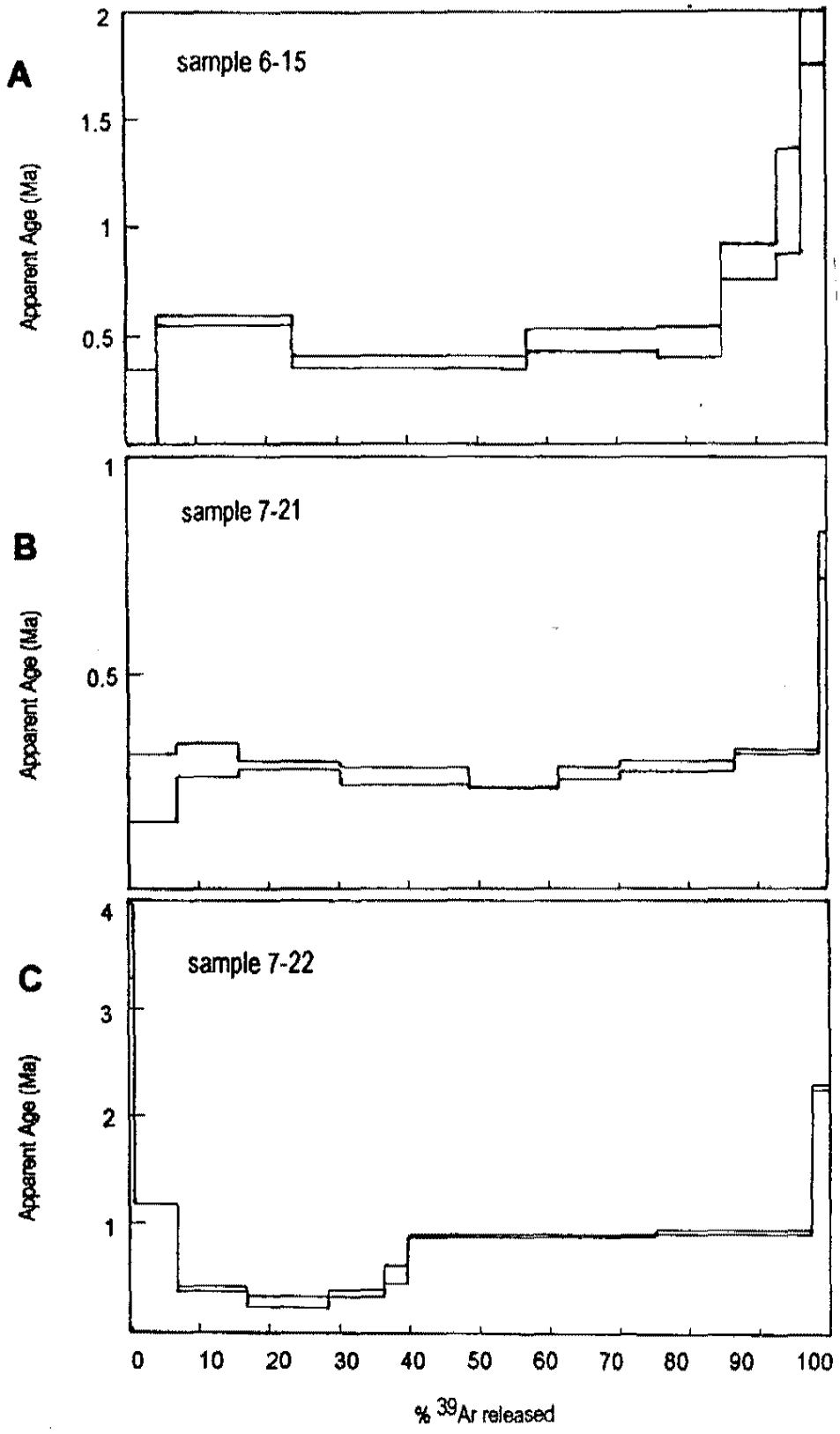


Figure 4. Age spectra of Hurricane samples.

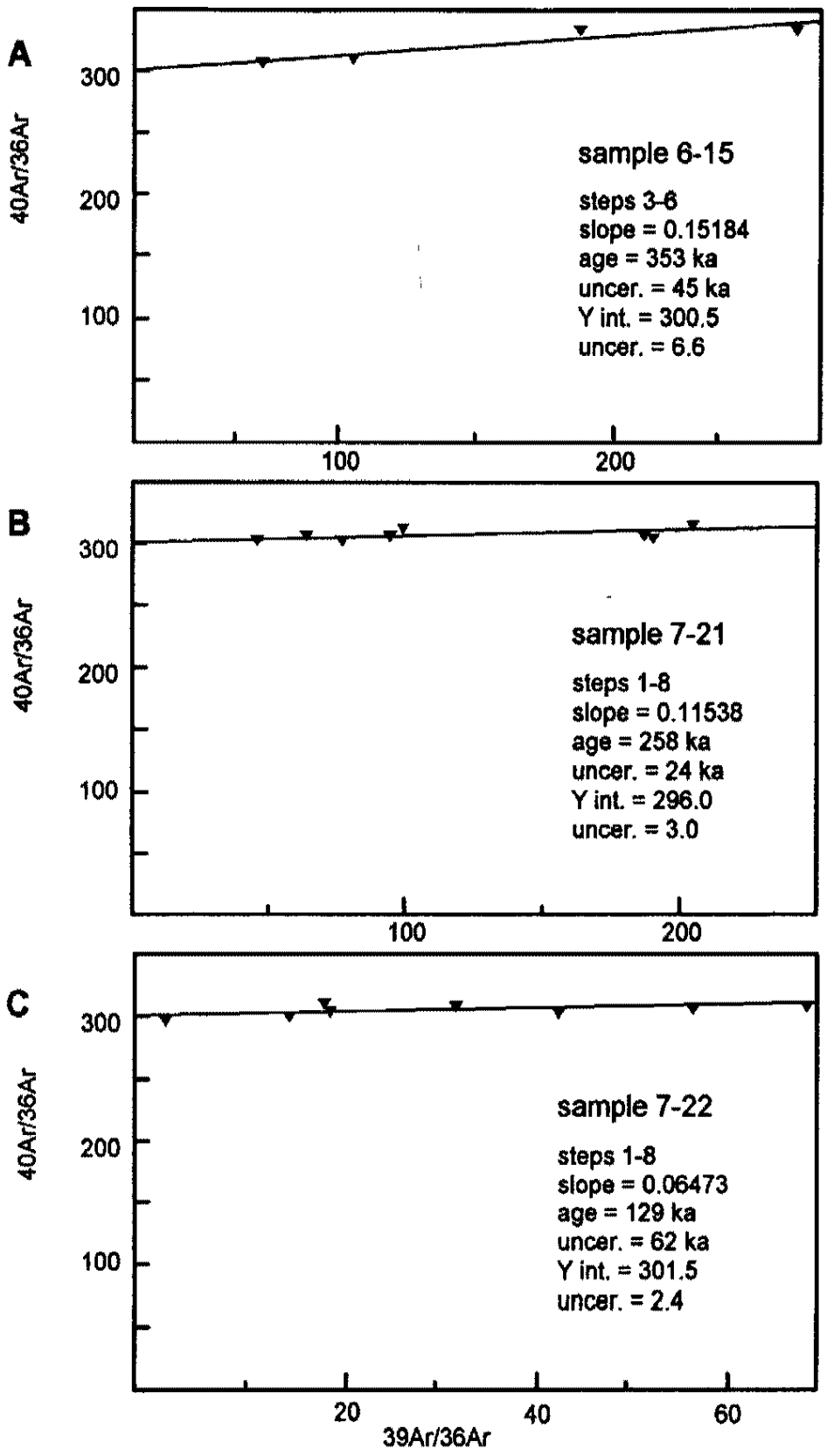


Figure 5. 39Ar/36Ar versus 40Ar/36Ar isochron plots.

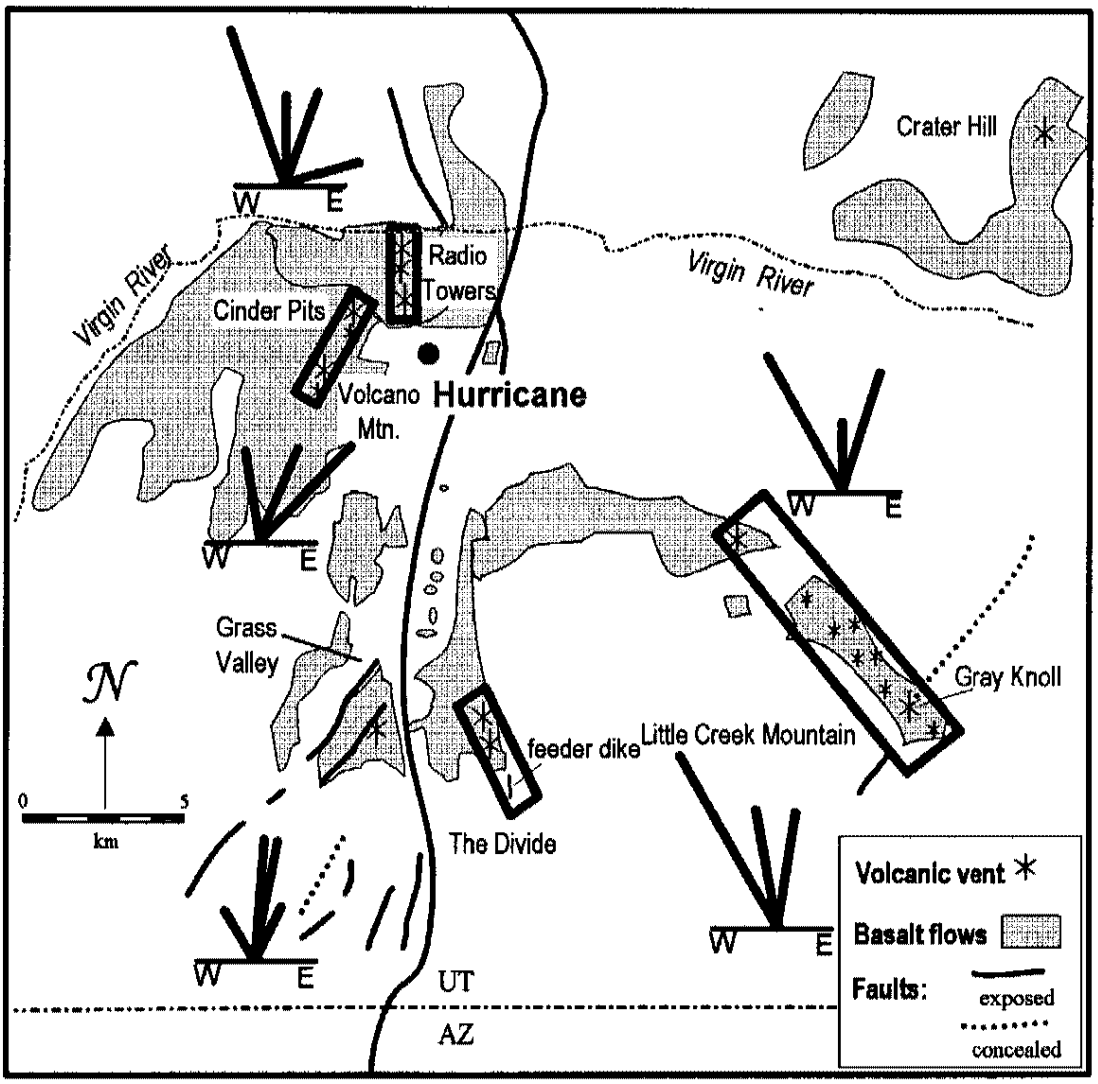


Figure 6. Map of the Hurricane volcanic field vent alignments (rectangles). Joint maxima data is from Lefebvre (1961). Note that the two vent alignments east of the Hurricane fault (The Divide and Gray Knoll on Little Creek Mtn.) come close to matching the largest joint nodes (N30°W) for those areas. West of the fault, Volcano Mtn. and Cinder Pits vents form an alignment (N30°E) that matches a secondary joint node in that area. The cone south of Grass Valley is on an array of faults that strike N35°E. The three cones at the Radio Towers locations form a north trending alignment which matches a minor joint node in that area.

# CHAPTER 3

## GEOCHEMISTRY - EVOLUTION OF THE VOLCANIC FIELD AND POLYGENETIC VS. MONOGENETIC VOLCANISM

Geochemistry of basaltic rocks can be used to address three problems concerning magmatism in the Basin-and-Range / Colorado Plateau Transition Zone. These problems are: (1) the properties of the mantle under the Transition Zone, (2) the evolution of the mafic magma after partial melting, and (3) the history of eruption of individual centers (polygenetic vs. monogenetic[1] ). The physical properties of the mantle beneath the Transition Zone can be determined indirectly by studying basalts erupted in this area. Basaltic rocks can be used as probes of the mantle because mafic magma spends a relatively short time in transit to the surface and is thought not to have evolved significantly. The geochemical study will also be used to demonstrate that some cinder cones and vent complexes in this area are polygenetic.

### Geochemistry and Petrology of Mafic Rocks in the Hurricane Volcanic Field

The volcanic rocks from the Hurricane volcanic field have olivine phenocrysts making up 10% to 30% of the rock volume. Phenocrysts are commonly 1 mm euhedral to

[1] Polygenetic describes a case where magmas from different sources erupted at one center and monogenetic refers to a single magma source.

3 mm x 6 mm lath shaped crystals and are generally fresh, except in some of the older flows (the Remnants) where olivine crystals are rimmed by iddingsite. Lava flows from The Divide, Radio Towers, and some from Volcano Mountain and the Cinder Pits cones, are very fine-grained and have a distinctive black color. They contain small (1 mm) pale green olivine crystals as the only phenocryst phase. Other lavas from Volcano Mountain and the Grass Valley cone are medium gray in color, fine- to medium-grained with small (1 mm) euhedral to lath shaped (3 x 6 mm) olivine crystals that are pale to dark green in color. At The Divide, two dikes have phenocrysts of clinopyroxene and hornblende in addition to olivine. The dike rock has 25%, 1 to 3 mm, pale green euhedral olivine crystals (some larger olivine crystals are rimmed with clinopyroxene); 15%, 1 x 1 mm, black, clinopyroxene crystals; and 5%, 1 x 3 mm, black, hornblende needles commonly forming star-shaped aggregates. Xenoliths of the Moenkopi Formation are numerous in this dike. At the Radio Towers cones, some bombs are cored by xenoliths of the Navajo Sandstone.

Chemical data for the samples included in this study are listed in Appendix I. The volcanic rocks from the Hurricane area are divided into three groups and classified as low-silica basanites, basanites, and alkali basalts based on the total alkali vs. silica (TAS) diagram of Le Bas et al. (1986) and normative plagioclase (An) vs. normative nepheline (ne) plus leucite (lc) and hypersthene (hy) (Figure 7). $Al_2O_3$ wt. % increases while MgO, $TiO_2$ and CaO wt. % decrease with increasing $SiO_2$ wt. % (Figure 8). Normative quartz is not present in any of the rocks. Low-silica basanites contain $SiO_2$ concentrations of 41.5 to 42.1%, MgO and CaO average 13.6% and 12.5%, respectively, and $TiO_2 < 1.9\%$. The mean magnesium number (Mg#; see Appendix IV for the definition of Mg#) for this group is 69.7 which is close to the typical Mg# of 71 for primary mantle-derived basalts (e.g., Green et al., 1974). Low-silica basanites are nepheline-normative (ne = 15 to 18). Normative plagioclase composition varies from $An_{96}$ to $An_{100}$. Basanites have a $SiO_2$

range from 43.2 to 46%, a MgO average of 11.7%, a CaO average of 10.6% and $TiO_2$ > 2.25%. Mg#s for the basanites range from 59.6 to 68.7 and average 63.9. These rocks are nepheline-normative (ne = 5 to 12). Normative plagioclase composition ranges from $An_{50}$ to $An_{74}$. The alkali basalt group has $SiO_2$ ranging from 46 to 51.6%, a MgO average of 7.5%, CaO average of 9.5% and $TiO_2$ < 1.9%. Mg#s for this group range from 49.6 to 62.8 and form two clusters at 61 and 54.8. These rocks have normative plagioclase compositions of $An_{42}$ to $An_{52}$ and are nepheline- to hypersthene-normative (ne < 4 to hy < 19).

Some incompatible trace element (Ba, Sr, Th and Nb) concentrations for each group are shown in Figure 9. Note that incompatible trace element concentrations decrease as $SiO_2$ wt. % increases. For example, low-silica basanites ($SiO_2 \cong 42$ wt. %) contain ≅ 80 ppm Nb and alkali basalts ($SiO_2 \cong 48$-50 wt. %) have about 10-30 ppm Nb. Incompatible trace element and rare-earth elements (REE) concentrations normalized to ocean island basalt (OIB) abundance from Fitton et al. (1991) are shown on Figure 10. The trace elements are listed on the x-axis of the plot to reflect increasing compatibility in mantle minerals from left to right. All groups from Hurricane show an enriched concentration in the large ion lithophile elements (LILE) and the light rare earth elements (LREE) relative to the high field strength elements (HFSE) and the heavy rare earth elements (HREE). Exceptions to this trend are depletions in Rb, a LILE, and enrichments in Nb, a HFSE.

Low-silica basanites have high Ba, Nb and Sr concentrations (>2300, > 72, and > 1180 ppm). This group has a Ba peak and troughs at Rb and K but not at Nb (Figure 10A). This pattern and overall trace elements are similar to mafic lavas from the Colorado Plateau. An olivine melilitite from Woodruff Butte, Arizona (Fitton et al., 1991) is shown as an example of a typical mafic lava from the Colorado Plateau (Figure 10A). The low-silica basanites also show an interesting similarity to rocks from the Oregon Cascades

called analcimites (Conrey, 1990). The analcimites commonly exhibit low $K_2O$ (0.70 wt. %), high $TiO_2$, $P_2O_5$ (3.6 and 1.23 wt. %), and Nb, Sr, Ta concentrations (77, 1038, and 3.45 ppm), and 8.5 % normative nepheline. The analcimites, however, are different in that they are relatively enriched in Rb, Ti, P, and depleted in Ba compared to the low-silica basanites from Hurricane (Figure 10A). Conrey suggests that the analcimites in Oregon were generated by very small partial melts at relatively shallow depths (~ 45-50 km).

The basanite spider diagram shows a pattern with a Ba peak and Rb trough but no K-Nb trough (Figure 10B). Ba and Rb concentrations range from 498 to 1266 ppm and 13.7 to 26.7 ppm, respectively. Basanites are definitely enriched in Nb (47 to 72 ppm) and have a slight enrichment in trace elements from La to Y compared to the Fitton et al. (1991) average of basaltic rocks younger than 5 Ma from the Transition Zone.

Rb, Ba and Nb in the Hurricane alkali basalts range from 8.3 to 16.9 ppm, 255 to 1281 ppm and 13 to 33 ppm respectively. The group produces a spider diagram pattern that is very similar to the average Transition Zone basalt younger than 5 Ma of Fitton et al. (1991) (Figure 10C). This similarity suggests that Hurricane alkali basalts are chemically like other Transition Zone alkali basalts.

Concentrations of compatible trace elements (Ni, Co, Cr and Sc) are summarized in Figure 11. Average values for the low-silica basanites are 312, 56, 607 and 32 ppm, respectively. These relatively high values coupled with the high Mg# (69.7) suggest that this rock is a relatively primitive basalt. Basanites also have relatively high concentrations of compatible trace elements although they are somewhat lower than the low-silica basanites. Cr concentrations in basanite range from 568 to 367 ppm, Co ranges from 50 to 68 ppm and Ni ranges from 114 to 475 ppm and clusters at ~350 and ~200 ppm. Sc for both the basanites and the alkali basalts has a range from 24 to 29 ppm. Cr and Ni in alkali basalt have two clusters (Cr at ~300 and ~150 ppm; Ni at ~60 and ~150). Co ranges from 40 to 50 ppm in the alkali basalts.

The Hurricane samples have $^{143}Nd/^{144}Nd$ ratios that range from 0.512253 to 0.512718 ($\varepsilon_{Nd}$ values -7.5 to +1.6; see Appendix IV for the definition of $\varepsilon_{Nd}$) while initial $^{87}Sr/^{86}Sr$ ranges from 0.703678 to 0.704882 (Figure 12). For clarity in the remainder of this work, the magmas which the volcanic rocks represent are divided into four magma types (Table 2). Basanites were formed from a magma referred to as magma type A. The basanites have initial $^{87}Sr/^{86}Sr$ values of 0.7040 to 0.7043, $\varepsilon_{Nd}$ values of -0.2 to -1.8 and $^{206}Pb/^{204}Pb$ values of about 18.35. Alkali basalts from Grass Valley were derived from magma type B. Grass Valley alkali basalts have initial $^{87}Sr/^{86}Sr$ values of 0.7035 to 0.7040, $\varepsilon_{Nd}$ values of +1.6 to -0.5 and $^{206}Pb/^{204}Pb$ values of about 18.05. Alkali basalts from Ivan's Knoll were derived from magma type C. These alkali basalts have initial $^{87}Sr/^{86}Sr$ values of 0.7046 to 0.7049, $\varepsilon_{Nd}$ values of -6.2 to -7.5 and $^{206}Pb/^{204}Pb$ values of about 17.5. Low-silica basanite from the Remnants is from magma type D and has $^{87}Sr/^{86}Sr$ values of 0.7046 to 0.7048, $\varepsilon_{Nd}$ values of -1 to -1.4 and $^{206}Pb/^{204}Pb$ values of about 18.7. On an initial $^{87}Sr/^{86}Sr$ versus $\varepsilon_{Nd}$ diagram, types A, B and D plot just to the left and below a mantle array (data from Bradshaw, 1991 and Feuerbach et al., 1994) produced by the mixing between OIB and lithospheric mantle end members (Figure 13A). Basalts from magma types A, B and D plot in a field defined by the range of isotopic variation of basalts on the Colorado Plateau. Falling outside this field is type C, from Ivan's Knoll and the flow underlying Hurricane Valley which have significantly lower $^{143}Nd/^{144}Nd$ ratios (0.512253 to 0.512322 and $\varepsilon_{Nd}$ values -6.2 to -7.5). Magma type C plots below the mantle and Colorado Plateau arrays. All samples from Hurricane plot above the Northern Hemisphere Reference Line (NHRL) and form a trend of decreasing $^{206}Pb/^{204}Pb$ with slightly decreasing $^{207}Pb/^{204}Pb$ on lead isotope ratio-ratio plots (Figure 12C).

Table 2. Summary of chemistry for Hurricane volcanic field magma types.

| Magma type | A | B | C | D |
|---|---|---|---|---|
| Time stage | Stage IVa, IVb | Stage III | Stage IIb | Stage IIa |
| rock class. | basanite | alkali basalt | alkali basalt | low-$SiO_2$ basanite |
| $SiO_2$ wt. % | 43.3 - 45.9 % | 47.2 - 49.6% | 48.4 - 51.6% | 41.5 - 42.5% |
| Mg# ave. | 63.9 | 61.0 | 54.8 | 69.7 |
| Ba/Nb ave. | 14.2 | 15.2 | 42.9 | 27.6 |
| initial $^{87}Sr/^{86}Sr$ | 0.704189 | 0.703810 | 0.704751 | 0.704687 |
| $\varepsilon_{Nd}$ | -0.2 to -1.8 | +1.6 to -0.5 | -6.2 to -7.5 | -1.0 to -1.4 |
| $^{206}Pb/^{204}Pb$ | 18.31 | 18.03 | 17.49 | 18.64 |

A comparison of chemical features of the basalts from Toquerville reported by Schramm (1994) (see chapter 5) and the Hurricane volcanic field shows many similarities. Both groups of rocks plot as basalts on a TAS diagram (Figure 14A). Alkali basalts from Ivan's Knoll (magma type C) are similar in chemistry to those from Toquerville in that they contain similar concentrations of compatible elements (Cr for example) (Figure 14C) and incompatible elements (K and Zr for example) (Figures 14B and 14D).

## Evolution of the Volcanic Field

Problems concerning the evolution of basalts in the Hurricane volcanic field are: (1) the chemistry of their source, (2) the effect of crustal contamination, (3) the petrogenetic relationship between the general rock groups (basanite, alkali basalt etc.), and (4) the variations of chemistry within the general rock groups.

### The Mantle Source

Low-silica basanite and basanite magmas rose rapidly from the site of partial melting to the surface as indicated by their primitive chemistry (high MgO, Mg# and high concentrations of compatible elements). The chemistry of these magmas, therefore, may directly reflect the composition of the mantle source. The nature of this source can be inferred by plotting ratios of trace elements that are compatible in mineral phases in equilibrium at high pressures and depths (i.e., Yb which is compatible with garnet).

In Figure 15A, a La/Yb vs. Nb/La diagram, magmas with a high La/Yb value may indicate smaller degrees of partial melting if garnet were in the source. Yb is highly compatible in garnet and would remain in the residual phase (garnet) if the source were a garnet-peridotite. However, high La/Yb ratios are not always indicative of a garnet bearing source. Perhaps a better indication of the presence of garnet in the source is a steep slope on a chondrite normalized REE diagram (Figure 15B). Normalized heavy REE values should approach 1 if garnet is in the source. Hurricane basalts have chondrite normalized Lu of between 5 and 10 (Figure 15B). These values are too high and are indicative of a garnet free mantle source. High Nb/La magmas probably originate in the asthenospheric mantle because this part of the mantle is enriched in high field strength elements (Nb) with respect to light rare earth elements (La). Lower Nb/La ratios suggest that the addition of a lithospheric mantle component. Figure 15A, therefore, can be used to determine the relative contribution of asthenospheric mantle and lithospheric mantle in the source, but can not be used to estimate the amount of partial melting. Isotopic types A, B and D (Grass Valley alkali basalts, basanites and low-silica basanites) have relatively high Nb/La values indicating that their source is asthenosphere mantle (OIB-like). The lower Nb/La values for alkali basalts from Ivan's Knoll (isotopic type C) indicate the presence of a lithospheric component in its source. Volcanic rocks from Hurricane, therefore, represent magmas that have an OIB-like garnet free source (perhaps spinel peridotite) but show variable amounts of mixing with lithospheric mantle sources.

## Crustal Contamination

Magmas can assimilate different parts of the crust as they rise to the surface. Crustal xenoliths incorporated in mafic lavas provide a sample of potential contaminants in the upper and lower crust. Lower crust typically has low $\varepsilon_{Nd}$ and initial $^{87}Sr/^{86}Sr$ while upper crust has high initial $^{87}Sr/^{86}Sr$ and low $\varepsilon_{Nd}$ values (see below). Hurricane mafic lavas exhibit lower $\varepsilon_{Nd}$ values with little or no increase in initial $^{87}Sr/^{86}Sr$. Therefore, a

lower crustal component with low $\varepsilon_{Nd}$ and initial $^{87}Sr/^{86}Sr$ may be the source of contamination of Hurricane magmas.

Previous studies on the Colorado Plateau have identified or proposed four lower crustal components that may be likely contaminants of Hurricane magmas. Nealey and Unruh (1991) described mafic crustal xenoliths from Tule Tank, Arizona that have isotopic ratios of 0.70255 to 0.70294 for $^{87}Sr/^{86}Sr$ and 0.511664 to 0.511897 for $^{143}Nd/^{144}Nd$. Unruh et al. (1994) proposed a mafic lower crustal component beneath the St. George basin that is identified by $^{87}Sr/^{86}Sr \geq 0.707$, $\varepsilon_{Nd} \leq -12$ and $^{206}Pb/^{204}Pb \sim 17.5$-17.9. Unruh et al. (1994) define this component on the basis of isotopic data from 23 basalt samples collected in the St. George basin. This lower crustal component is different from one believed to lie beneath the Markagunt Plateau ($^{87}Sr/^{86}Sr \leq 0.704$, $\varepsilon_{Nd} \leq -10$ and $^{206}Pb/^{204}Pb \leq 17$) by Nealey et al. (1993) just to the northeast to the St. George basin. A lower crustal component ($^{87}Sr/^{86}Sr \geq 0.705$, $\varepsilon_{Nd} \leq -18$) is proposed by Perry et al. (1987) to lie under the Taos Plateau on the eastern edge of the Colorado Plateau. A range of isotope values for the lower crust were shown by Arculus and Gust (1995) to exist beneath the San Francisco volcanic field in northern Arizona based on their studies of crustal xenoliths (Figure 13).

The isotopic arrays for each magma group (Figures 12 and 13A) can be explained by the addition of a lower crustal component to mafic magmas. Either two step or single step contamination models are possible. Lower crustal contamination may occur both before or during fractional crystallization (FC) (see below). A two step assimilation fractional crystallization (AFC) model for the evolution of Hurricane magmas requires the addition of both Tule Tank and St. George basin components (Figure 13B). Assimilation of Tule Tank type crust during fractional crystallization should produce evolution vectors that extend from the mantle array toward the field defined by Tule Tank compositions on isotope diagrams (Figure 13B). Although the Hurricane samples fall below the mantle

array, they are aligned sub-parallel to the array and do not trend toward the compositions of Tule Tank xenoliths (Figure 13B). In fact, the isotopic arrays for Hurricane alkali basalts and basanites trend in the general direction of the St. George basin lower crustal component proposed by Unruh et al. (1994). These observations indicate that a lower crustal component like Tule Tank possibly was not being assimilated *during* fractional crystallization. A lower crustal component, however, may have been assimilated *prior* to FC to produce the most primitive magmas in the field. Thus, it is possible that the basalts from the Hurricane volcanic field experienced two lower crustal contamination events. The first, contamination by the Tule Tank component (~10%) prior to FC, would draw the isotope values of the most primitive Hurricane basalts below the mantle array on Figure 13B. The Tule Tank component can affect melts at any point within the mantle array. For example, the most primitive magmas within groups B and D might reflect separate contamination events. (Figure 13B). A second assimilation event with up to eighteen percent of the St. George basin component during FC would produce the trends of the isotopic arrays of magma groups A and B observed on Figure 13B. Assimilation of from 19 to 50% of this lower crustal component would be required to produce magma group C. This second contamination event may not be required to produce the isotopic variation within magma group D. The disadvantage of the two step model is that it requires a fairly complex history and possibly a long residence time in the crust for the rising magma to be affected by two crustal components. This history is counter to the chemical evidence which suggests that these primitive alkali magmas rose to the surface quickly. Another disadvantage of this model is that the large amounts of contamination may not be thermodynamically possible.

An alternative model of lower crustal contamination requires only one step. The isotopic array defined by the Hurricane lavas also trend toward a lower crustal component under the Taos Plateau on the eastern edge of the Colorado Plateau proposed by Perry et

al. (1987) and toward a range of isotope values for lower crustal material as shown by Arculus and Gust (1995) to lie beneath the San Francisco volcanic field (Figure 13C). Therefore, contamination by *one* of these lower crustal components may explain both the position of the Hurricane lavas below the mantle array and the trend of the isotopic arrays for each magma group. This model is simple but has the disadvantage that it requires the addition of from 28 to 60% of lower crust components not demonstrated to exist beneath the Hurricane area. This amount of contamination is probably not thermodynamically possible. The contaminant composition, however, may lie anywhere within the field shown on Figure 13C. The estimates of contamination, therefore, represent maximum values. Without additional evidence, the single step assimilation model is preferred even though it has serious problems mentioned above.

## Variation Between and Within Rock Groups

Three types of models will be evaluated to determine the processes that are responsible for chemical variation between and within magma groups. These are fractional crystallization (FC), assimilation and fractional crystallization (AFC), and mixing of isotopically different basaltic melts. These models require the addition of a lower crustal component(s) in order to explain the isotopic variation (discussed above) within each magma group. However, the effects of the lower crustal component(s) on trace element variations can not be evaluated due to lack of trace element data for these component(s). Computer modeling of these processes was done using IGPETWIN software written by Carr (1994) and an EXCEL spreadsheet, using the DePaolo (1981) AFC equation, developed by Bradshaw (1991) and modified by Smith (1993, pers. comm.). Minor oxide and trace element distribution coefficients used in the modeling are given in Appendix IV.

Fractional crystallization does not seem likely to explain the variation between groups for three reasons. (1) The isotopic ratios of the groups are different (Figure 12). Fractional crystallization of phenocrysts in equilibrium with liquid does not produce

changes in isotopic ratios. (2) Incompatible trace element amounts decrease with increasing silica content (Figure 9). Incompatible trace elements like Th, Ba and Nb should increase in abundance during fractional crystallization because these elements are conserved in the liquid phase. (3) Incompatible vs. compatible trace element plots show a positive correlation (e.g., Ni concentrations are generally higher for greater abundance of the incompatible element Rb) (Figure 16A). The fractionation process is not expected to produce such a correlation between incompatible and compatible trace elements because the compatible element is conserved in the solid phase while the incompatible element is conserved in the liquid phase. Thus, concentrations of compatible elements should decrease while incompatible element abundances increase during fractional crystallization.

Fractional crystallization (FC) models quantitatively establish these observations (Figures 16, 17 and 18). Three models were attempted to relate the basanites to the alkali basalts by FC. Sample 6-10 from The Divide is used as a parent in these models because it is the most mafic and primitive of the basanite samples. This sample is from a dike that contains 25% olivine, 15% clinopyroxene and 5% hornblende phenocrysts. A FC model involving the fractionation of olivine and plagioclase in a ratio of 3:7 does produce a model that relates the basanites and alkali basalts, but an unreasonably high amount of fractionation is required (90%) (Figure 18). A second model requires the removal of olivine, clinopyroxene and hornblende in a 35:55:10 ratio and produces a variation trend that explains the production of the Radio Towers basanite from the more primitive basanites at The Divide by only 18% fractionation (line 1, Figures 16 and 17). Fractionation of olivine alone produces a similar model (line 2, Figures 16 and 17). Both of these models successfully imitate the evolution of magma type A basanites, but neither explains the production of the alkali basalts from the basanites (Figures 16A and 17A). Earlier work by Best and Brimhall (1974) indicated that FC is not responsible for

producing hawaiite and alkali olivine basalt from basanite. This observation was based on the major elements alone for equivalent rock types in the western Grand Canyon region.

Because FC models do not explain the chemical evolution of the entire Hurricane field, AFC models involving the mixing of independent mantle melts must be considered. Mixing of different melts would explain the differences in isotopic ratios, the decrease in incompatible trace elements with evolution and the positive correlation on compatible-incompatible trace element plots. A three stage model using FC and mixing processes represents the variation of Hurricane basanites, Grass Valley alkali basalts and some alkali basalts from Volcano Mountain. (1) The first stage of the model employs FC models discussed earlier which successfully imitate the evolution of isotopic type A basanites (lines 1 and 2, Figures 16 and 17). (2) Next, mixing of evolved type A basanite with type B alkali basalt produces the variation observed between the Radio Towers basanite and Cinder Pits, Volcano Mountain and Grass Valley samples (line XY, Figures 16B and 17B). The basanite end-member sample 5-6 (X on Figures 16B and 17B) is the earliest flow from the Radio Towers cones and one of the more mafic Radio Towers basanites (Ni=233 and Cr=445 ppm) . Sample 5-5 (Y on Figures 16B and 17B) is from a lava lake at the Cinder Pits satellite cone. (3) The last step involves FC of magma with a composition along mixing line XY. FC models for alkali basalt evolution from line XY are successful in explaining petrologic differences of Grass Valley (magma type B) and the Cinder Pits center. Samples used as the parent for each model are those that are the most mafic and closest to the mixing line X-Y. Alkali basalts at Grass Valley are modeled by about 8% olivine fractionation using sample 7-4 as the parent (line 3, Figures 16B and 17B). Alkali basalts at the Cinder Pits required slightly over 10% olivine FC to produce differences observed (line 4, Figure 16B). The FC model used sample 5-7 as the parent although in theory any point on the mixing line from the basanites could be the starting point.

This three stage model does not explain the production of magma type C, Ivan's Knoll alkali basalt, and type D, the Remnants low-silica basanite. Variation within magma type C (alkali basalts from Ivan's Knoll) or magma type D (low-silica basanites from the Remnants) can not be modeled by FC. These rocks may have reached the surface so rapidly that the FC process could not occur. These magma types (C and D) are interpreted as independent melts that did not interact with other magma types. A flowchart depicting the genesis of Hurricane magmas is shown on Figure 19. The time line shown on this figure refers only to the eruptions of volcanoes in the field and not to the magma differentiation processes.

## Geochemistry of Individual Centers

The chemistry of the volcanic rocks found at each center in the Hurricane volcanic field is described below. These data are used to determine if each center was monogenetic or polygenetic.

### Cinder Pits

The two vents of the Cinder Pits erupted alkali basalts (48.3% $SiO_2$) that are transitional in their chemistry between the basanite from Volcano Mountain and the alkali basalts from Ivan's Knoll. Concentrations of some major element oxides and trace elements approach the values of the basanites found at Volcano Mountain and Radio Towers locations. For example, sample 1-3 has a Cr concentration of 326 ppm and high Zr, Y and Ba values (241, 28.7 and 1281 ppm). Sample 5-5 has 8.5% MgO and contains 220 ppm Ni. No isotopic analyses were done on samples from this location.

### Grass Valley

The volcanic rocks at Grass Valley are alkali basalts (47.2 to 49.6% $SiO_2$). Chemical and isotopic analyses cluster for almost all elements. Some average major

element oxide wt % values are $Al_2O_3$ = 16%, $Fe_2O_3$ = 10%, CaO = 8.5-9.8% and $TiO_2$ = 1.8%. Trace elements values for Rb, Zr, Sr and Nb cluster at 11.5, 250, 700 and 27 ppm respectively. Cr and Ni concentrations range from 226 to 375 ppm and 107 to 194 ppm. Initial $^{87}Sr/^{86}Sr$, $^{143}Nd/^{144}Nd$ isotopic ratios cluster at 0.7038 and 0.51265. $^{206}Pb/^{204}Pb$, $^{207}Pb/^{204}Pb$ and $^{208}Pb/^{204}Pb$ values are 18, 15.5 and 38, respectively.

## Radio Towers

The Radio Towers vents erupted basanite (43.9 to 45.5% $SiO_2$). Other major element oxide wt % average values are $Al_2O_3$ = 13%, $Fe_2O_3$ = 12.5%, CaO = 10.5%. MgO and $TiO_2$ range from 9-12% and 2.2-2.6% respectively. Some trace element concentrations are Rb = 17-27 ppm, Zr = 250-300 ppm, Nb = 48-72 ppm and Sr ≅ 900 ppm. Ni concentrations cluster at 200 ppm while Cr values range from 350 to 500 ppm. Initial $^{87}Sr/^{86}Sr$, $^{143}Nd/^{144}Nd$ isotopic ratios have ranges of 0.7040 to 0.7043 and 0.51255 to 0.51262. $^{206}Pb/^{204}Pb$, $^{207}Pb/^{204}Pb$ and $^{208}Pb/^{204}Pb$ values are 18.35, 15.5 and 38.2, respectively.

## The Divide

At The Divide, basanite (43.3 to 45% $SiO_2$) was erupted from at least two vents. These basanites are slightly more primitive than other basanites in the Hurricane field because they have higher Mg# and compatible trace element concentrations. The average Mg# for these samples is 62.9 and Ni and Cr concentration ranges are 215-490 and 350-550 ppm. Some major element oxide wt % average values are $Al_2O_3$ = 11.5%, $Fe_2O_3$ = 13% and CaO = 11%. MgO and $TiO_2$ range from 10.5-14% and 2.4-2.8% respectively. Nb, Th and Sr concentration ranges are 60-70, 18-19.7 and 800-1000 ppm. No isotopic analyses were done on these samples.

## The Remnants

Low-silica basanite flows have an ultrabasic composition ($SiO_2$ wt. % of 41.5 to 42.1%). The low-silica basanites are quite primitive because compatible trace element average concentrations are high (Cr=607 and Ni=312 ppm) and Mg# averages 69.7. This group is depleted in Rb, K and Ti and heavily enriched in all other trace elements (Ba> 2080, Nb> 73, Th> 18 and Sr> 1180) (Figure 9). REE are also enriched (Figure 10). Isotopic ratio ranges are 0.7046 to 0.704759 for $^{87}Sr/^{86}Sr$ and 0.512568 to 0.512589 for $^{143}Nd/^{144}Nd$. Lead isotopic ratios average 18.64, 15.56 and 38.51 for $^{206}Pb/^{204}Pb$, $^{207}Pb/^{204}Pb$ and $^{208}Pb/^{204}Pb$ respectively and plot above the NHRL on lead ratio-ratio diagrams (Figure 12C).

## Volcano Mountain-Ivan's Knoll

Rocks erupted from vents at the Volcano Mountain-Ivan's Knoll complex form two groups: basanites (44-46% $SiO_2$) and alkali basalts (48.5-51.6% $SiO_2$). In general the chemistry of the groups do not overlap with the exception of one sample. The samples from the nearby Cinder Pits vent, however, are transitional from basanite to alkali basalt. The basanites have isotopic ratios similar to magma type A ($\varepsilon_{Nd}$ = -0.8 to -1.8 and $^{87}Sr/^{86}Sr$ = 0.7040 to 0.7042). Alkali basalts from Ivan's Knoll represent magma type C. The basanites are slightly more enriched in trace and LREE than the alkali basalts (Figure 20).

Table 3. Summary of average chemical analyses from each volcanic center in the Hurricane volcanic field. Oxide values in wt. %, trace element values in ppm.

| | Remnants (low-silica basanite) | The Divide (basanite) | Radio Towers (basanite) | Volcano Mtn. (basanite) | Cinder Pits (alk. basalt) | Ivan's Knoll (alk. basalt) | Grass Valley (alk. basalt) |
|---|---|---|---|---|---|---|---|
| magma | D | A | A | A | - | C | B |
| $SiO_2$ | 42.0 | 44.0 | 45.4 | 45.6 | 48.3 | 49.5 | 48.6 |
| $Al_2O_3$ | 12.0 | 11.3 | 13.0 | 12.8 | 15.0 | 16.0 | 16.0 |
| $Fe_2O_3$ | 11.7 | 13.1 | 12.6 | 12.8 | 11.1 | 11.1 | 10.1 |
| MgO | 13.6 | 12.5 | 10.4 | 10.6 | 7.7 | 7.1 | 8.0 |
| $TiO_2$ | 1.86 | 2.58 | 2.28 | 2.43 | 1.74 | 1.58 | 1.79 |
| Mg# | 69.7 | 65.3 | 62.6 | 62.1 | 58.1 | 54.8 | 61.0 |
| Rb | 12.2 | 19.0 | 20.0 | 17.3 | 13.5 | 12.1 | 12.1 |
| Ba | 2243 | 766 | 993 | 990 | 823 | 678 | 381 |
| Nb | 81.8 | 64.2 | 53.4 | 50.9 | 30.2 | 17.8 | 25.2 |
| Th | 18.65 | 7.50 | 7.01 | 6.49 | 5.02 | 2.03 | 3.39 |
| Sr | 1230 | 885 | 890 | 890 | 664 | 614 | 756 |
| Cr | 607 | 466 | 421 | 414 | 300 | 181 | 294 |
| Ni | 312 | 360 | 198 | 215 | 143 | 68 | 157 |

## Polygenetic Volcanism at Volcano Mountain

Cinder cones are traditionally thought to form over short periods of time (less than 100 years) and to have simple evolutionary histories involving a single magma source. Consequently cinder cones were classified as monocyclic (single event) and monogenetic (evolved from a single source) volcanoes. When eruptions from a single volcano occur over periods longer than the lifetime of the near surface magma chamber, the term "polycyclic" is used. Polycyclic refers to eruptions that occur over a period of time but their magmas are derived from a single source and are probably related at depth by fractional crystallization and/or a melting process. Polycyclic centers may be monogenetic or polygenetic. The term "polygenetic" is often used synonymously with polycyclic however, recent work (e.g., Bradshaw and Smith, 1994) shows cases where magmas erupted at one center are derived from more than one source. In this discussion polygenetic is used to describe a volcano that erupts magmas from different sources.

Most volcanoes in the Hurricane volcanic field are monogenetic. The Cinder Pits cones may be polygenetic based on chemical data (major oxide and trace element). Trace element data (Ba/Nb = 18.9 to 40.5) suggest the possibility that two magma types erupted

from this center. Isotopic data of samples from the Cinder Pits cones are needed to verify this conclusion. The Volcano Mountain cone complex is the only documented example of a polygenetic center in the Hurricane field (see below).

The Volcano Mountain complex contains of several overlapping cones. Volcano Mountain is the youngest cinder cone in the complex. Other older cones include Ivan's Knoll and possibly several now buried centers directly south of Volcano Mountain. Volcanism in the Volcano Mountain complex may have occurred over a period of 100 t.y. Lava flows of at least two and possibly three of Hamblin's time stages are associated with this complex. A flow that may have erupted from Ivan's Knoll was dated at 352 ± 45 ka and a flow from the flank of Volcano Mountain is 258 ± 24 ka (both dates from this work and by the $^{40}Ar/^{39}Ar$ technique).

Volcano Mountain is made entirely of basanite, magma type A ($^{87}Sr/^{86}Sr$ = 0.7041 to 0.7042, $\varepsilon_{Nd}$ = 0 to -2 and $^{206}Pb/^{204}Pb$ = 18.16 to 18.34). Alkali basalt erupted from Ivan's Knoll is magma type C ($^{87}Sr/^{86}Sr$ = 0.7046, $\varepsilon_{Nd}$ = -6 and $^{206}Pb/^{204}Pb$ = 17.60). As demonstrated earlier, magma type A is not related by fractional crystallization or assimilation to magma type C (Figures 16 and 17). Mixing between the two magma types does not seem to be possible because no rocks with chemistry or isotope values intermediate between basanites and alkali basalts occur at this complex. Independent magma melts, therefore, generated in the mantle followed the same pathway to the surface and are responsible for the compositional variation of rocks erupted from Volcano Mountain/Ivan's Knoll complex. This chemical and isotopic evidence coupled with the fact that volcanism at the complex occurred over a relatively long time period (100 t.y.) indicate that the complex is polygenetic and polycyclic.

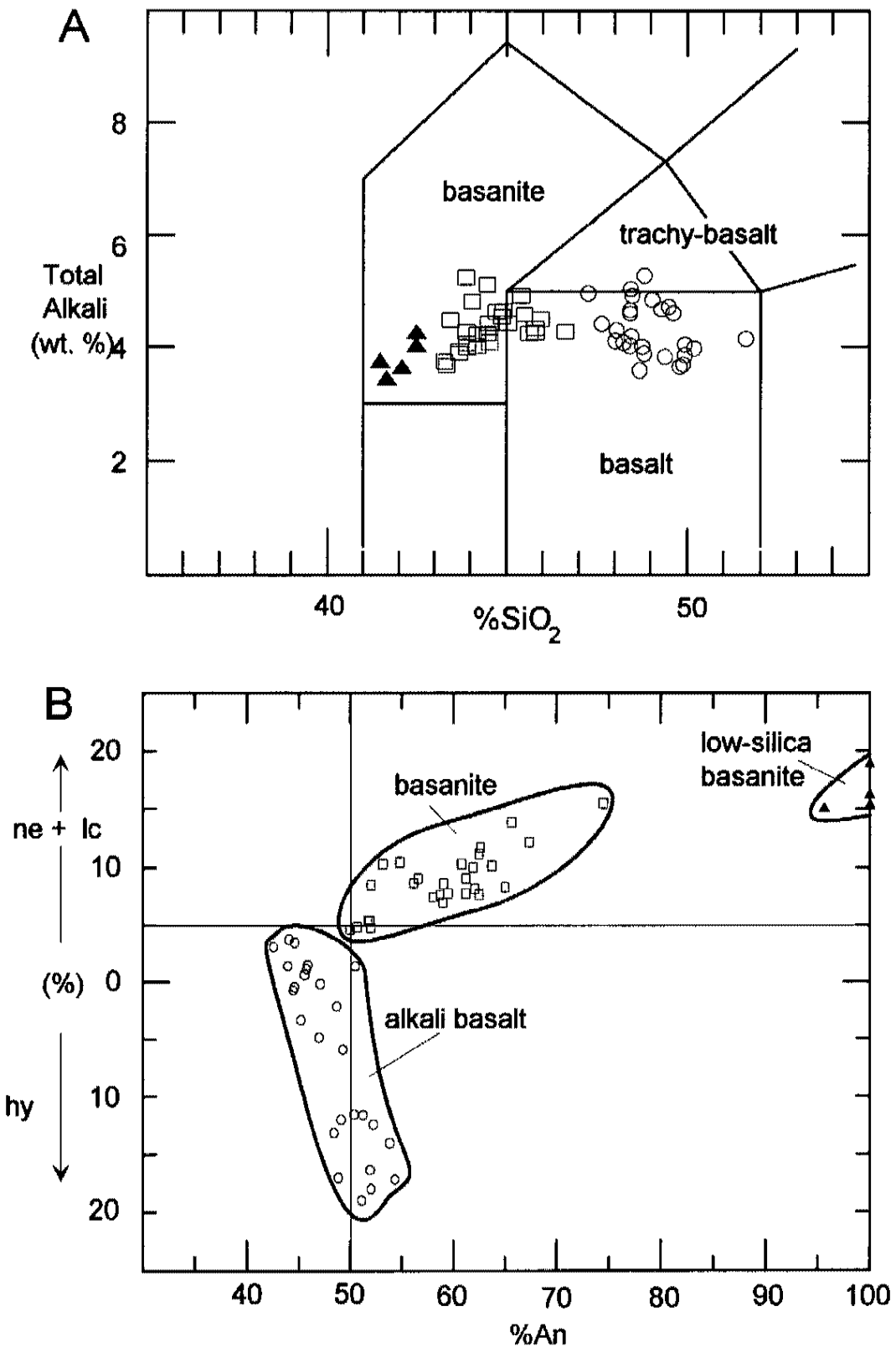


Figure 7. Rock classification diagrams. (A) Total alkali vs. silica diagram (after La Bas et al., 1986). (B) Normative plagioclase vs. normative nepheline + leucite and hypersthene (field boundaries after Best and Brimhall, 1974). ▲ - low-silica basanite; □- basanite; o - alkali basalts.

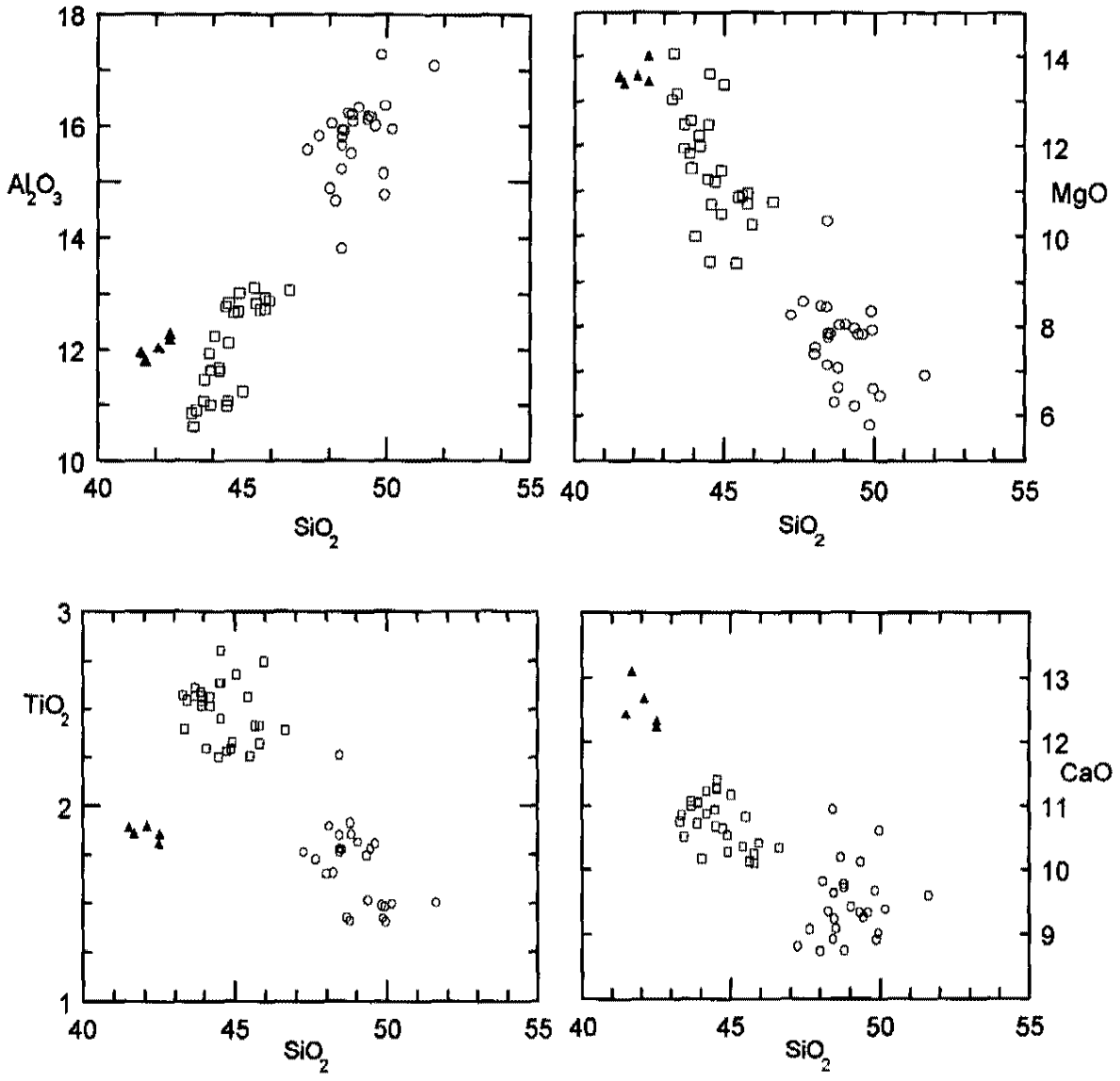


Figure 8. SiO2 (wt. %) vs. selected wt. % of major oxides. ▲ - alkali basanite; □- basanite; o - alkali basalts. MgO, TiO2 and CaO decrease and Al2O3 increases with increasing silica content.

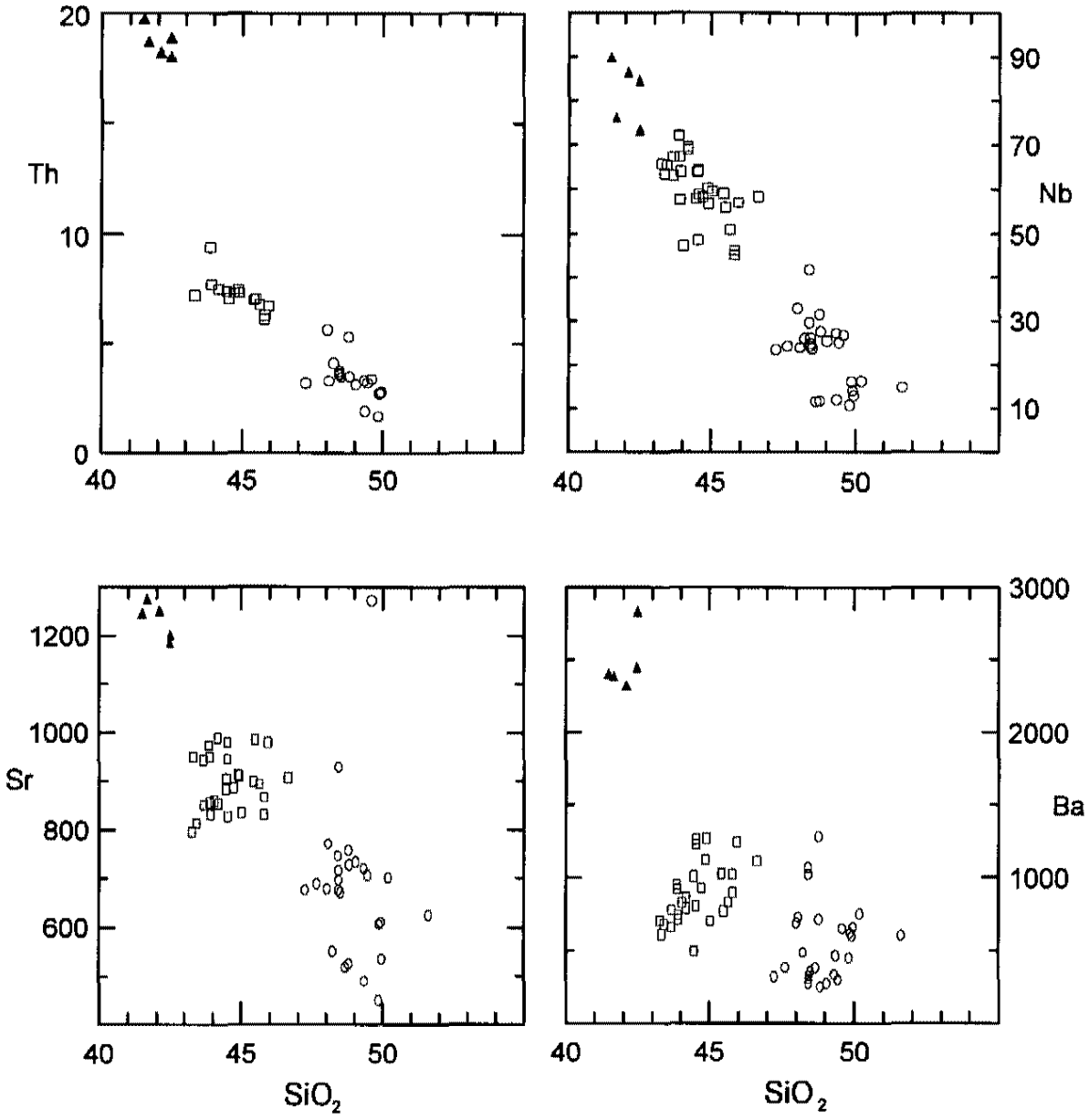


Figure 9. SiO2 (wt. %) vs. selected incompatible trace element concentrations (ppm). Concentrations of trace elements decrease with increasing silica.
▲ - alkali basanite; □- basanite; o - alkali basalts.

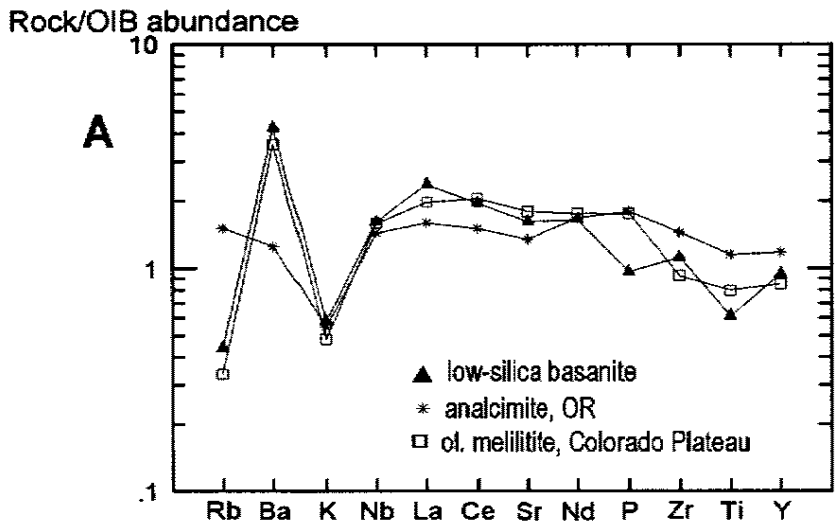


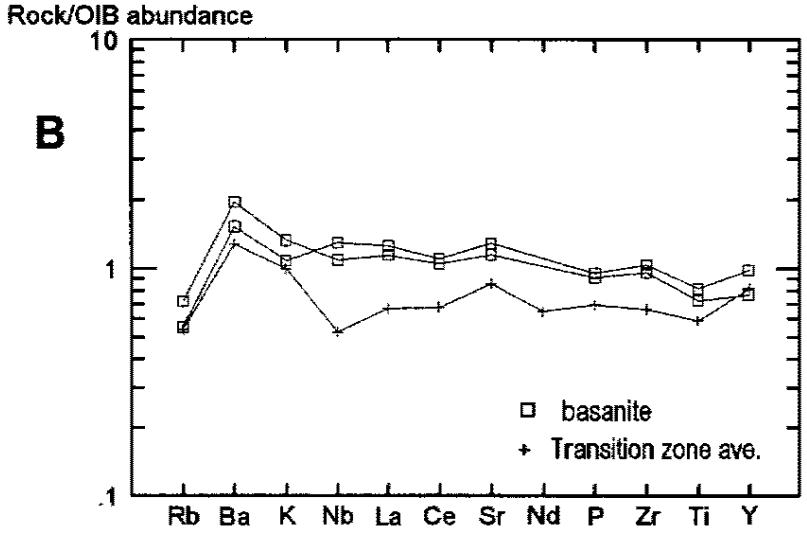


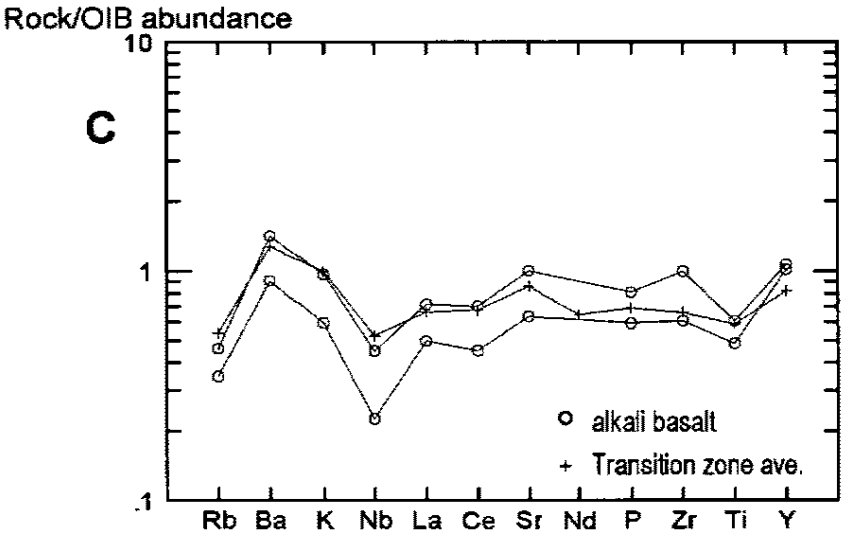


Figure 10. Trace elements normalized to OIB abundance values from Fitton et al. (1991). (A) A selected low-silica basanite plots close to a olivine melilitite (Fitton et al., 1991) from the Colorado Plateau. Note Rb and K depletion and Ba and Nb enrichment. (B) Selected basanites show a pattern of enrichment of Nb and slight enrichment in LREE compared to the average of transition zone <5 Ma basalts (Fitton et al., 1991). (C) Selected alkali basalts display a pattern very similar to the Fitton et al. (1991) average of transition zone <5 Ma basalts. Note the trough at Nb.

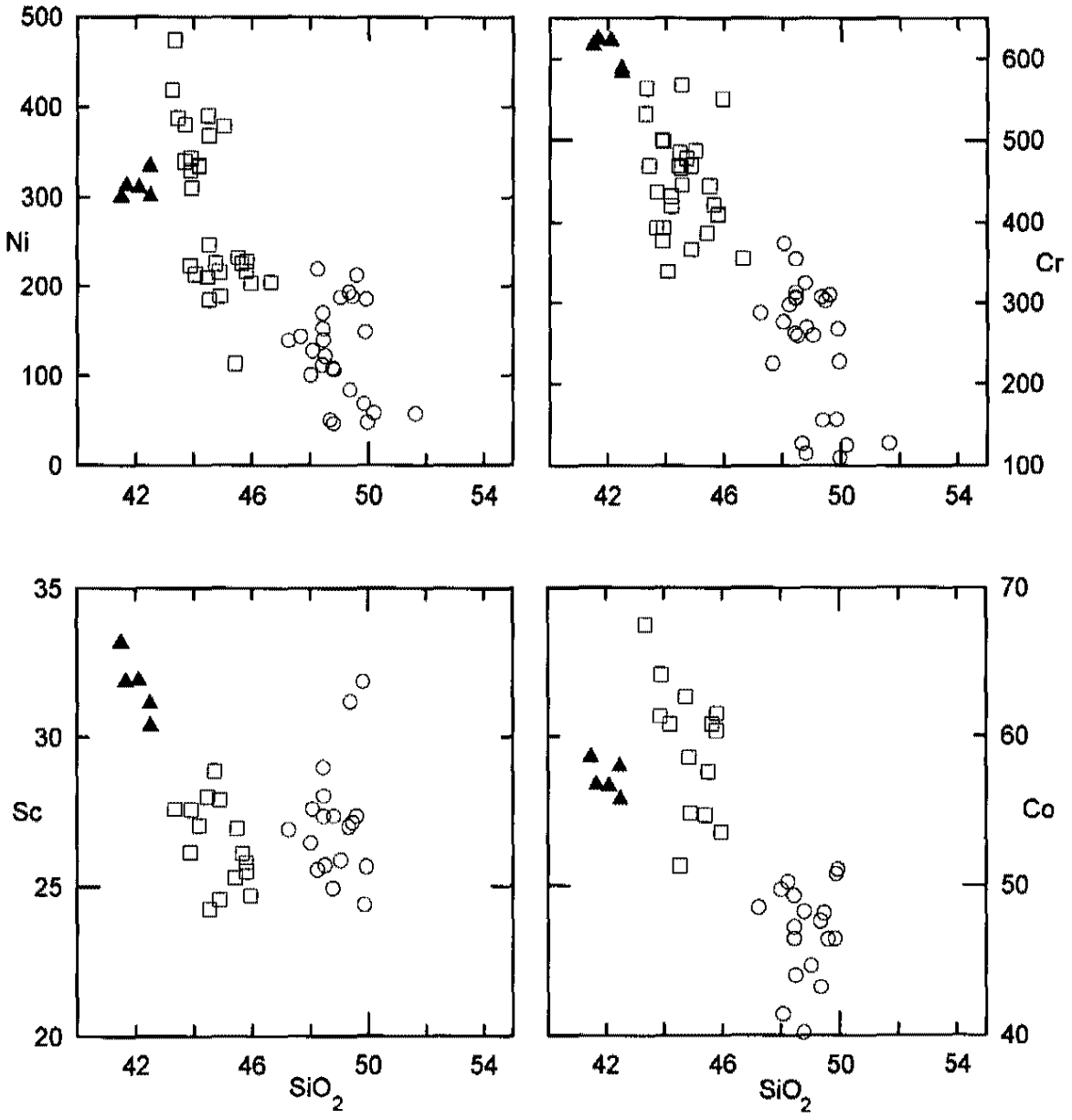


Figure 11. $SiO_2$ (wt. %) vs. compatible trace elements (ppm). Concentrations of trace elements decrease with increasing silica.
▲ - alkali basanite; □- basanite; o - alkali basalts.

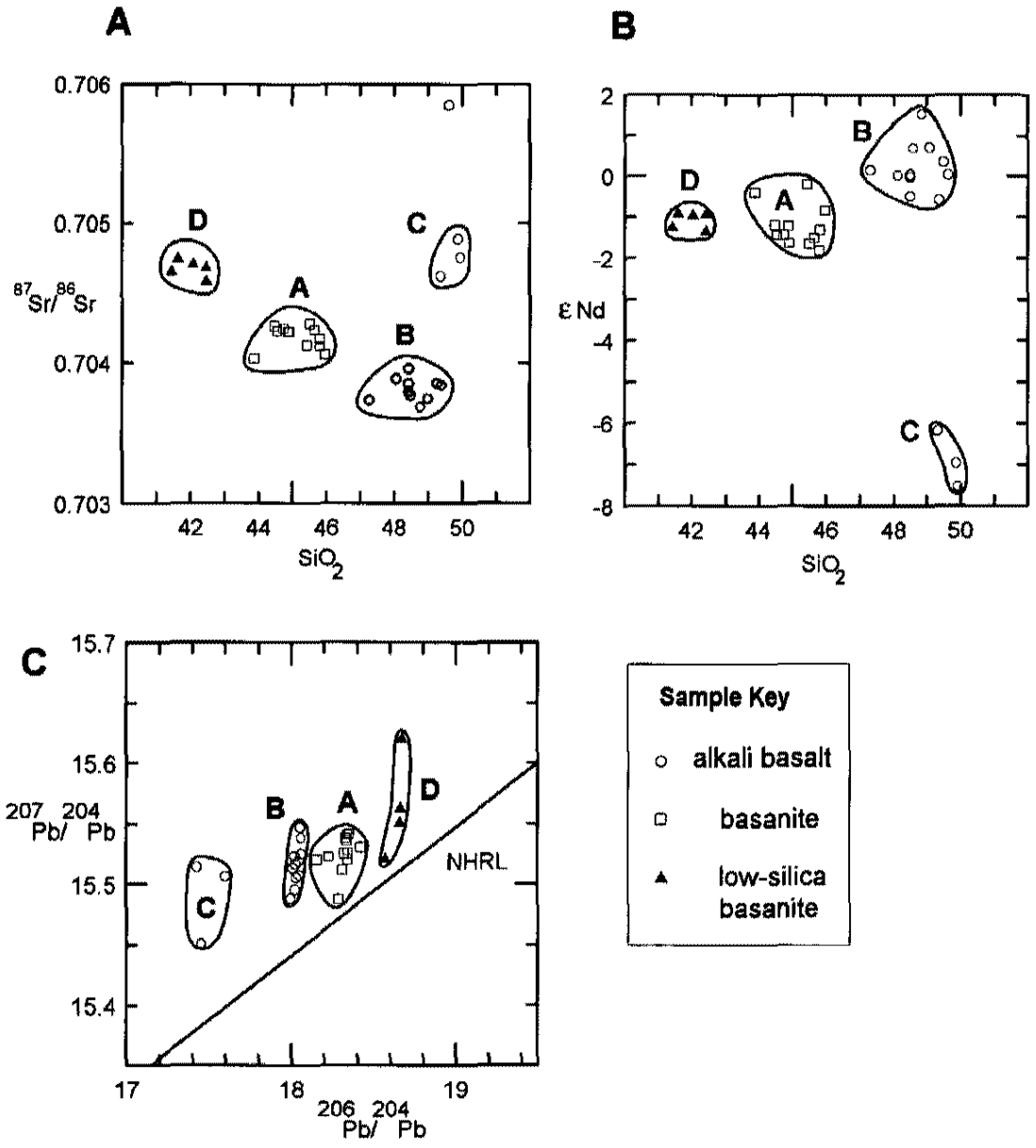


Figure 12. Isotopic plots of lavas in the Hurricane volcanic field. (A) Silica versus initial Sr. (B) Silica versus epsilon Nd. (C) 206Pb/204Pb versus 207Pb/204Pb.

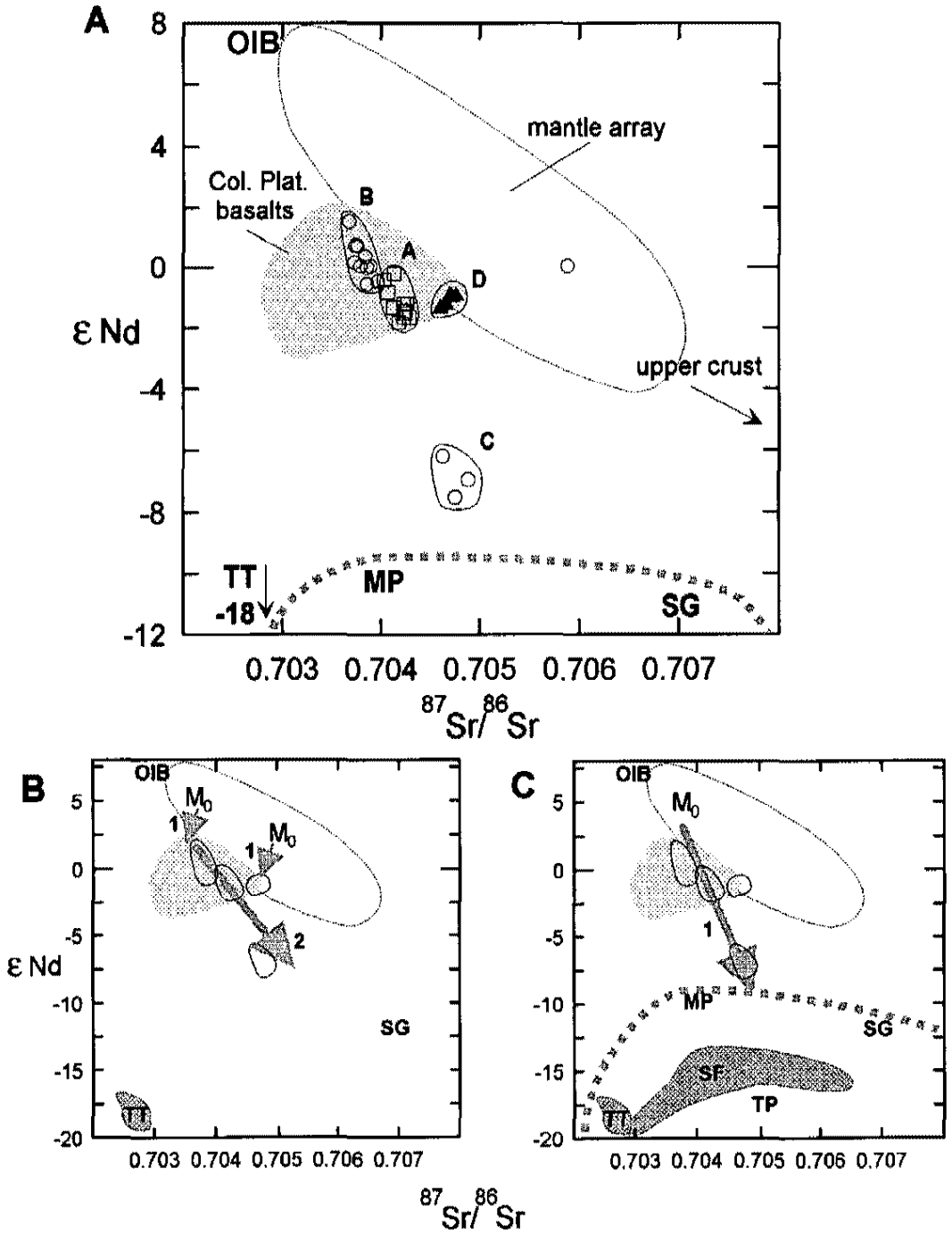


Figure 13. (A) Epsilon Nd vs. initial Sr diagram. Hurricane magma types plot below the mantle array with Colorado Plateau basalts and trend toward a range of lower crustal components, enclosed by dashed line. **TT**, Tule Tank, AZ (Nealey and Unruh, 1991; **TP**, Taos Plateau, NM (Perry et al., 1987); **MP**, Markagunt Plateau, UT and **SG**, St. George basin, UT (Unruh et al., 1994); **SF**, San Francisco volcanic field, AZ (Arculus and Gust, 1995). (B) The model shows isotope variation produced by two steps of contamination from a (1) Tule Tank component (TT) then (2) the proposed lower crustal component under the St. George basin (SG) of Unruh et al. (1994). (C) An alternative single step contamination model. Initial magmas ($M_0$) are contaminated by some lower crustal component as they rise to the surface.

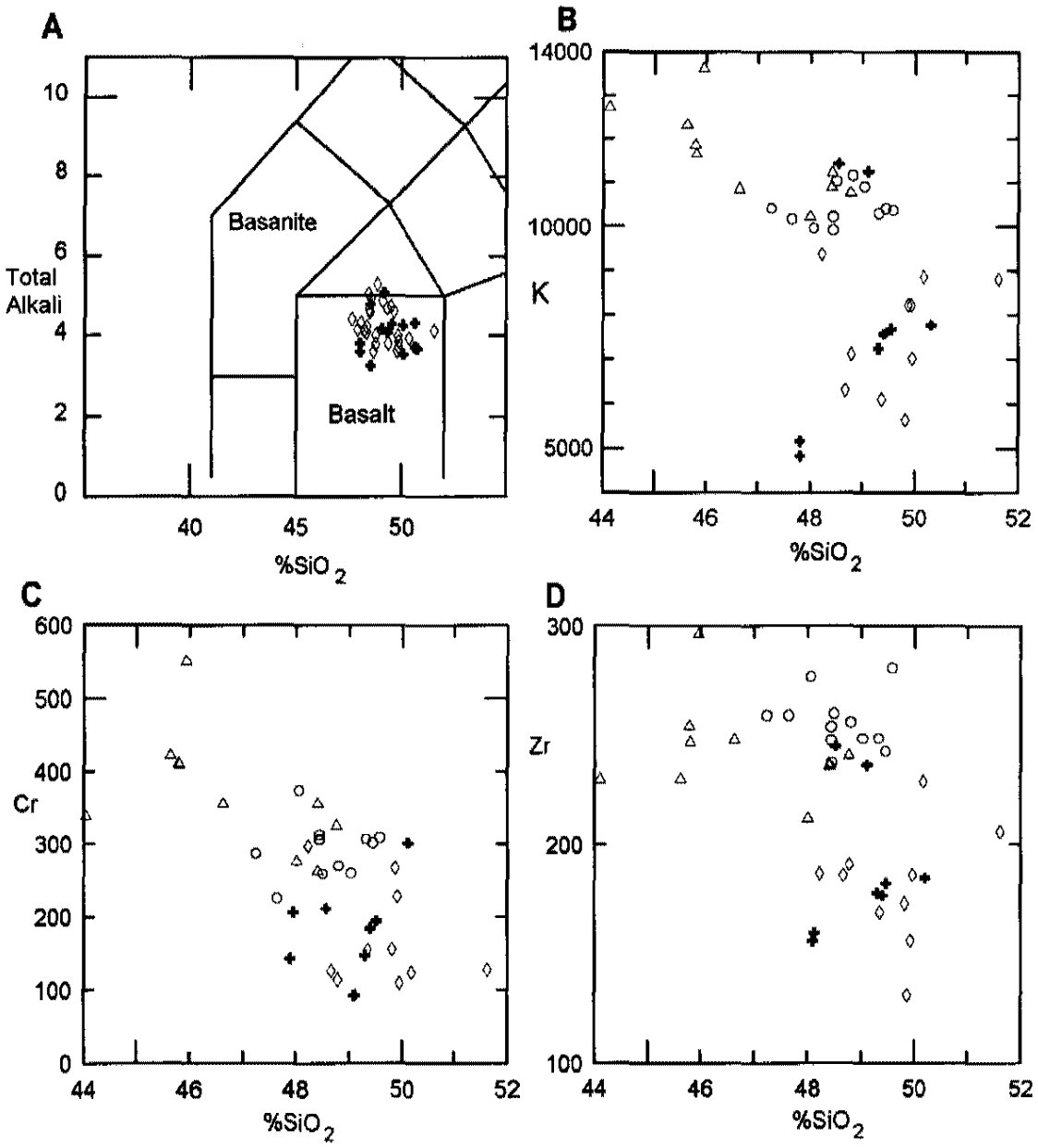


Figure 14. Chemical diagrams of Hurricane and Toquerville basalts. Similarities between Hurricane magma type C alkali basalts and Toquerville basalts (Schramm, 1994) are shown. (A) TAS diagram (after Le Bas et al., 1986); all Hurricane alkali basalts are ♦, Toquerville basalts are ✚. (B) (C) (D) Hurricane samples are; ▲- basanites (magma type A), o -magma type B alkali basalt, ♦ - magma type C alkali basalt; ✚ - Toquerville basalts. Magma type C alkali basalts from Ivan's Knoll and basalts from Toquerville have similar chemical features.

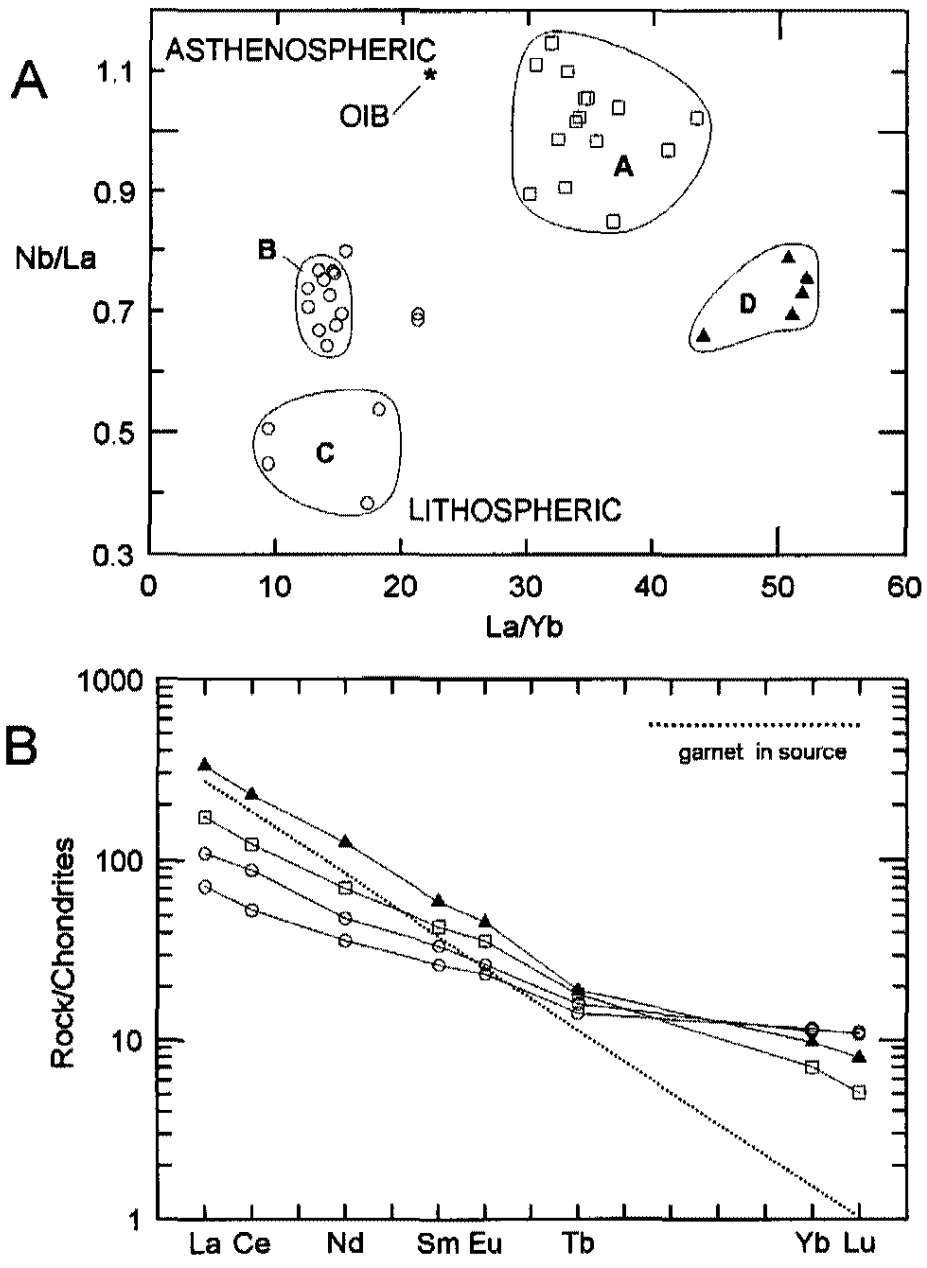


Figure 15. Ratio-ratio and rock normalized to chondrite plots. (A) La/Yb vs. Nb/La. Hurricane isotope types are A, basanite; B, Grass Valley alkali basalt; C, Ivan's Knoll alkali basalt; D, low-silica basanite, OIB is oceanic island basalt normalized abundance (from Fitton et al., 1991). Nb concentrations control the variation in Nb/La values. Rocks derived from an undepleted asthenospheric source will have high values of Nb/La. (B) Rare-earth element concentrations normalized to chrondrite. Extremely high concentrations of light REE suggest very small degrees of partial melting or a light REE enriched source. Very low concentrations of heavy REE would indicate the presence of garnet in the source (dotted line). Symbols are the same as in Figure 12.

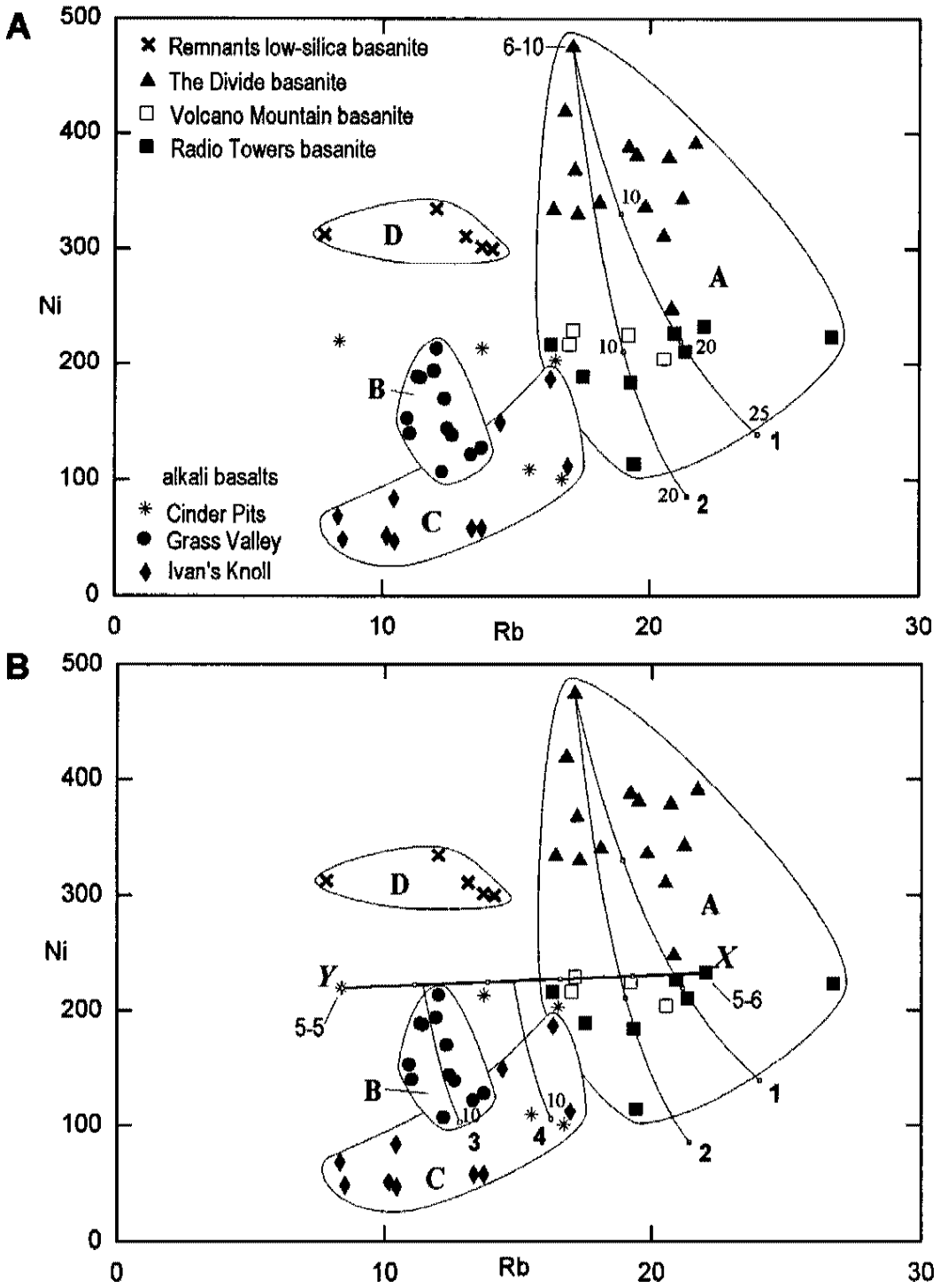


Figure 16. Rb vs. Ni plots; fields of magma types A (basanite), B and C (alkali basalt) and D (low-silica basanite) are outlined. (A) Fractional crystallization from sample 6-10 models; line 1 is cpx:ol:hb (55:35:10) to 25%, line 2 is pure olivine to 20%. These models only explain variation for type A (basanites). (B) Three stage model FC-mixing model explains types A and B magmas and Cinder Pits samples. Stage 1 is FC along line 1 or 2, stage 2 is mixing between points X and Y (samples 5-6 and 5-5), stage 3 is 10% olivine FC along lines 3 and 4. Magma types C and D (Ivan's Knoll alkali basalts and low-silica basanites) are not explained by this model and are interpreted as independent melts.

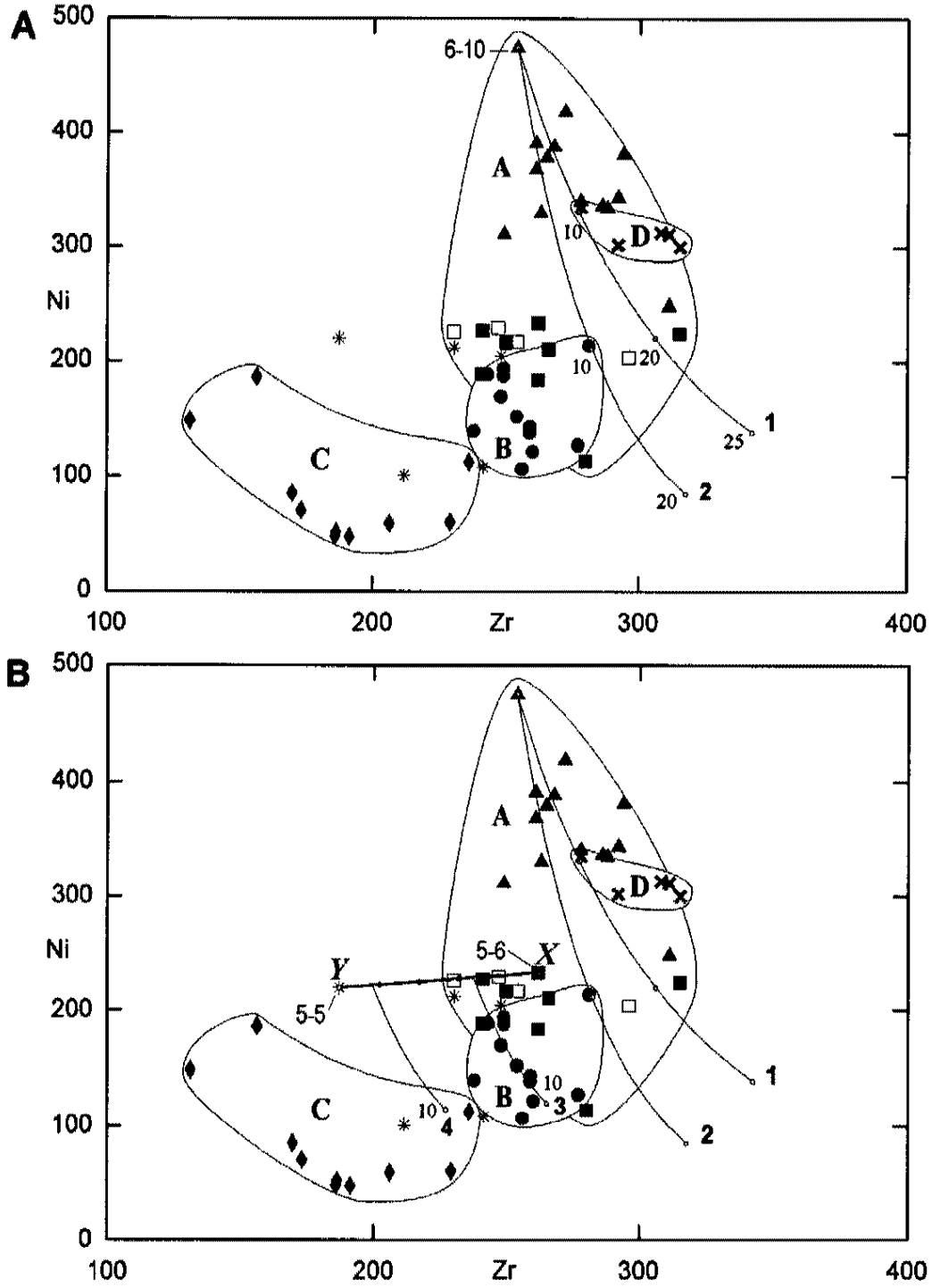


Figure 17. Zr vs. Ni plots, magma types A (basanite), B and C (alkali basalt) and D (low-silica basanite) are enclosed. (A) Fractional crystallization from sample 6-10 models; line 1 is cpx:ol:hb (55:35:10) to 25%, line 2 is pure olivine to 20%. These models only explain variation for type A (basanites). (B) Three stage model FC-mixing model explains types A and B magmas and Cinder Pits samples. Stage 1 is FC along line 1 or 2, stage 2 is mixing between points X and Y (samples 5-6 and 5-5), stage 3 is 10% olivine FC along lines 3 and 4. Magma types C and D (Ivan's Knoll alkali basalts and low-silica basanites) are not explained by this model and are interpreted as independent melts. Symbols are the same as in Figure 16.

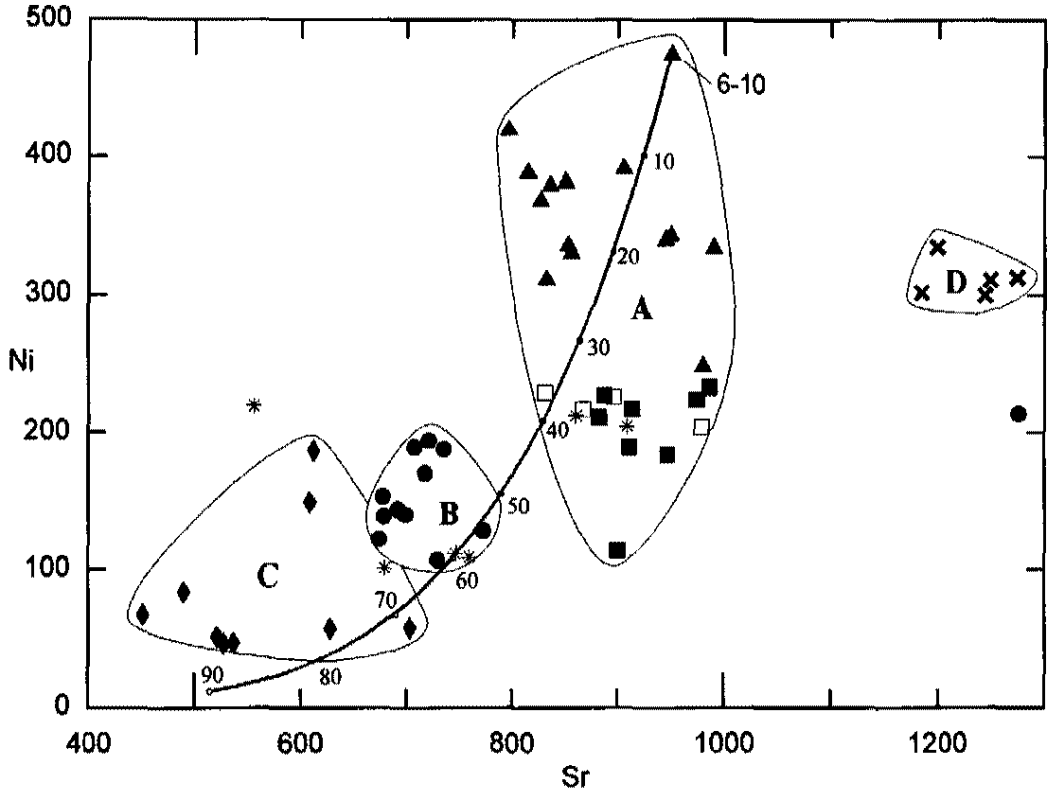


Figure 18. Sr vs. Ni plot, symbols and magma types as in Figure 16. The line models olivine:plagioclase fractionation (3:7) to 90% beginning from sample 6-10, a type A basanite from The Divide. This model requires an unreasonable amount of FC and does not include type D magma.

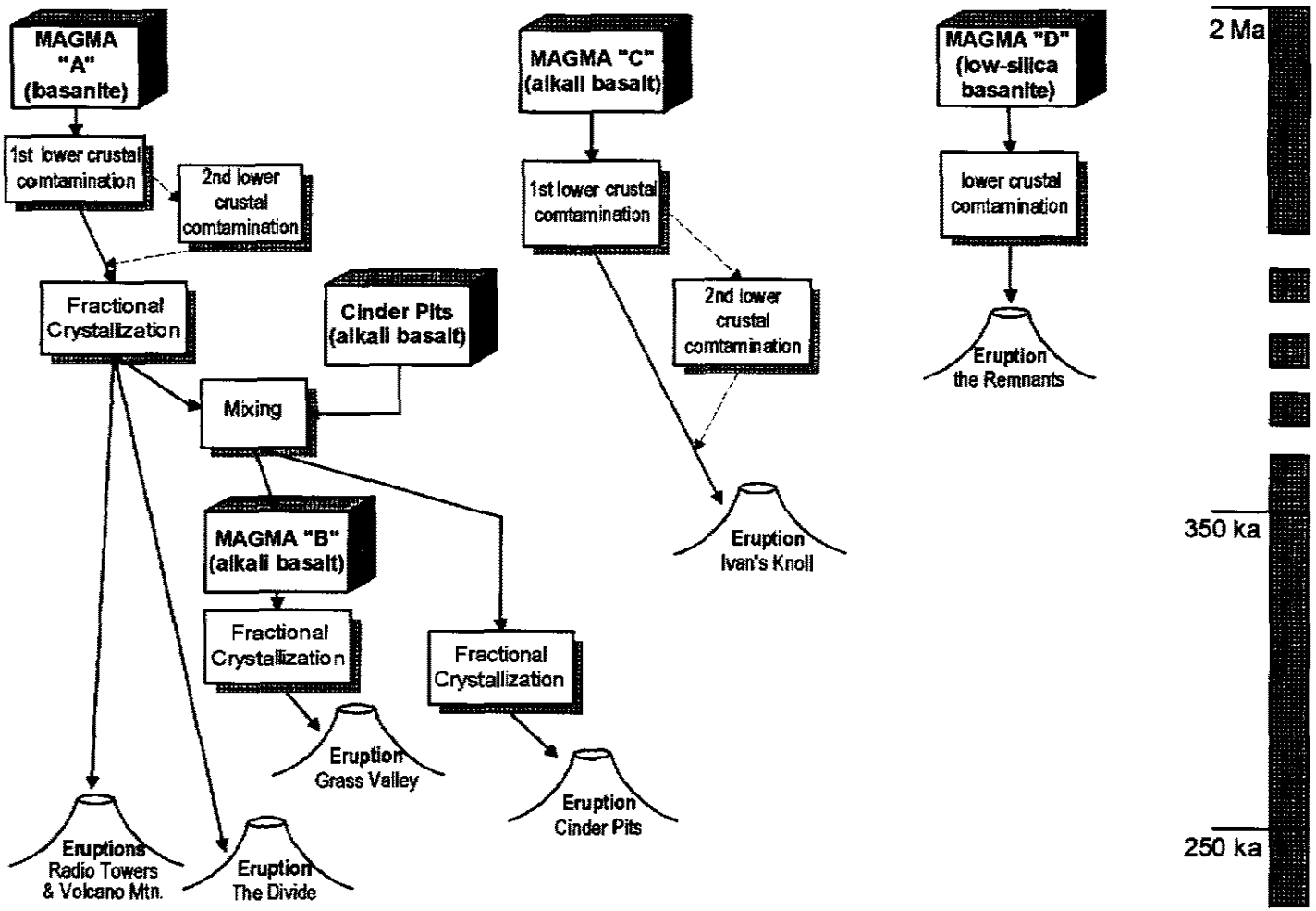


Figure 19. Magma genesis flowchart. Time line refers to eruptions only.

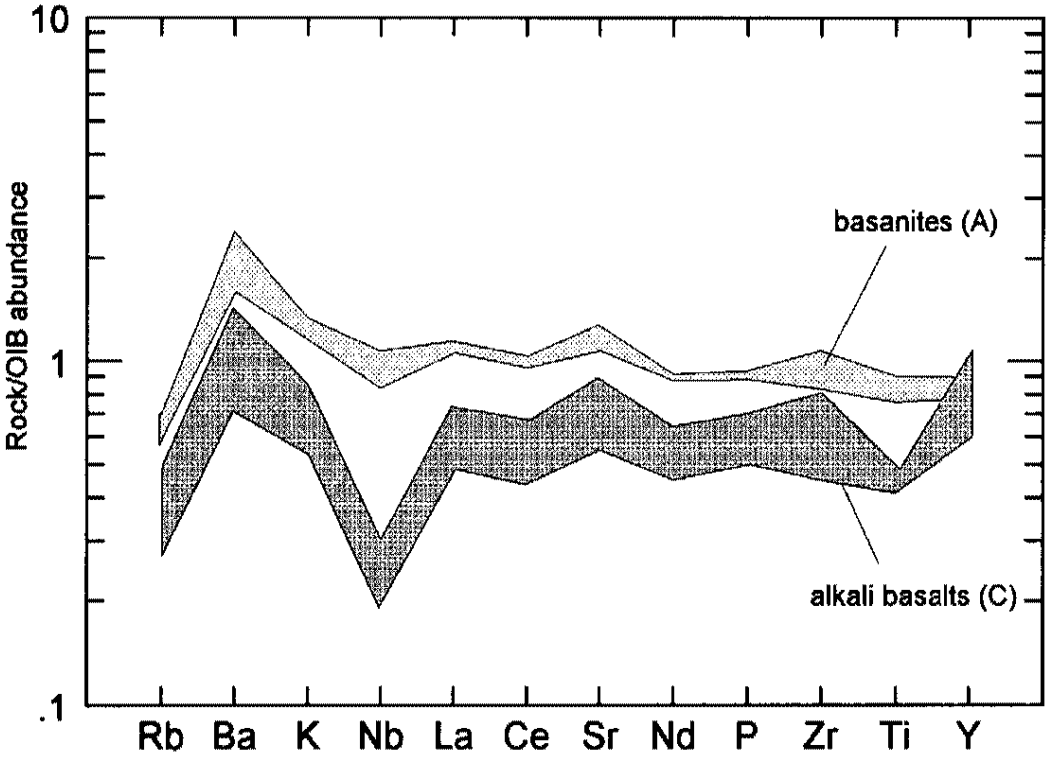


Figure 20. Volcano Mountain/Ivan's Knoll basalts normalized to OIB abundance from Fitton et al. (1991). Volcano Mountain basanites (magma type A) are slightly more enriched in trace elements and more OIB-like compared to the alkali basalts from Ivan's Knoll (magma type C). Also, the alkali basalts show negative anomalies at Nb and Ti and a positive anomaly at Y which suggest the magma sourceis in the lithospheric mantle.

# CHAPTER 4

## REGIONAL COMPARISON

The Hurricane volcanic field is in the Transition Zone between the Colorado Plateau and the Basin-and-Range provinces. Geochemistry of lavas from this field provides information on the composition of the mantle beneath the Transition Zone (see "The Mantle Source" section, chapter 3). In this section, the nature of the mantle beneath the Hurricane volcanic field is compared to adjacent physiographic provinces (Basin-and-Range and Colorado Plateau) and other areas of the Transition Zone. The Transition Zone separates the Basin-and-Range from the Colorado Plateau and comprises the eastern margin of the Great Basin and the northern margin of the southern Basin-and-Range. Mafic volcanism has occurred in each of these provinces since 25 Ma but this comparison will concentrate on mafic lavas produced in the last 5 m.y.

In this discussion all trace elements will be normalized to OIB abundance values of Fitton et al. (1991). Their database for OIB consists of nearly 900 analyses from each major oceanic island group and is thought to be representative of OIB compositions worldwide. OIB represents magma produced in the asthenosphere. Magmas with compositions different than OIB can not have been produced entirely from an OIB source and must have interacted with the lithosphere. Lower crustal components are typically thought to be the source of the lithospheric contamination. These lower crustal

components are enriched in Ba and sometimes Sr and depleted in Nb and Ti, and have low $^{143}Nd/^{144}Nd$ values (see section the "Crustal Contamination" in chapter 3).

### Hurricane Volcanic Field and the Basin-and-Range

The Basin-and-Range province is a region of fault bounded mountain ranges and intervening basins that developed in response to roughly east-west extension. As a result of the extension, the lithosphere thinned so that the asthenosphere is relatively close to the surface (~30 km) (Allmendinger et al., 1987). In the most extended parts of the Basin-and-Range, magmas have compositions very similar to OIB (Fitton et al., 1991). The average Basin-and-Range composition for volcanic rocks less than 5 Ma (Fitton et al., 1991) on a spider diagram normalized to OIB abundance (Figure 21) has a relatively horizontal pattern with values close to one (1). Figure 21A shows that trace elements from La to Y for Hurricane alkali basalts are similar to the Basin-and-Range average with samples from Ivan's Knoll slightly more depleted than Grass Valley samples. The Hurricane alkali basalts are similar to OIB except for depletion in Rb, K and Nb. Hurricane basanites are generally enriched in REE and especially enriched in Ba and depleted in Rb (Figure 21B). The low-silica basanites show greater enrichment and depletion for the same elements plus a depletion in K compared to the average OIB. Basaltic rocks erupted in the Great Basin have isotopic signatures ($\varepsilon_{Nd} \geq +4$, $^{87}Sr/^{86}Sr \leq 0.7038$; Farmer et al., 1989; Glazner and Farmer, 1992) that are asthenospheric. Hurricane basalts have lower $\varepsilon_{Nd}$ values (-7.5 to +1.6) and higher $^{87}Sr/^{86}Sr$ (0.70368 to 0.70488 ) than Great Basin OIB basalts.

### Hurricane Volcanic Field and the Colorado Plateau

Tertiary volcanism from the interior of the Colorado Plateau is represented by an olivine melilitite plug that forms Woodruff Butte, Arizona and nephelinite lavas and plugs from Hopi Buttes, Arizona (Fitton et al., 1991). Rocks from both of these areas are

somewhat enriched in elements from Nb to P and strongly enriched in Ba compared to OIB (Figure 22). Melilitites from Woodruff Butte are strongly depleted in Rb and K. Patterns of element abundance for Hurricane low-silica basanite and Woodruff Butte are very similar from Rb to Nd (Figure 22A). Hurricane basanite produces a pattern close to that of the nephelinite from Hopi Buttes except for Rb which is more highly depleted in the basanites (Figure 21A). Alkali basalts from Hurricane are depleted in all elements except for Rb when compared to the Colorado Plateau rocks (Figure 22B). Isotopically, basalts from the Colorado Plateau have variable $^{87}Sr/^{86}Sr$ of 0.7032 to 0.7071 and $\varepsilon_{Nd}$ values of -2.6 to +3.7 (Alibert et al., 1986). Rocks from Hurricane are within these ranges except for the type C alkali basalts which have lower $\varepsilon_{Nd}$ values (-6.2 to -7.5).

**Hurricane Volcanic Field and the Transition Zone**

Transition Zone mafic volcanic rocks less than 5 Ma (Fitton et al., 1991) display a pattern that is very much like Basin-and-Range OIB rocks of the same age except for lower Rb and Nb and higher Ba (Figure 23). Both the low-silica basanites and basanites from Hurricane have patterns that show enrichment of trace elements, except for Rb and K, compared to the average Transition Zone basalt (Figure 23A). The typical Transition Zone basalt is low in Nb but this anomaly is missing from the spider patterns of the Hurricane basanite and low-silica basanite. Hurricane alkali basalts produce patterns similar to other Transition Zone rocks (Figure 23B) except for lower Rb, Nb and Ti and higher Ba, Sr and Y. Basalts from the Transition Zone in the western Grand Canyon region have $^{87}Sr/^{86}Sr$ of 0.70344 to 0.70505 and $\varepsilon_{Nd}$ values from +5.4 to -7.1 (Wenrich et al., 1995). Basalts from Hurricane fall within these ranges except for one magma type C alkali basalt sample which has an $\varepsilon_{Nd} = -7.5$.

## Summary of Comparison

Rocks from the Hurricane volcanic field display trace element abundance patterns that have similarities to mafic volcanic rocks in the Basin-and-Range, Colorado Plateau and the Transition Zone. All Hurricane rock types have isotopic values that are like those of other Transition Zone basalts in that they have lower $\varepsilon_{Nd}$ values and higher $^{87}Sr/^{86}Sr$ than basalts from the Great Basin. Hurricane low-silica basanite, basanite and type B alkali basalts are like basalts found on the Colorado Plateau. The oldest rocks in the Hurricane volcanic field, the low-silica basanite, are similar in element abundance to Woodruff Butte, a volcanic plug on the Colorado Plateau. Alkali basalts in the Hurricane field are similar to other young, mafic volcanic rocks in the Transition Zone. The youngest rocks at Hurricane are more OIB like and similar to many young (<5 Ma) volcanic rocks of the Basin-and-Range. An important point is that mafic volcanic rocks in the Hurricane field become more OIB like with time.

## Discussion

Two points are brought out by this regional comparison of young, mafic volcanic rocks from the Basin-and-Range, Colorado Plateau and Transition Zone. (1) Basalts become more OIB-like with distance from the Colorado Plateau. (2) In each province, basalts become more OIB-like with time.

In a transect from the Colorado Plateau across the Transition Zone to the Basin-and-Range, the magnitude of lower crustal contamination in OIB magmas correlates directly with the lithospheric thickness in each tectonic province. The Fortification Hill volcanic field described by Feuerbach et al. (1993) lies in the northern Colorado River extensional corridor, an area of thin lithosphere in the Basin-and-Range. Isotopic values for the alkali basalts in this field lie within the mantle array between OIB and lithospheric mantle end-members (Figure 24). Isotopic ratios for alkali basalts in the Grand Wash

Trough (Cole, 1989) near the boundary between the Transition Zone and the Basin-and-Range have lower $\varepsilon_{Nd}$ values than the basalts of the Fortification Hill field and their data array has a steeper slope on the initial Sr vs. $\varepsilon_{Nd}$ diagram. Rocks from the Hurricane volcanic field in the Transition Zone have isotopic values that plot to the lower left of the mantle array with lower $\varepsilon_{Nd}$ and initial Sr. The trends defined by the three fields discussed above pivot at the OIB end-point and swing from the mantle array (Basin-and-Range) toward lower $\varepsilon_{Nd}$ and initial Sr values (Colorado Plateau and Transition Zone). The trend toward lower $\varepsilon_{Nd}$ and initial Sr is directly related to the change in the lithosphere from the Basin-and-Range (thin) to the Colorado Plateau (thick). Allmendinger et al. (1987) showed in a study of seismic refraction profiles that the thickness of the lithosphere thins from 40 to 25 km from the Colorado Plateau to the Great Basin. This profile agrees with modeling by Keen (1985; cited by Fitton et al., 1988) that results in the lithosphere thinning from 35 to 23 km at the margins of an extensional terrane. This change in lithospheric thickness is produced after 16 Ma of extension by a side-driven stretching model at a rate of 1 cm/yr over an initial horizontal distance of 240 km. These conclusions agree with the work of Fitton et al. (1991) and their conclusion that magmas generated farther away from the location of advanced extension (Basin-and-Range) undergo more contamination by a lithospheric component because magmas must rise through a thicker lithosphere.

Figure 24 also shows that as rocks in each area become younger they become more like OIB. This trend can be demonstrated by using the geochemical data and the relative time scale from the Hurricane volcanic field. Overall, Hurricane volcanic rocks are similar to OIB in their concentrations of trace elements except for enrichment in Ba and depletion in Rb, K and Nb. The differences in the relative concentrations of these elements (Ba, Rb, K and Nb) with respect to OIB are significant because the degree of Ba enrichment and Rb, K and Nb depletion (as depicted by La/Ba and La/Nb ratios) may be a measure of the

degree of lithospheric contamination. Lavas in the Hurricane volcanic field became more OIB-like with time. Low-silica basanites (magma type D) and alkali basalts (magma type C) are Stage IIa and IIb flows respectively, the oldest in the field. Both of these magma types plot outside of the OIB array on a La/Ba vs. La/Nb diagram (Figure 25). Type B alkali basalts are Stage III and type A basanites are Stages IVa and IVb are from some of the youngest rocks in the field. These magma types (basanites and other alkali basalts) plot partially within the OIB array. The same trend toward OIB composition with time is shown on Figure 24 for Fortification Hill and Grand Wash Trough mafic rocks. Fitton et al. (1991) describe a similar pattern when comparing mafic volcanic rocks greater than and less than 5 Ma from the southwestern United States (Figure 26, Figure 8 from Fitton et al., 1991). They concluded that this pattern is consistent with the theory of erosion and removal of the lithosphere by a mantle plume. The erosion of the lithosphere is most pronounced in areas of advanced extension (i.e., the Basin-and-Range) where OIB-like magma has erupted in the last 5 m.y.

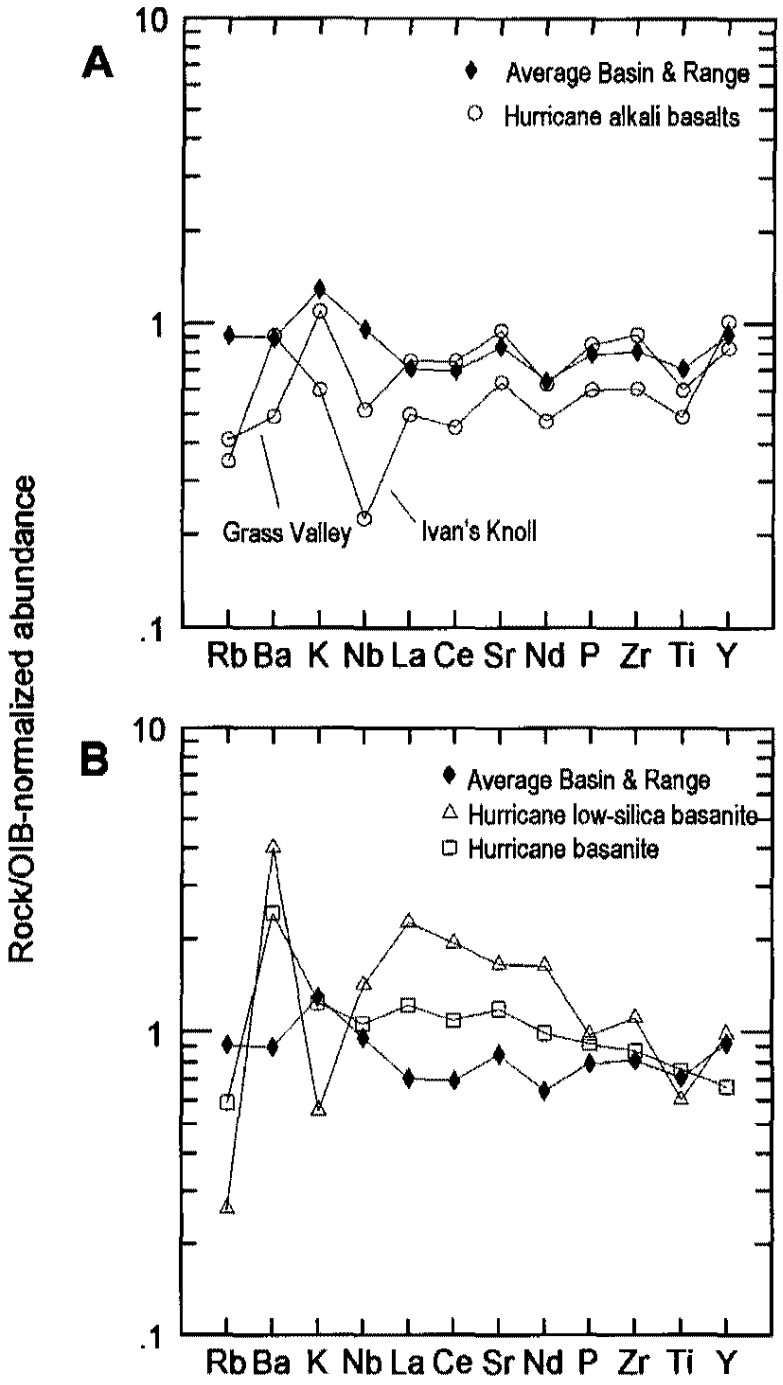


Figure 21. Average Basin & Range basalts <5 Ma (Fitton et al., 1991) compared to (A) Hurricane alkali basalts and (B) Hurricane basanite and low-silica basanite. The average Basin & Range basalt is OIB-like. Hurricane alkali basalts are similar to the average Basin & Range basalt but show depletion in Rb, K and Nb. Hurricane basanites and low-silica basanites are enriched in REE and Ba and depleted in Rb. Low-silica basanites are also depleted in K.

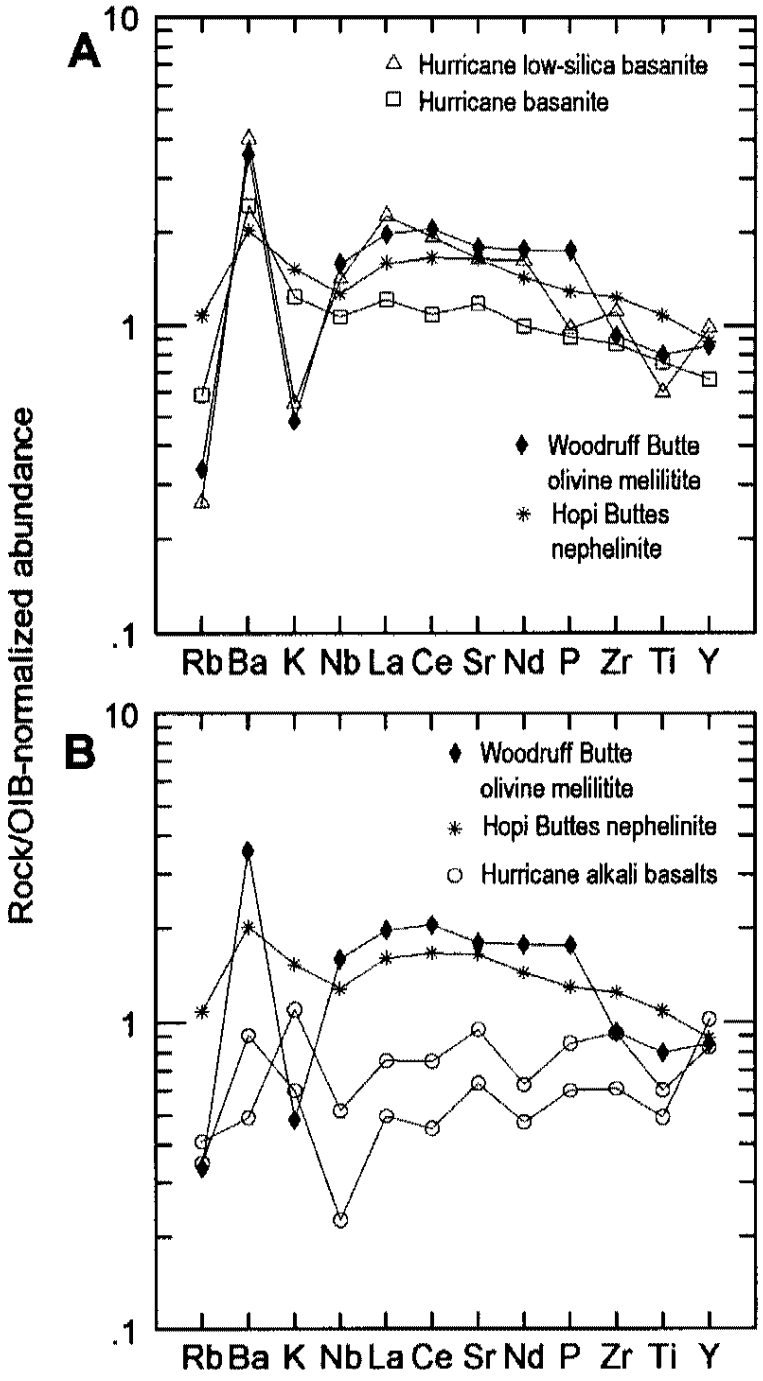


Figure 22. Two Colorado Plateau basalts compared to Hurricane basalts. An olivine melilitite from Woodruff Butte, Arizona and nephelinite from Hopi Buttes on the Colorado Plateau are compared to (A) Hurricane basanite and low-silica basanite and (B) Hurricane alkali basalts. Hurricane low-silica basanites are similar to the olivine melilitite; Hurricane basanites are similar to the nephelinite except for low Rb. Hurricane alkali basalts are depleted in all elements except Rb compared to the two Colorado Plateau rocks.

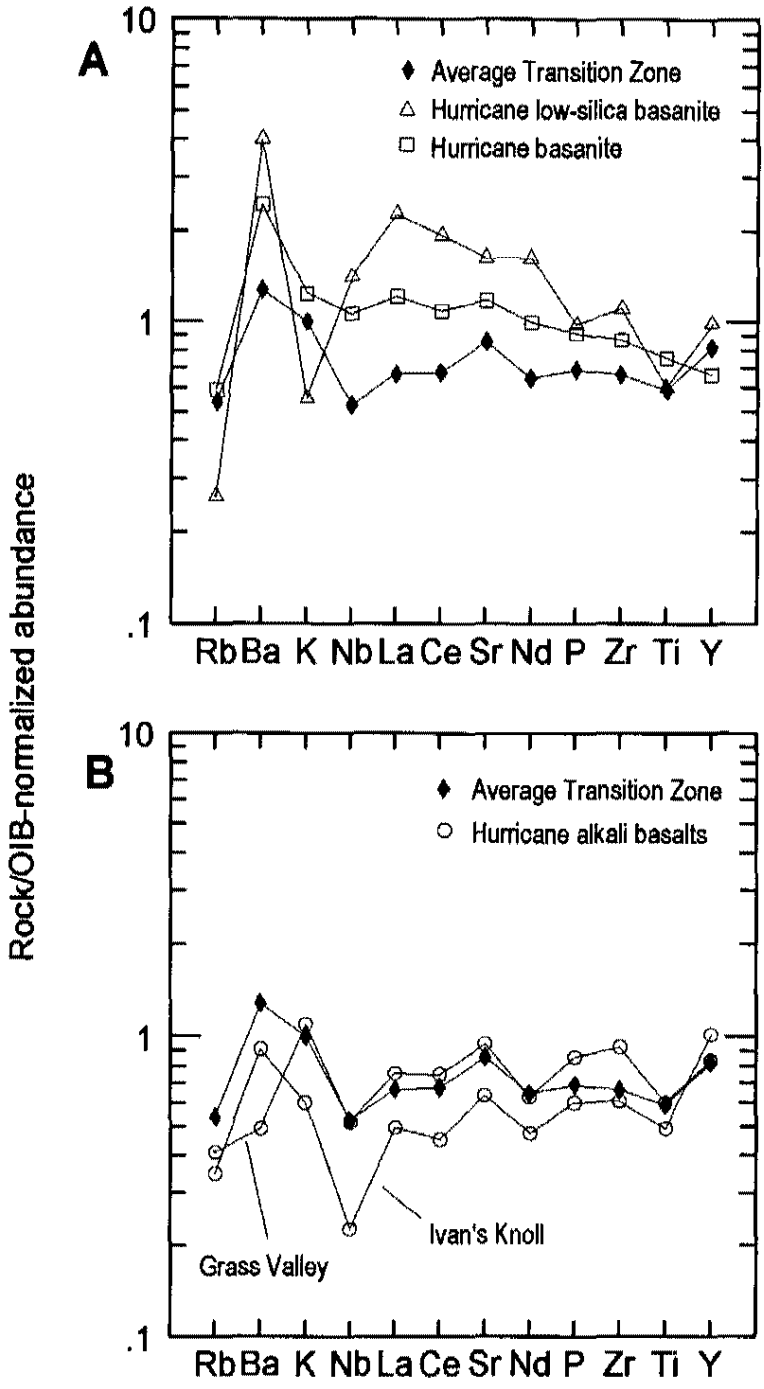


Figure 23. Average Transition Zone basalts <5 Ma (Fitton et al., 1991) compared to (A) Hurricane basanite and low-silica basanite and (B) Hurricane alkali basalts. The average Transition Zone basalt is OIB-like except for low Rb and Nb and higher Ba. Hurricane alkali basalts are similar to the average Transition Zone basalt. Hurricane basanites and low-silica basanites are missing the trough at Nb and are enriched in other elements except Rb.

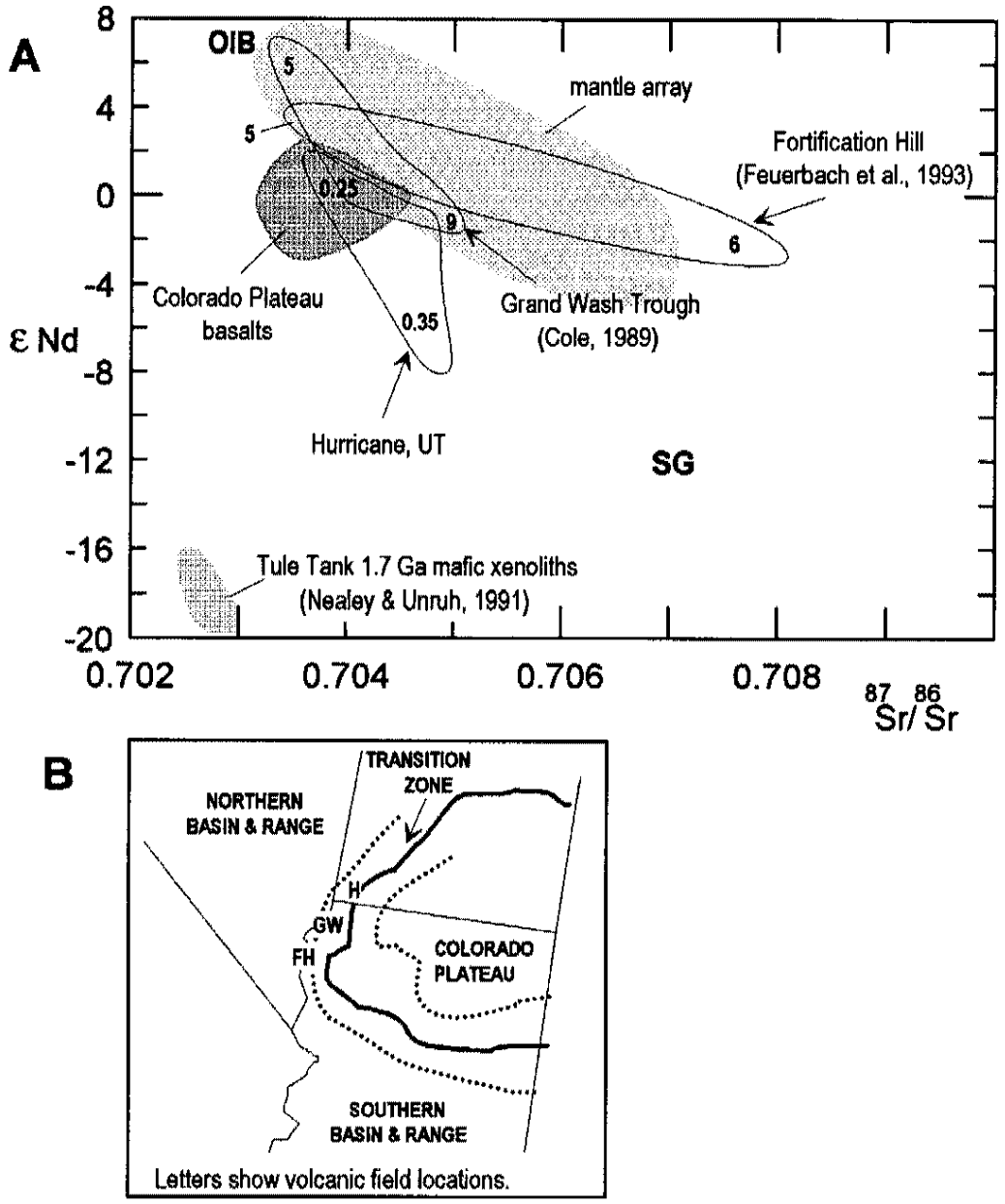


Figure 24. Comparison of volcanic fields along a transect from the Basin-and-Range to the Colorado Plateau. (A) Initial Sr vs. epsilon Nd isotope plot. Mafic volcanism shows more lower crustal material input with distance from the Basin-and-Range, (Tule Tank or St. George component). Also, as mafic volcanism becomes younger, magmas become more OIB like within each volcanic field. This observation correlates with models of lithosphere erosion and thinning with time from the Basin-and-Range to the Colorado Plateau. **SG** denotes the proposed lower crust component beneath the St. George basin, southwestern Utah (Unruh et al., 1994), **FH**, Fortification Hill; **GW**, Grand Wash Trough; **H**, Hurricane volcanic field. Number in fields (.35) are dates in Ma. (B) Map of the southwestern United States showing the locations of the volcanic fields and tectonic province boundaries. Dotted lines are the approximate limits of the Transition Zone, heavy solid line is the boundary between the Colorado Plateau and Basin-and-Range provinces.

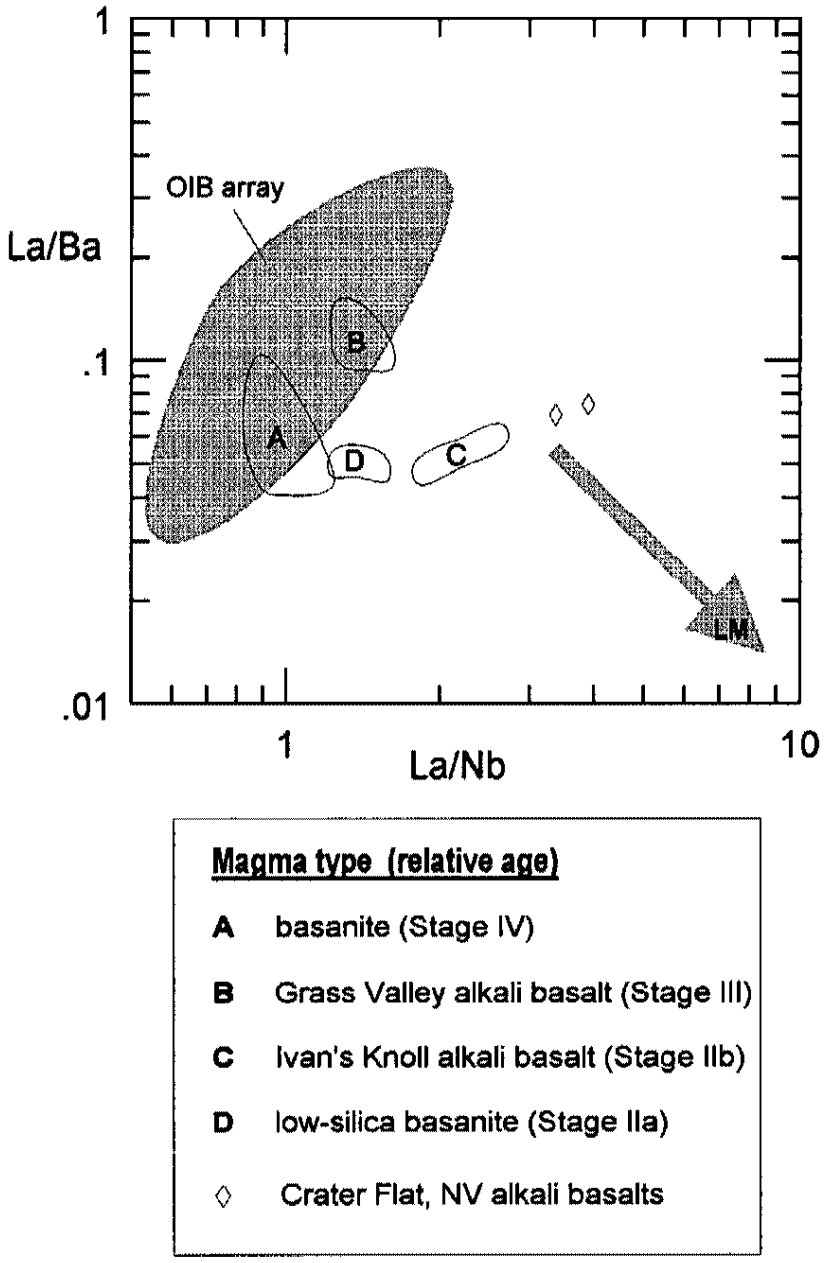


Figure 25. La/Ba vs. La/Nb diagram in Hurricane basalts. The arrow reflects an increasing subduction enriched lithospheric mantle component (LM) added to ocean island basalt (OIB) (data from Fitton et al., 1991). The LM should be enriched in Ba and depleted in Nb. Ba and Nb data for Hurricane samples agree with isotopic data in that types A and B are the most OIB-like and type C shows more LM contribution. Crater Flat, Nevada volcanic rocks are shown for comparison. They are interpreted as small partial melts of lithospheric mantle (Bradshaw and Smith, 1994).

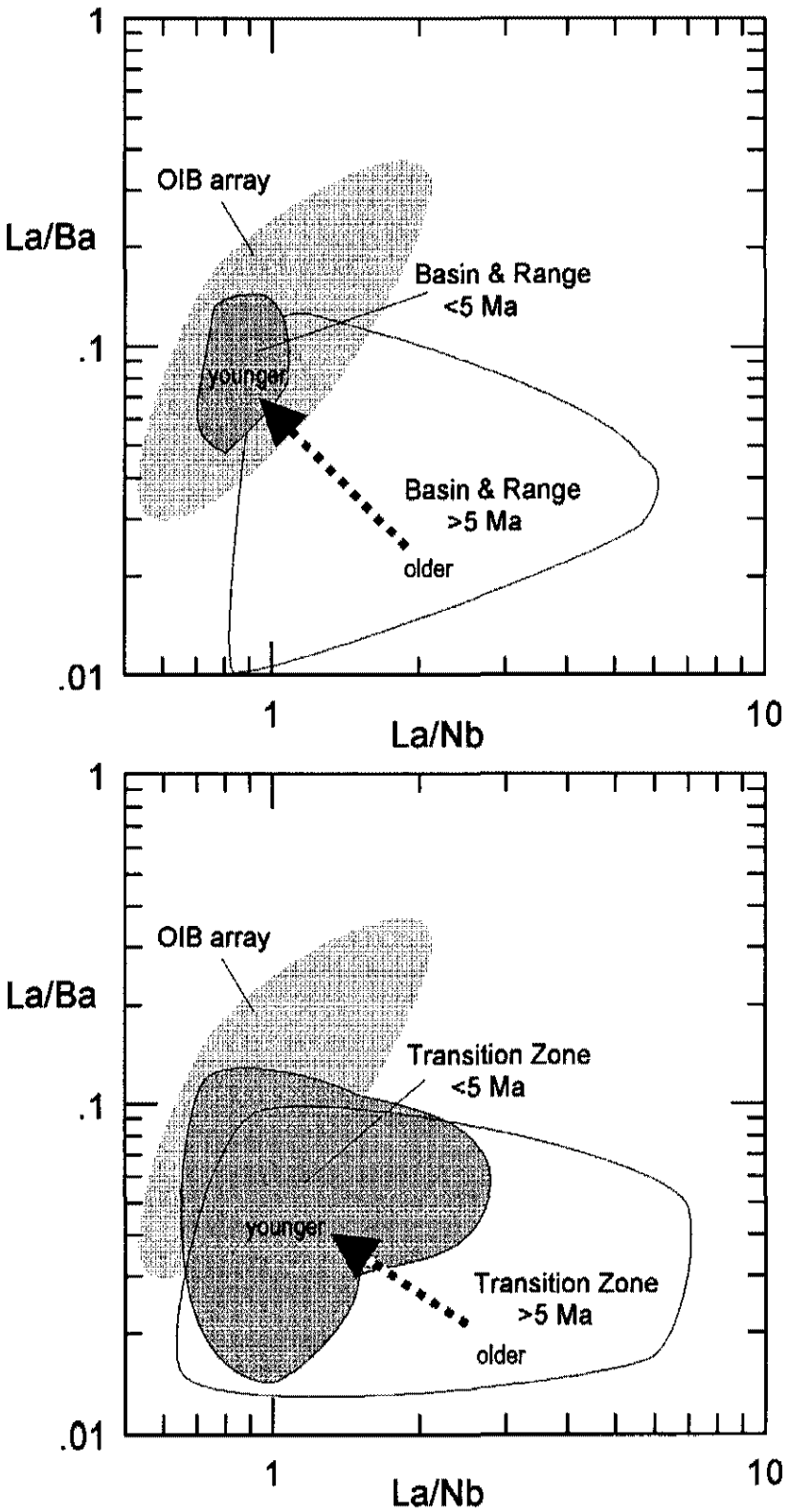


Figure 26. La/Ba vs. La Nb in late Cenozoic basalts from the Basin & Range and Transition Zone. Increases in Ba/Nb (from upper left to lower right in each plot ) reflect decreasing amounts of lithospheric mantle into an OIB-like mantle with time (modified after Fitton et al., 1991).

# CHAPTER 5

# GEOMORPHOLOGY

## A Problem - Correlating Flows Between Hurricane and Toquerville

The present morphology of the Transition Zone in the Hurricane area is the product of uplift and erosion; the dominant geologic processes, besides volcanism, that occurred in the region during Late Cenozoic time. Landforms in the Transition Zone are the result of differential uplift of the crust and the erosion of the uplifted rocks at rates reflecting their relative resistance to weathering. In general, the areas east of the Hurricane fault on the Colorado Plateau have been uplifted relative to the areas to the west of the fault (Cook, 1960).

Many workers concluded that the Hurricane fault has had at least two periods of movement (Huntington and Goldthwaite, 1904; Gregory, 1950; Cook, 1960; Watson, 1968). The lava flows in volcanic fields cut by the Hurricane fault may provide additional information on the history of the fault. Using the lava flows as a marker, Cook (1960) concluded that the second period of vertical displacement was 150 m near Hurricane and about 460 m near Pintura, 18 km to the north (Figure 27). Schramm (1994) confirmed these observations in a study of the fault near Toquerville, Utah. Schramm proposed that the flows can be used as piercing points and in combination with the fault geometry demonstrated that motion on the Hurricane fault was dominantly normal dip-slip. Schramm used trace element analysis to correlate flows from the hanging wall to the footwall of the fault. Schramm's analysis assumed that flows occupied channels that

crossed the fault and that the flows were not laterally extensive along strike of the fault in the footwall.

Lava flows that underlie the Hurricane Valley have a similar petrology and chemistry to lava flows studied by Schramm (1994) that crop out 12 km to the north near Toquerville, Utah (Figure 27) as demonstrated earlier in chapter 3. In both areas, the lava flows are offset by the Hurricane fault. The flows at Hurricane were possibly erupted from vent(s) at Ivan's Knoll or an older vent near Volcano Mountain. A source for the flows near Toquerville has not been discovered but the most reasonable location of the source of these flows is Ivan's Knoll in the Volcano Mountain vent complex. Evidence for this association is the chemical similarities between the Ivan's Knoll deposit and the Toquerville flows. The important question is, therefore; if the Hurricane and Toquerville flows erupted from a vent near Volcano Mountain, how did lava flows reach Toquerville that now lies uphill from Volcano Mountain? This question is important because the answer affects models regarding the displacement history of the Hurricane fault.

Three possible models are presented to answer the question posed above. The first suggests that basal flows at Hurricane and basalt near Toquerville are coeval and correlative. This model requires a drainage reversal between the time of the eruption of the flows and the present. The second model suggests that flows in both areas erupted from vents near Volcano Mountain, but that they have different ages. The third model theorizes that flows at Toquerville had a different source than those at Hurricane. This source is now eroded or covered.

## Models

1. Drainage reversal, coeval flows.

Schramm (1994) demonstrated that the Gunlock-Grand Wash and Washington faults have offsets that increase to the south. The Hurricane fault increases in displacement to the north from Hurricane (Schramm, 1994). Ash Creek presently flows to

the south and parallels the Hurricane fault for 32 km from the Virgin River north. If the creek gradient is restored to a gradient that existed before the second period of movement on the fault, assuming that the offset along the fault is greater to the north by about 300 m, the gradient of the creek could have been shallow or reversed at the time of eruption. The northward sloping stream gradient would allow lava flows erupted from Ivan's Knoll to fill the Hurricane Valley and flow toward Toquerville in the Ash Creek drainage (Figure 28). Ash Creek has basalt flows along parts of its drainage north of the Virgin River (Figure 27).

2. Different Age, same vent - drainage reversal.

This model assumes that flows erupted from Ivan's Knoll at different times. Initially only those near Toquerville were produced. The age of the Toquerville flows is unknown. These eruptions were followed by faulting and a change of the gradient of Ash Creek to the south. Finally, additional eruptions from Ivan's Knoll produced flows 353 ka ± 45 ka old that filled the Hurricane Valley and part of the southern Ash Creek drainage. The younger flows were then offset 150 m by the Hurricane fault at Hurricane.

3. Different age and vent

This model assumes that the flows near Toquerville and at Hurricane have different sources and significantly different ages. Twelve km north of Toquerville on Black Ridge just north of Pintura, Utah are basalt flows dated at 1.0 ± 0.1 Ma (K-Ar, Best at al., 1980). The vent associated with these older flows (1 Ma) may now be eroded or covered. It is possible that the Toquerville flows may be related to the flows near Pintura rather than the Volcano Mountain/Ivan's Knoll center. If this is the case, the basalts near Toquerville could be 900 to 600 ka older than the Hurricane basalts. Unfortunately no chemical data is available for the Pintura basalts, so this correlation can not be tested at the present time. A drainage reversal is not required if the flows erupted from a now hidden vent in the Toquerville area or if the source of the flows is to the north near Pintura.

## Discussion of Models

Models 1 and 2 require variable displacement along strike on the Hurricane fault (Figure 28). Cook (1960) and Schramm (1994) indicate that vertical motion of the footwall of the fault would have to increase toward the north from the town of Hurricane relative to the hanging wall. However, models 1 and 2 require a hanging wall block with greater vertical movement in the north relative to the south, to explain the drainage reversal (Figure 28). Model 2 would also require a relatively continuous eruption at Ivan's Knoll/Volcano Mountain. Both of these models require that lava flows travel at least 12 km from their source. If this is correct then the Ivan's Knoll-Toquerville flow would be the longest in the area. One of the longer lava flows in the region at Crater Hill, near Zion Canyon, flowed 10 km down gradient from its source (Threet, 1958).

Model 3 simply suggests that the cinder cone that erupted the Toquerville flows is covered or deeply eroded. This model does not require a reversal of drainage but suggests that the age of Toquerville flows is significantly older than flows at Hurricane. Toquerville flows may be closer in age to a lava flow from Black Ridge north of Pintura dated at $1.0 \pm 0.1$ Ma. This flow is as far north of Toquerville as Hurricane is south, (12 km). The source of the Toquerville flows may never be located, in fact, cinder cones for flows of the same age (Stage II) are rarely found. Model 3 is certainly the most compelling model, however, it can not be tested until flows at Toquerville are dated and a detailed study of the rocks at Black Ridge has been completed.

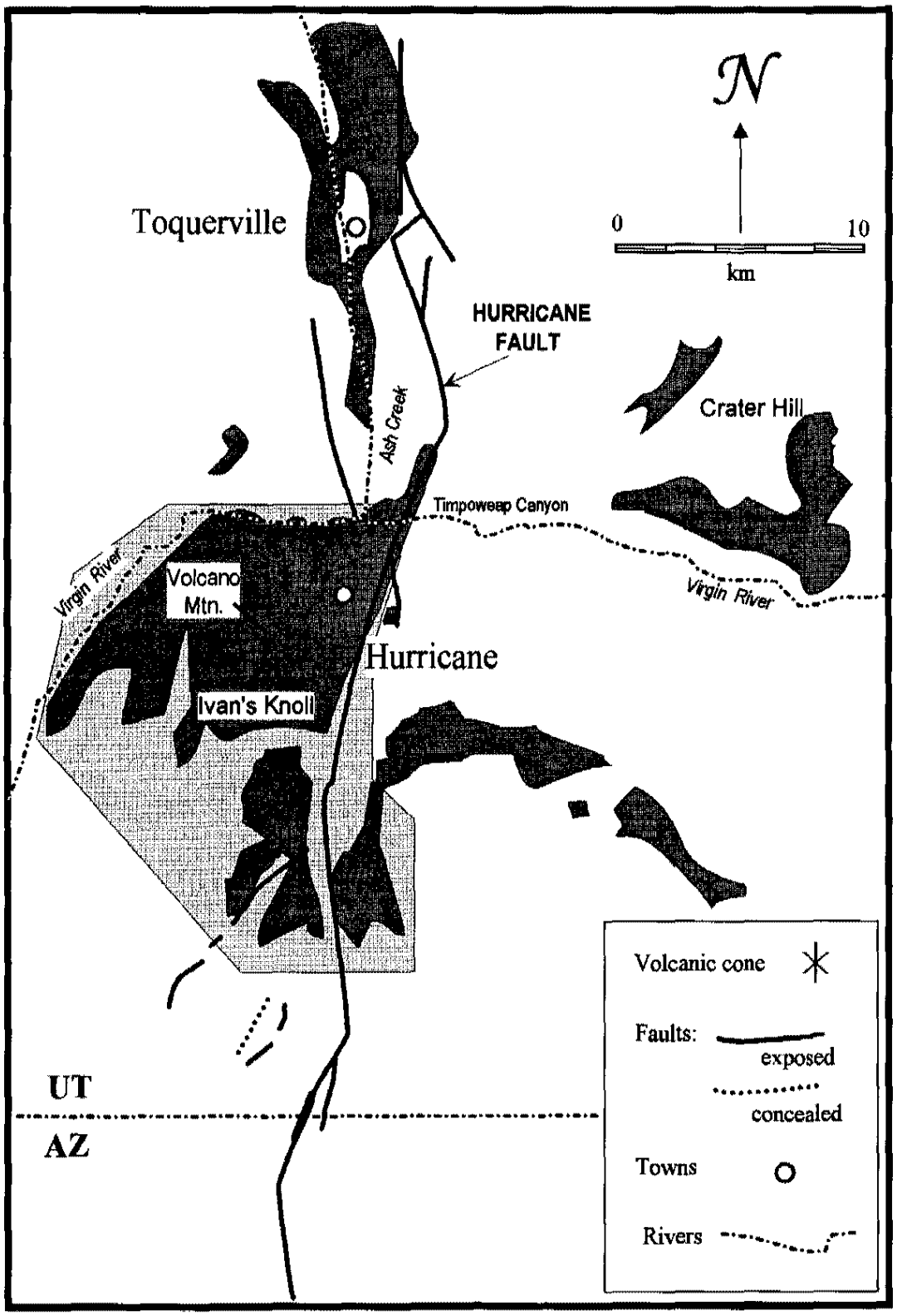


Figure 27. Map of the Hurricane fault between Toquerville and the Arizona-Utah border. Lava flows (dark areas) in the Hurricane and Toquerville, Utah area shown, study area shown enclosed in light gray polygon, structural geology after Hintze (1960).

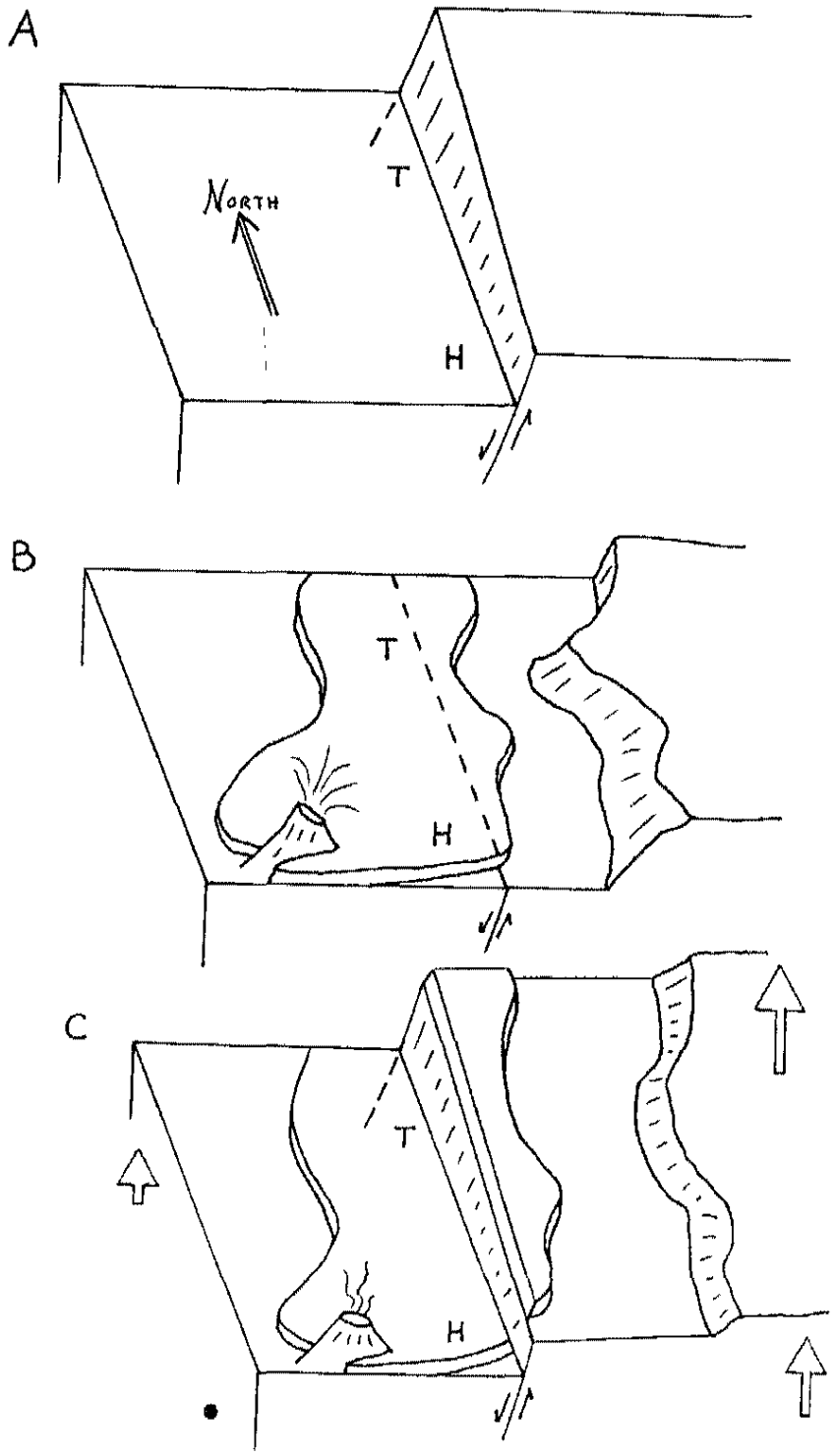


Figure 28. Schematic block diagram depicting variable movement on the Hurricane fault. The locations of Toquerville and Hurricane are indicated by the capital letters. (A) Normal faulting with displacement increasing toward the north on the Hurricane fault before volcanism. (B) Volcanism produces lavas that flow over the fault (now leveled by erosion). (C) A period of normal faulting after volcanism. Variable displacement with direction and magnitude indicated by the block arrows produces the post basalt throw seen at present.

# CHAPTER 6

## SUMMARY

1. The Hurricane volcanic field is a small-volume mafic volcanic field in the Colorado Plateau / Basin & Range Transition Zone of the southwestern United States. The total volume of the field is about 0.48 $km^3$ with the volume of individual centers ranging from 0.05 to 0.30 $km^3$. Strombolian-Hawaiian style eruptions produced thin (10 m) a'a lava flows and cinder (scoria) cones composed of vesicular basalt, bombs and agglutinate.

2. The relative time scale based on the geomorphic criteria established by Hamblin (1970b) for the western Grand Canyon region places the volcanoes and flows in Stages II to IV. Radiometric dating ($^{40}Ar/^{39}Ar$) yielded dates of 353 ± 45 ka for a Stage IIb flow and 258 ± 24 ka for a Stage IVb flows. These dates and geologic relationships demonstrate that volcanoes near Hurricane formed over a period of at least 100,000 years. Also, the dates suggest that the post basalt throw on the Hurricane fault has occurred in the last 350 thousand years (t.y.) and perhaps in as short a time as 100 t.y.

3. In the upper crust, magma rose along joints in sedimentary rocks. East of the Hurricane fault, chains of vents follow a joint orientation maxima of N30°W. Vent chains west of the fault follow a joint maxima of N30°E.

4. Lava flows at Toquerville, 12 km north of Hurricane, are chemically similar to some flows in the Hurricane volcanic field. The flows at Toquerville are not associated

with any vent and may have erupted from the Ivan's Knoll/Volcano Mountain complex in the Hurricane field. The correlation problem between the Toquerville flows and the Hurricane field can not be solved without radiometric dating of the Toquerville lavas.

5. Three rock groups, low-silica basanite (<42% $SiO_2$), basanite (43-46% $SiO_2$) and alkali basalt (>46% $SiO_2$), originated by the partial melting of four isotopically distinct garnet-free mantle sources. Limited mixing occurred between two of the four types of magmas (A and B). AFC processes may explain intra-element variation of basanites and some alkali basalts.

6. Hurricane mafic lavas have relatively high La/Ba and La/Nb and $^{87}Sr/^{86}Sr$ and lower $\varepsilon_{Nd}$ values compared to Basin-and-Range basalts less than 5 m.y. old. These observations indicate that magmas originated in the lithospheric mantle and interacted with lower crustal component(s) whereas Basin-and-Range basalts are similar to OIB and probably originated in the asthenosphere and rose to the surface with little or no lithospheric contamination. Isotope and trace element analyses indicate that the Hurricane magmas interacted with a lower crustal component(s) in one or two steps. A single step could explain the isotope variation in the Hurricane volcanic field if the lower crustal component beneath the field has isotope values between those of the Markagunt Plateau and the St. George basin. A two step model with a component which underlies the Colorado Plateau (Tule Tank) and a second which lies beneath the St. George basin also explains the isotope variation. With distance from the Colorado Plateau and time, Hurricane magmas like those in other areas of the Transition Zone become more OIB-like. The lack of a lower crustal component for the Basin-and-Range basalts and its presence in the Transition Zone reflects the thick lithosphere beneath the Transition Zone and Colorado Plateau. The transition toward OIB source for Hurricane lavas with time may reflect the thinning of the lithosphere during extension.

7. Differences in chemical and isotopic characteristics of volcanic rocks erupted from the Volcano Mountain/Ivan's Knoll complex indicate that the complex is polygenetic. Geochronological data indicate that the complex erupted over a period of at least 100 t.y. Therefore it is also polycyclic.

8. Two of the findings of this work have implications for volcanic hazard assessment in the region around Yucca Mountain, Nevada and the proposed high-level nuclear waste repository. (a) Jointing in the upper crust controls volcano locations in the Hurricane volcanic field. Jointing is the most frequent structural feature observed at the surface in this area. Structural features observed at the surface should be a factor when determining high-risk zones for volcanism. (b) Polygenetic volcanism occurs when magmas use established pathways to the surface. Therefore, if a volcano is demonstrated to be polygenetic the chance increases that the same volcano or a site nearby will be the site of future eruptions.

# APPENDIX I

## GEOCHEMICAL DATA

Whole rock chemical analyses of samples from the Hurricane volcanic field are grouped by rock type. Totals values for the major oxides (analyzed by XRF) do not include loss on ignition (LOI) values. Only three samples were analyzed for LOI; 7-16, 7-24 and 7-26. The results, 0.90, 0.53 and 0.55%, respectively, are believed to be representative of all samples. Total iron is reported as $Fe_2O_3T$. Blank spaces indicate that no analysis was performed.

# Whole Rock Chemical Analyses

| Rock type | *Low-Silica Basanite* | | | | | *Basanite* | | | | |
|---|---|---|---|---|---|---|---|---|---|---|
| Sample | 6-3 | 6-11 | 6-12 | 7-11 | 7-18 | 1-2 | 1-4 | 1-6 | 5-2 | 5-3 |
| long (°W) | 113.303 | 113.294 | 113.294 | 113.325 | 113.306 | 113.385 | 113.295 | 113.274 | 113.298 | 113.292 |
| lat (°N) | 37.072 | 37.094 | 37.094 | 37.105 | 37.119 | 37.172 | 37.187 | 37.065 | 37.080 | 37.071 |
| | | | | | *X-Ray Fluorescence Analyses, wt %* | | | | | |
| $SiO_2$ | 42.5 | 42.1 | 41.5 | 42.5 | 41.7 | 45.9 | 44.5 | 44.5 | 43.9 | 43.7 |
| $TiO_2$ | 1.85 | 1.89 | 1.88 | 1.80 | 1.85 | 2.75 | 2.45 | 2.80 | 2.57 | 2.57 |
| $Al_2O_3$ | 12.2 | 12.0 | 11.9 | 12.3 | 11.8 | 12.9 | 12.8 | 12.1 | 11.0 | 11.5 |
| $Fe_2O_3T$ | 11.8 | 11.9 | 11.7 | 11.5 | 11.7 | 13.0 | 12.4 | 13.2 | 13.2 | 13.0 |
| MnO | 0.21 | 0.21 | 0.20 | 0.19 | 0.20 | 0.17 | 0.17 | 0.18 | 0.19 | 0.19 |
| MgO | 13.99 | 13.55 | 13.54 | 13.41 | 13.37 | 10.26 | 9.45 | 10.69 | 12.59 | 11.93 |
| CaO | 12.2 | 12.7 | 12.4 | 12.3 | 13.1 | 10.4 | 11.3 | 11.4 | 11.0 | 11.1 |
| $Na_2O$ | 3.05 | 2.89 | 2.94 | 2.84 | 2.72 | 2.84 | 2.70 | 2.74 | 2.66 | 2.55 |
| $K_2O$ | 1.17 | 0.72 | 0.78 | 1.15 | 0.69 | 1.66 | 1.54 | 1.34 | 1.39 | 1.34 |
| $P_2O_5$ | 0.65 | 0.66 | 0.65 | 0.66 | 0.66 | 0.63 | 0.63 | 0.65 | 0.65 | 0.66 |
| Total | 99.56 | 98.54 | 97.54 | 98.63 | 97.72 | 100.54 | 97.93 | 99.63 | 99.23 | 98.47 |
| | | | | | *X-Ray Fluorescence Analyses, ppm* | | | | | |
| Rb | 12.0 | 13.1 | 14.1 | 13.7 | 7.8 | 20.5 | 19.3 | 20.8 | 21.2 | 18.1 |
| Ba | 2827 | 2316 | 2390 | 2435 | 2375 | 1242 | 1262 | 1227 | 718 | 664 |
| Nb | 84.3 | 86.1 | 89.6 | 73.0 | 75.8 | 57.1 | 48.6 | 58.8 | 63.9 | 63.0 |
| Sr | 1199 | 1249 | 1244 | 1184 | 1274 | 979 | 947 | 980 | 950 | 945 |
| Zr | 278 | 311 | 315 | 292 | 308 | 296 | 262 | 311 | 292 | 278 |
| Y | 27.7 | 28.9 | 28.2 | 25.3 | 30.0 | 23.9 | 26.6 | 33.9 | 30.9 | 29.6 |
| Cr | 583 | 623 | 617 | 588 | 624 | | | 568 | | 393 |
| Ni | 335 | 311 | 300 | 302 | 313 | 204 | 184 | 248 | | 340 |
| | | | | | *Instrumental Neutron Activation Analyses, ppm* | | | | | |
| Ba | 2316 | 2199 | 2302 | 2316 | 2082 | 971 | 1251 | | 766 | |
| Th | 18.8 | 18.1 | 19.7 | 18.0 | 18.6 | 6.7 | 7.1 | | 7.7 | |
| Ta | 4.85 | 4.83 | 5.04 | 4.61 | 4.70 | 3.30 | 3.07 | | 4.12 | |
| La | 115.6 | 114.1 | 113.8 | 110.8 | 109.3 | 54.9 | 57.2 | | 58.1 | |
| Ce | 203.8 | 199.7 | 211.9 | 196.8 | 198.0 | 105.6 | 106.3 | | 115.3 | |
| Nd | 79.2 | 78.6 | 72.4 | 84.1 | 88.6 | 47.2 | 55.1 | | 40.1 | |
| Sm | 13.12 | 13.35 | 13.14 | 12.71 | 12.77 | 8.96 | 8.82 | | 10.51 | |
| Hf | 6.18 | 6.16 | 6.16 | 6.07 | 6.11 | 5.62 | 5.24 | | 6.27 | |
| Eu | 3.51 | 3.54 | 3.61 | 3.24 | 3.54 | 2.68 | 2.78 | | 3.45 | |
| Tb | 1.36 | 1.36 | 1.00 | 0.97 | 0.90 | 1.03 | 0.85 | | 1.13 | |
| Yb | 2.23 | 2.19 | 2.24 | 2.52 | 2.14 | 1.48 | 1.56 | | 1.75 | |
| Lu | 0.34 | 0.33 | 0.31 | 0.29 | 0.27 | 0.21 | 0.17 | | 0.18 | |
| Sc | 31.1 | 31.9 | 33.2 | 30.4 | 31.9 | 24.7 | 24.2 | | 27.6 | |
| Cr | 590 | 617 | 628 | 588 | 638 | 551 | 446 | | 499 | |
| Co | 57.9 | 56.6 | 58.6 | 55.7 | 56.7 | 53.6 | 51.4 | | 64.1 | |
| Ni | 295 | 285 | 318 | 293 | 304 | 267 | 236 | | 343 | |
| | | | | | *Isotope Dilution Analyses, ppm* | | | | | |
| Pb | 10.73 | | 10.62 | 10.67 | 10.32 | 6.75 | 7.57 | | | |
| Nd | 78.5 | 79.8 | 81.2 | 78.0 | 78.5 | 44.0 | 44.5 | | | |
| Sm | 12.01 | 12.26 | 12.45 | 11.85 | 12.08 | 8.24 | 8.16 | | | |

| Rock type | *Basanite* | | | | | | | | | |
|---|---|---|---|---|---|---|---|---|---|---|
| Sample | 5-6 | 5-7 | 6-1 | 6-2 | 6-4 | 6-5 | 6-6 | 6-7 | 6-8 | 6-9 |
| long (°W) | 113.316 | 113.322 | 113.274 | 113.298 | 113.292 | 113.275 | 113.279 | 113.277 | 113.276 | 113.268 |
| lat (°N) | 37.197 | 37.185 | 37.066 | 37.072 | 37.089 | 37.078 | 37.078 | 37.072 | 37.072 | 37.052 |
| | *X-Ray Fluorescence Analyses, wt %* | | | | | | | | | |
| $SiO_2$ | 45.5 | 44.0 | 43.9 | 44.2 | 44.5 | 43.4 | 44.5 | 45.0 | 43.9 | 44.2 |
| $TiO_2$ | 2.26 | 2.30 | 2.55 | 2.56 | 2.64 | 2.55 | 2.64 | 2.68 | 2.52 | 2.52 |
| $Al_2O_3$ | 12.8 | 12.3 | 11.6 | 11.7 | 11.1 | 10.9 | 11.0 | 11.2 | 11.6 | 11.6 |
| $Fe_2O_3T$ | 12.5 | 12.6 | 13.0 | 13.2 | 13.4 | 12.6 | 13.3 | 13.6 | 12.8 | 12.9 |
| MnO | 0.18 | 0.18 | 0.18 | 0.19 | 0.19 | 0.18 | 0.19 | 0.19 | 0.19 | 0.19 |
| MgO | 10.85 | 10.00 | 11.82 | 12.22 | 13.61 | 13.19 | 12.47 | 13.39 | 11.49 | 11.99 |
| CaO | 10.8 | 10.2 | 11.1 | 11.2 | 11.3 | 10.5 | 10.9 | 11.2 | 11.0 | 10.9 |
| $Na_2O$ | 2.93 | 3.27 | 2.86 | 2.85 | 3.01 | 2.97 | 2.81 | 3.01 | 2.63 | 2.64 |
| $K_2O$ | 1.65 | 1.55 | 1.41 | 1.37 | 1.42 | 1.51 | 1.42 | 1.42 | 1.37 | 1.37 |
| $P_2O_5$ | 0.59 | 0.63 | 0.65 | 0.66 | 0.65 | 0.64 | 0.65 | 0.65 | 0.65 | 0.64 |
| Total | 100.09 | 97.03 | 99.04 | 100.16 | 101.82 | 98.54 | 99.82 | 102.40 | 98.27 | 98.91 |
| | *X-Ray Fluorescence Analyses, ppm* | | | | | | | | | |
| Rb | 22.0 | 13.7 | 17.3 | 16.4 | 17.2 | 19.2 | 21.7 | 20.7 | 20.5 | 19.8 |
| Ba | 773 | 830 | 925 | 790 | 807 | 680 | 498 | 706 | 746 | 864 |
| Nb | 55.9 | 47.1 | 67.3 | 69.0 | 64.2 | 65.4 | 64.0 | 59.5 | 57.6 | 69.5 |
| Sr | 986 | 860 | 856 | 990 | 827 | 814 | 905 | 836 | 832 | 853 |
| Zr | 262 | 230 | 263 | 288 | 261 | 268 | 261 | 265 | 249 | 286 |
| Y | 23.8 | 19.7 | 28.5 | 30.0 | 26.5 | 25.0 | 29.2 | 31.0 | 31.2 | 29.9 |
| Cr | | 339 | 377 | | 467 | 469 | 485 | 487 | 393 | 420 |
| Ni | | 214 | 330 | | 368 | 388 | 391 | 379 | 311 | 336 |
| | *Instrumental Neutron Activation Analyses, ppm* | | | | | | | | | |
| Ba | 963 | | | 831 | | | | | | |
| Th | 7.1 | | | 7.5 | | | | | | |
| Ta | 3.43 | | | 3.88 | | | | | | |
| La | 56.6 | | | 60.2 | | | | | | |
| Ce | 107.3 | | | 113.2 | | | | | | |
| Nd | 37.5 | | | 51.4 | | | | | | |
| Sm | 8.99 | | | 10.76 | | | | | | |
| Hf | 5.81 | | | 6.11 | | | | | | |
| Eu | 2.74 | | | 3.17 | | | | | | |
| Tb | 0.99 | | | 1.19 | | | | | | |
| Yb | 1.75 | | | 1.89 | | | | | | |
| Lu | 0.28 | | | 0.22 | | | | | | |
| Sc | 27.0 | | | 27.0 | | | | | | |
| Cr | 445 | | | 432 | | | | | | |
| Co | 57.6 | | | 60.8 | | | | | | |
| Ni | 233 | | | 334 | | | | | | |
| | *Isotope Dilution Analyses, ppm* | | | | | | | | | |
| Pb | 7.21 | | | | | | | | | |
| Nd | 46.1 | | | | | | | | | |
| Sm | 8.41 | | | | | | | | | |

| Rock type | *Basanite* | | | | | | | | | |
|---|---|---|---|---|---|---|---|---|---|---|
| Sample | 6-10 | 6-13 | 6-14 | 7-21 | 7-22 | 7-23 | 7-25 | 7-26 | 7-27 | 7-29 |
| long (°W) | 113.268 | 113.279 | 113.275 | 113.335 | 113.324 | 113.335 | 113.305 | 113.310 | 113.301 | 113.302 |
| lat (°N) | 37.052 | 37.087 | 37.059 | 37.166 | 37.160 | 37.169 | 37.189 | 37.190 | 37.197 | 37.197 |
| | *X-Ray Fluorescence Analyses, wt %* | | | | | | | | | |
| $SiO_2$ | 43.3 | 43.7 | 43.3 | 45.8 | 45.6 | 45.8 | 45.4 | 44.5 | 43.9 | 44.9 |
| $TiO_2$ | 2.40 | 2.61 | 2.57 | 2.32 | 2.42 | 2.42 | 2.57 | 2.25 | 2.59 | 2.29 |
| $Al_2O_3$ | 10.6 | 11.1 | 10.8 | 12.7 | 12.7 | 12.9 | 13.1 | 12.8 | 11.9 | 12.7 |
| $Fe_2O_3T$ | 12.7 | 13.3 | 13.3 | 12.6 | 12.8 | 12.7 | 12.6 | 12.5 | 13.5 | 12.8 |
| MnO | 0.18 | 0.18 | 0.19 | 0.18 | 0.18 | 0.18 | 0.18 | 0.19 | 0.19 | 0.19 |
| MgO | 14.08 | 12.46 | 13.06 | 10.94 | 10.89 | 10.72 | 9.42 | 11.23 | 11.84 | 11.43 |
| CaO | 10.9 | 11.0 | 10.8 | 10.1 | 10.1 | 10.2 | 10.4 | 10.7 | 10.7 | 10.5 |
| $Na_2O$ | 2.40 | 2.51 | 2.41 | 2.83 | 2.73 | 2.88 | 3.24 | 3.45 | 3.39 | 3.44 |
| $K_2O$ | 1.27 | 1.41 | 1.34 | 1.42 | 1.50 | 1.45 | 1.68 | 1.66 | 1.86 | 1.11 |
| $P_2O_5$ | 0.63 | 0.64 | 0.65 | 0.62 | 0.61 | 0.60 | 0.62 | 0.63 | 0.66 | 0.62 |
| Total | 98.48 | 98.85 | 98.36 | 99.60 | 99.63 | 99.92 | 99.22 | 100.37 | 100.58 | 99.94 |
| | *X-Ray Fluorescence Analyses, ppm* | | | | | | | | | |
| Rb | 17.1 | 19.5 | 16.8 | 17.1 | 19.2 | 17.0 | 19.4 | 21.3 | 26.7 | 16.3 |
| Ba | 611 | 780 | 703 | 895 | 835 | 1023 | 1025 | 1011 | 951 | 1122 |
| Nb | 63.3 | 67.0 | 65.6 | 45.2 | 51.0 | 46.4 | 58.9 | 58.0 | 72.1 | 60.3 |
| Sr | 950 | 851 | 796 | 831 | 895 | 867 | 900 | 882 | 974 | 913 |
| Zr | 254 | 294 | 272 | 247 | 230 | 254 | 280 | 266 | 315 | 250 |
| Y | 31.3 | 29.0 | 28.8 | 23.7 | 24.3 | 26.9 | 23.4 | 23.4 | 24.3 | 22.1 |
| Cr | | 437 | 533 | | | | | | | |
| Ni | | 381 | 419 | | | | | | | |
| | *Instrumental Neutron Activation Analyses, ppm* | | | | | | | | | |
| Ba | 627 | | | 852 | 810 | 926 | 922 | 980 | 1090 | 969 |
| Th | 7.2 | | | 6.3 | 6.8 | 6.1 | 7.0 | 7.4 | 9.4 | 7.5 |
| Ta | 3.80 | | | 3.19 | 3.37 | 3.18 | 3.71 | 7.26 | 4.69 | 3.53 |
| La | 56.9 | | | 50.4 | 51.8 | 51.1 | 57.9 | 54.9 | 70.4 | 57.1 |
| Ce | 106.6 | | | 98.6 | 105.2 | 98.8 | 110.7 | 107.5 | 135.7 | 110.3 |
| Nd | 54.6 | | | 47.9 | 43.4 | 28.8 | 51.4 | 43.4 | 57.6 | 52.9 |
| Sm | 10.18 | | | 8.76 | 8.86 | 8.81 | 9.29 | 9.08 | 10.94 | 9.48 |
| Hf | 5.90 | | | 5.93 | 5.95 | 5.40 | 6.18 | 6.01 | 7.13 | 5.99 |
| Eu | 3.17 | | | 2.48 | 2.49 | 2.47 | 2.49 | 2.42 | 3.15 | 2.59 |
| Tb | 1.18 | | | 0.95 | 1.01 | 1.05 | 1.07 | 1.11 | 1.23 | 0.87 |
| Yb | 1.86 | | | 1.67 | 1.46 | 1.55 | 1.71 | 1.59 | 1.62 | 1.64 |
| Lu | 0.21 | | | 0.28 | 0.27 | 0.28 | 0.27 | 0.18 | 0.26 | 0.27 |
| Sc | 27.6 | | | 25.5 | 26.1 | 25.8 | 25.3 | 28.0 | 26.1 | 27.9 |
| Cr | 564 | | | 409 | 422 | 411 | 387 | 469 | 501 | 469 |
| Co | 67.5 | | | 61.6 | 60.8 | 60.4 | 54.7 | 178.4 | 61.3 | 58.6 |
| Ni | 475 | | | 229 | 226 | 217 | 114 | 211 | 224 | 217 |
| | *Isotope Dilution Analyses, ppm* | | | | | | | | | |
| Pb | | | | 6.20 | 5.81 | 6.62 | 7.02 | 6.92 | 7.26 | 7.73 |
| Nd | | | | 42.1 | 43.6 | 43.2 | 47.9 | 46.8 | 58.9 | 48.0 |
| Sm | | | | 7.96 | 8.22 | 8.18 | 8.89 | 8.58 | 10.62 | 8.79 |

| Rock type | *Basanite* | | *Alkali Basalt* | | | | | | | |
|---|---|---|---|---|---|---|---|---|---|---|
| Sample | 7-30 | 7-31 | 1-1 | 1-3 | 1-5 | 5-5 | 5-8 | 5-9 | 6-15 | 7-1 |
| long (°W) | 113.302 | 113.303 | 113.385 | 113.319 | 113.308 | 113.318 | 113.352 | 113.354 | 113.280 | 113.321 |
| lat (°N) | 37.191 | 37.194 | 37.164 | 37.184 | 37.062 | 37.188 | 37.174 | 37.173 | 37.180 | 37.073 |
| *X-Ray Fluorescence Analyses, wt %* | | | | | | | | | | |
| $SiO_2$ | 44.9 | 44.7 | 48.4 | 48.8 | 48.1 | 48.2 | 46.6 | 49.9 | 49.9 | 49.3 |
| $TiO_2$ | 2.33 | 2.28 | 1.85 | 1.91 | 1.90 | 1.66 | 2.39 | 1.40 | 1.42 | 1.75 |
| $Al_2O_3$ | 13.0 | 12.7 | 15.2 | 15.5 | 16.1 | 14.7 | 13.1 | 16.4 | 15.1 | 16.1 |
| $Fe_2O_3T$ | 12.7 | 12.6 | 11.3 | 11.3 | 10.2 | 11.6 | 13.0 | 10.5 | 11.9 | 10.2 |
| MnO | 0.18 | 0.19 | 0.16 | 0.16 | 0.16 | 0.16 | 0.18 | 0.16 | 0.17 | 0.17 |
| MgO | 10.51 | 11.21 | 7.15 | 7.10 | 7.54 | 8.50 | 10.78 | 6.60 | 8.35 | 7.99 |
| CaO | 10.3 | 10.7 | 8.9 | 9.8 | 9.8 | 9.4 | 10.4 | 10.6 | 8.9 | 9.3 |
| $Na_2O$ | 3.09 | 3.08 | 2.86 | 2.69 | 3.10 | 2.95 | 2.94 | 3.19 | 2.70 | 3.44 |
| $K_2O$ | 1.54 | 1.56 | 1.33 | 1.31 | 1.22 | 1.15 | 1.33 | 0.86 | 0.99 | 1.26 |
| $P_2O_5$ | 0.62 | 0.61 | 0.52 | 0.58 | 0.56 | 0.49 | 0.61 | 0.38 | 0.38 | 0.54 |
| Total | 99.16 | 99.59 | 97.79 | 99.10 | 98.66 | 98.78 | 101.31 | 100.05 | 99.90 | 100.12 |
| *X-Ray Fluorescence Analyses, ppm* | | | | | | | | | | |
| Rb | 17.5 | 20.9 | 16.9 | 15.5 | 13.7 | 8.4 | 16.5 | 8.5 | 14.4 | 11.9 |
| Ba | 1266 | 930 | 1072 | 1281 | 737 | 493 | 1114 | 663 | 627 | 341 |
| Nb | 56.8 | 58.4 | 29.7 | 31.6 | 24.0 | 26.1 | 58.4 | 13.1 | 16.1 | 27.2 |
| Sr | 911 | 887 | 746 | 759 | 772 | 552 | 908 | 536 | 608 | 721 |
| Zr | 241 | 241 | 236 | 241 | 277 | 187 | 248 | 186 | 131 | 249 |
| Y | 20.2 | 21.8 | 27.8 | 28.7 | 32.6 | 22.1 | 20.3 | 26.0 | 18.7 | 26.5 |
| Cr | | | 263 | | | | 356 | 110 | 268 | |
| Ni | | | 112 | 109 | 128 | | 205 | 48 | 149 | |
| *Instrumental Neutron Activation Analyses, ppm* | | | | | | | | | | |
| Ba | 1144 | 936 | | 920 | 799 | 514 | | | 731 | 421 |
| Th | 7.4 | 7.4 | | 5.3 | 3.3 | 4.1 | | | 2.7 | 3.3 |
| Ta | 3.48 | 3.78 | | 1.63 | 1.44 | 1.49 | | | 0.85 | 1.65 |
| La | 58.5 | 57.0 | | 46.1 | 34.5 | 32.6 | | | 30.0 | 35.5 |
| Ce | 111.0 | 116.0 | | 84.9 | 72.0 | 65.4 | | | 59.0 | 70.5 |
| Nd | 29.2 | 40.4 | | 57.4 | 30.7 | 34.0 | | | 23.5 | 43.8 |
| Sm | 8.95 | 9.22 | | 7.02 | 6.20 | 5.80 | | | 5.52 | 6.46 |
| Hf | 5.91 | 5.96 | | 4.56 | 5.06 | 4.62 | | | 3.45 | 5.09 |
| Eu | 2.64 | 2.71 | | 1.93 | 2.18 | 2.01 | | | 1.70 | 2.56 |
| Tb | 0.90 | 1.05 | | 0.88 | 1.04 | 0.94 | | | 0.50 | 0.96 |
| Yb | 1.42 | 1.67 | | 2.17 | 2.27 | 2.11 | | | 1.65 | 2.46 |
| Lu | 0.28 | 0.23 | | 0.45 | 0.28 | 0.26 | | | 0.22 | 0.33 |
| Sc | 24.6 | 28.9 | | 24.9 | 27.6 | 25.6 | | | 24.4 | 27.0 |
| Cr | 367 | 479 | | 326 | 375 | 298 | | | 309 | 308 |
| Co | 54.8 | 62.6 | | 40.2 | 41.5 | 50.3 | | | 50.8 | 47.7 |
| Ni | 189 | 227 | | 146 | 134 | 220 | | | 154 | 194 |
| *Isotope Dilution Analyses, ppm* | | | | | | | | | | |
| Pb | 7.67 | 7.15 | | | 4.52 | | | | 5.75 | 4.63 |
| Nd | 47.7 | 47.5 | | | 30.3 | | | | 26.8 | 30.7 |
| Sm | 8.66 | 8.70 | | | 5.92 | | | | 5.07 | 5.97 |

| Rock type | *Alkali Basalt* | | | | | | | | | |
|---|---|---|---|---|---|---|---|---|---|---|
| Sample | 7-2 | 7-3 | 7-4 | 7-5 | 7-6 | 7-7 | 7-8 | 7-9 | 7-10 | 7-12 |
| long (°W) | 113.326 | 113.327 | 113.316 | 113.315 | 113.316 | 113.318 | 113.320 | 113.311 | 113.330 | 113.351 |
| lat (°N) | 37.070 | 37.064 | 37.070 | 37.069 | 37.071 | 37.071 | 37.071 | 37.085 | 37.087 | 37.123 |
| | *X-Ray Fluorescence Analyses, wt %* | | | | | | | | | |
| $SiO_2$ | 48.4 | 49.4 | 49.6 | 48.4 | 49.0 | 48.8 | 47.2 | 48.5 | 47.6 | 50.2 |
| $TiO_2$ | 1.77 | 1.78 | 1.81 | 1.78 | 1.82 | 1.86 | 1.77 | 1.78 | 1.73 | 1.50 |
| $Al_2O_3$ | 15.9 | 16.2 | 16.0 | 15.8 | 16.4 | 16.1 | 15.6 | 15.9 | 15.8 | 15.9 |
| $Fe_2O_3T$ | 10.0 | 10.3 | 10.2 | 10.1 | 10.2 | 10.2 | 10.1 | 10.0 | 10.1 | 10.5 |
| MnO | 0.16 | 0.17 | 0.16 | 0.16 | 0.16 | 0.16 | 0.16 | 0.16 | 0.16 | 0.16 |
| MgO | 7.87 | 7.86 | 7.83 | 7.80 | 8.07 | 8.05 | 8.27 | 7.84 | 8.57 | 6.44 |
| CaO | 9.6 | 9.3 | 9.3 | 9.6 | 9.4 | 8.8 | 8.8 | 9.1 | 9.1 | 9.4 |
| $Na_2O$ | 3.45 | 3.46 | 3.36 | 3.36 | 3.54 | 3.93 | 3.70 | 3.59 | 3.17 | 2.91 |
| $K_2O$ | 1.21 | 1.27 | 1.27 | 1.25 | 1.33 | 1.36 | 1.27 | 1.35 | 1.25 | 1.09 |
| $P_2O_5$ | 0.55 | 0.50 | 0.50 | 0.53 | 0.56 | 0.58 | 0.57 | 0.58 | 0.55 | 0.46 |
| Total | 99.02 | 100.24 | 100.05 | 98.81 | 100.43 | 99.79 | 97.45 | 98.77 | 98.07 | 98.58 |
| | *X-Ray Fluorescence Analyses, ppm* | | | | | | | | | |
| Rb | 12.3 | 11.3 | 12.0 | 11.0 | 11.4 | 12.2 | 12.6 | 13.3 | 12.4 | 13.4 |
| Ba | 279 | 305 | 656 | 309 | 277 | 255 | 325 | 358 | 390 | 753 |
| Nb | 26.2 | 25.1 | 26.8 | 24.7 | 25.6 | 27.6 | 23.5 | 23.6 | 24.2 | 16.5 |
| Sr | 717 | 707 | 1275 | 698 | 735 | 729 | 678 | 673 | 691 | 703 |
| Zr | 248 | 243 | 281 | 238 | 249 | 256 | 259 | 260 | 259 | 229 |
| Y | 25.2 | 25.9 | 25.9 | 23.5 | 22.8 | 25.3 | 30.0 | 28.3 | 28.7 | 31.9 |
| Cr | | | | | | | | | 226 | 125 |
| Ni | | | | | | | | | 144 | 59 |
| | *Instrumental Neutron Activation Analyses, ppm* | | | | | | | | | |
| Ba | 637 | 422 | 818 | 378 | 414 | 402 | 463 | 520 | | |
| Th | 3.6 | 3.2 | 3.4 | 3.7 | 3.1 | 3.5 | 3.2 | 3.4 | | |
| Ta | 1.67 | 1.63 | 1.50 | 1.48 | 1.66 | 1.91 | 1.73 | 1.78 | | |
| La | 36.1 | 34.0 | 34.9 | 34.9 | 34.1 | 36.2 | 35.2 | 36.7 | | |
| Ce | 73.6 | 69.4 | 71.8 | 70.2 | 69.2 | 76.5 | 70.5 | 70.9 | | |
| Nd | 49.4 | 28.8 | 24.9 | 40.6 | 30.7 | 29.7 | 38.8 | 23.4 | | |
| Sm | 6.42 | 6.37 | 6.44 | 6.38 | 6.30 | 6.86 | 6.69 | 6.88 | | |
| Hf | 5.22 | 5.15 | 5.19 | 5.42 | 5.22 | 5.89 | 5.46 | 5.49 | | |
| Eu | 2.30 | 2.14 | 2.11 | 2.15 | 2.11 | 2.06 | 2.00 | 1.91 | | |
| Tb | 0.90 | 0.92 | 0.81 | 0.88 | 0.90 | 0.75 | 0.99 | 0.85 | | |
| Yb | 2.53 | 2.72 | 2.62 | 2.78 | 2.49 | 2.48 | 2.62 | 2.61 | | |
| Lu | 0.29 | 0.29 | 0.30 | 0.43 | 0.31 | 0.38 | 0.40 | 0.37 | | |
| Sc | 28.0 | 27.1 | 27.4 | 27.3 | 25.9 | 27.4 | 26.9 | 25.7 | | |
| Cr | 314 | 303 | 310 | 308 | 261 | 271 | 288 | 260 | | |
| Co | 47.3 | 48.2 | 46.5 | 46.5 | 44.7 | 48.3 | 48.6 | 44.0 | | |
| Ni | 170 | 189 | 214 | 140 | 188 | 107 | 139 | 122 | | |
| | *Isotope Dilution Analyses, ppm* | | | | | | | | | |
| Pb | 4.61 | 4.39 | 4.32 | 4.69 | 4.01 | 4.47 | 4.66 | 4.34 | | |
| Nd | 31.1 | 31.2 | 30.1 | 30.1 | 29.9 | 30.3 | 31.3 | 32.4 | | |
| Sm | 6.04 | 5.88 | 5.84 | 5.84 | 5.85 | 5.92 | 6.12 | 6.15 | | |

| Rock type | *Alkali Basalt* | | | | | | | | |
|---|---|---|---|---|---|---|---|---|---|
| Sample | 7-13 | 7-14 | 7-15 | 7-16 | 7-17 | 7-19 | 7-20 | 7-24 | 7-28 |
| long (°W) | 113.347 | 113.336 | 113.334 | 113.333 | 113.334 | 113.321 | 113.395 | 113.315 | 113.303 |
| lat (°N) | 37.129 | 37.154 | 37.154 | 37.156 | 37.156 | 37.069 | 37.162 | 37.190 | 37.197 |
| | *X-Ray Fluorescence Analyses, wt %* | | | | | | | | |
| $SiO_2$ | 51.6 | 48.8 | 49.4 | 48.7 | 49.8 | 48.4 | 48.4 | 48.0 | 49.9 |
| $TiO_2$ | 1.50 | 1.41 | 1.52 | 1.43 | 1.49 | 1.78 | 2.26 | 1.65 | 1.48 |
| $Al_2O_3$ | 17.1 | 16.2 | 16.2 | 16.2 | 17.3 | 15.7 | 13.8 | 14.9 | 14.8 |
| $Fe_2O_3T$ | 10.8 | 10.3 | 10.9 | 10.3 | 11.7 | 10.3 | 12.5 | 10.4 | 12.1 |
| MnO | 0.16 | 0.17 | 0.17 | 0.16 | 0.18 | 0.17 | 0.19 | 0.17 | 0.17 |
| MgO | 6.91 | 6.61 | 6.20 | 6.29 | 5.79 | 8.45 | 10.35 | 7.40 | 7.96 |
| CaO | 9.6 | 9.7 | 10.1 | 10.2 | 9.7 | 9.2 | 11.0 | 8.7 | 9.0 |
| $Na_2O$ | 3.06 | 2.99 | 3.09 | 2.81 | 2.98 | 3.81 | 2.64 | 2.86 | 2.86 |
| $K_2O$ | 1.08 | 0.88 | 0.75 | 0.79 | 0.70 | 1.25 | 1.38 | 1.26 | 0.99 |
| $P_2O_5$ | 0.46 | 0.39 | 0.41 | 0.38 | 0.36 | 0.53 | 0.59 | 0.48 | 0.52 |
| Total | 102.31 | 97.44 | 98.76 | 98.19 | 99.93 | 99.58 | 103.13 | 96.38 | 99.83 |
| | *X-Ray Fluorescence Analyses, ppm* | | | | | | | | |
| Rb | 13.7 | 10.4 | 10.4 | 10.1 | 8.3 | 10.9 | 14.5 | 16.7 | 16.3 |
| Ba | 607 | 717 | 471 | 386 | 455 | 335 | 1024 | 694 | 601 |
| Nb | 14.8 | 11.8 | 12.1 | 11.5 | 10.9 | 24.2 | 41.9 | 33.0 | 13.9 |
| Sr | 627 | 527 | 490 | 520 | 451 | 677 | 929 | 680 | 612 |
| Zr | 206 | 191 | 169 | 186 | 173 | 254 | 237 | 212 | 156 |
| Y | 29.1 | 30.2 | 31.0 | 29.5 | 29.8 | 29.2 | 24.1 | 23.6 | 19.9 |
| Cr | 128 | 115 | | 127 | | | 356 | | 228 |
| Ni | 58 | 47 | | 51 | | | | | |
| | *Instrumental Neutron Activation Analyses, ppm* | | | | | | | | |
| Ba | | | 670 | | 578 | 510 | | 764 | 723 |
| Th | | | 1.9 | | 1.7 | 3.6 | | 5.6 | 2.8 |
| Ta | | | 0.60 | | 0.71 | 1.85 | | 1.91 | 0.97 |
| La | | | 23.9 | | 24.3 | 35.7 | | 47.5 | 36.2 |
| Ce | | | 46.2 | | 48.3 | 74.3 | | 90.6 | 70.7 |
| Nd | | | 18.0 | | 23.4 | 31.9 | | 46.8 | 26.0 |
| Sm | | | 5.38 | | 5.54 | 6.68 | | 7.50 | 6.22 |
| Hf | | | 4.01 | | 4.08 | 5.85 | | 4.94 | 3.60 |
| Eu | | | 1.82 | | 1.79 | 2.17 | | 2.22 | 1.96 |
| Tb | | | 0.67 | | 0.75 | 0.85 | | 0.88 | 0.71 |
| Yb | | | 2.55 | | 2.59 | 2.42 | | 2.23 | 2.10 |
| Lu | | | 0.37 | | 0.42 | 0.35 | | 0.37 | 0.36 |
| Sc | | | 31.2 | | 31.9 | 29.0 | | 26.5 | 25.7 |
| Cr | | | 156 | | 157 | 306 | | 277 | 276 |
| Co | | | 43.3 | | 46.5 | 49.4 | | 49.8 | 51.1 |
| Ni | | | 85 | | 69 | 153 | | 101 | 187 |
| | *Isotope Dilution Analyses, ppm* | | | | | | | | |
| Pb | | | 4.51 | | | 4.43 | | | 6.51 |
| Nd | | | 22.8 | | | 31.9 | | | 31.7 |
| Sm | | | 4.86 | | | 6.22 | | | 5.77 |

Isotope Ratios

| Magma type | D (Low-silica basanite) | | | | |
|---|---|---|---|---|---|
| Sample | 6-3 | 6-11 | 6-12 | 7-11 | 7-18 |
| $^{87}Sr/^{86}Sr_i$ | .704600 | .704715 | .704665 | .704694 | .704759 |
| $^{143}Nd/^{144}Nd$ | .512568 | .512588 | .512573 | .512589 | .512589 |
| $\varepsilon_{Nd}$ | -1.4 | -1.0 | -1.3 | -1.0 | -1.0 |
| $^{206}Pb/^{204}Pb$ | 18.67 | | 18.66 | 18.57 | 18.66 |
| $^{207}Pb/^{204}Pb$ | 15.62 | | 15.56 | 15.52 | 15.55 |
| $^{208}Pb/^{204}Pb$ | 38.67 | | 38.55 | 38.34 | 38.49 |

| Magma type | A (Basanite) | | | | | |
|---|---|---|---|---|---|---|
| Sample | 1-2 | 1-4 | 5-6 | 7-21 | 7-22 | 7-23 |
| $^{87}Sr/^{86}Sr_i$ | .704069 | .704235 | .704286 | .704127 | .704240 | .704179 |
| $^{143}Nd/^{144}Nd$ | .512595 | .512564 | .512554 | .512570 | .512560 | .512545 |
| $\varepsilon_{Nd}$ | -0.8 | -1.4 | -1.6 | -1.3 | -1.5 | -1.8 |
| $^{206}Pb/^{204}Pb$ | 18.34 | 18.33 | 18.29 | 18.23 | 18.34 | 18.16 |
| $^{207}Pb/^{204}Pb$ | 15.52 | 15.54 | 15.49 | 15.52 | 15.54 | 15.52 |
| $^{208}Pb/^{204}Pb$ | 38.25 | 38.27 | 38.14 | 38.20 | 38.41 | 38.16 |

| Magma type | A (Basanite) | | | | | |
|---|---|---|---|---|---|---|
| Sample | 7-25 | 7-26 | 7-27 | 7-29 | 7-30 | 7-31 |
| $^{87}Sr/^{86}Sr_i$ | .704134 | .704266 | .704033 | .704227 | .704228 | .704247 |
| $^{143}Nd/^{144}Nd$ | .512628 | .512576 | .512616 | .512575 | .512555 | .512565 |
| $\varepsilon_{Nd}$ | -0.2 | -1.2 | -0.4 | -1.2 | -1.6 | -1.4 |
| $^{206}Pb/^{204}Pb$ | 18.34 | 18.32 | 18.42 | 18.33 | 18.31 | 18.35 |
| $^{207}Pb/^{204}Pb$ | 15.53 | 15.53 | 15.53 | 15.54 | 15.51 | 15.54 |
| $^{208}Pb/^{204}Pb$ | 38.22 | 38.18 | 38.34 | 38.26 | 38.16 | 38.26 |

| Magma type | B (Alkali basalt) | | | | | | |
|---|---|---|---|---|---|---|---|
| Sample | 1-5 | 7-1 | 7-2 | 7-3 | 7-4 | 7-5 | 7-6 |
| $^{87}Sr/^{86}Sr_i$ | .703890 | .703856 | .703854 | .703840 | .705884 | .703966 | .703741 |
| $^{143}Nd/^{144}Nd$ | .512640 | .512610 | .512638 | .512657 | .512641 | .512615 | .512677 |
| $\varepsilon_{Nd}$ | 0.0 | -0.5 | 0.0 | 0.4 | 0.1 | -0.4 | 0.8 |
| $^{206}Pb/^{204}Pb$ | 18.03 | 18.02 | 18.00 | 18.05 | 18.02 | 18.01 | 18.06 |
| $^{207}Pb/^{204}Pb$ | 15.51 | 15.52 | 15.49 | 15.55 | 15.52 | 15.51 | 15.53 |
| $^{208}Pb/^{204}Pb$ | 37.96 | 37.99 | 37.90 | 38.07 | 38.01 | 37.97 | 38.01 |

| Magma type | B (Alkali basalt) | | | | C (Alkali basalt) | | |
|---|---|---|---|---|---|---|---|
| Sample | 7-7 | 7-8 | 7-9 | 7-19 | 6-15 | 7-15 | 7-28 |
| $^{87}Sr/^{86}Sr_i$ | .703678 | .703728 | .703761 | .703791 | .704882 | .704619 | .704753 |
| $^{143}Nd/^{144}Nd$ | .512718 | .512647 | .512675 | .512642 | .512282 | .512322 | .512253 |
| $\varepsilon_{Nd}$ | 1.6 | 0.2 | 0.7 | 0.1 | -6.9 | -6.2 | -7.5 |
| $^{206}Pb/^{204}Pb$ | 18.05 | 18.05 | 18.04 | 18.02 | 17.45 | 17.60 | 17.42 |
| $^{207}Pb/^{204}Pb$ | 15.51 | 15.54 | 15.52 | 15.50 | 15.45 | 15.51 | 15.52 |
| $^{208}Pb/^{204}Pb$ | 37.95 | 38.05 | 37.98 | 37.91 | 37.58 | 37.62 | 37.63 |

# APPENDIX II

## DATA PRECISION AND ACCURACY

Geochemical standards for calibration of XRF spectometer are USGS standards unless noted.

| | | | | | | | | | |
|---|---|---|---|---|---|---|---|---|---|
| **Major elements** | | | | | | | | | |
| SCO-1 | STM-1 | GSP-1 | DNC-1 | RGM-1 | BHVO-1 | PCC-1 | AGV-1 | QLO-1 | AL-I* |
| **Trace elements** | | | | | | | | | |
| G-2 | W-2 | BIR-1 | RGM-1 | QLO-1 | BHVO-1 | PCC-1 | SCO-1 | AGV-1 | DNC-1 |
| **Cr** | | | | | | | | | |
| PCC-1 | W-2 | Mica-Fe† | GSP-1 | BHVO-1 | DR-N§ | SCO-1 | GS-N§ | BE-N§ | MAG-1 |
| **Ni** | | | | | | | | | |
| W-2 | Mica-Fe† | BHVO-1 | BR† | Mica-Mg† | **H94-6-10** | **H94-6-2** | GS-N§ | SCO-1 | |

*- Groupe International de Travail-International Working Group (GIT-IWG); † - CRPG geochemical standard; § - Association Nationale de la Recherche Technique (ANRT). Values for samples in boldface were obtained from INAA data from this work.

Analytical precision is one standard deviation (1 σ) expressed as a percentage of the mean for repeat analyses of standards. Other values are in weight percent (wt. %) or parts per million (ppm). Data precision and accuracy for geochemical standards used for XRF analysis.

| USGS BIR-1 | | | | | | | | | | | |
|---|---|---|---|---|---|---|---|---|---|---|---|
| element (wt. %) | SiO2 | Al2O3 | TiO2 | Fe2O3 | MgO | CaO | Na2O | K2O | MnO | P2O5 | Total |
| published value | 47.77 | 15.65 | 0.96 | 11.26 | 9.68 | 13.24 | 1.75 | 0.027 | 0.171 | 0.046 | 100.55 |
| no. | 17 | 17 | 17 | 17 | 17 | 17 | 17 | 17 | 17 | 17 | 17 |
| mean | 47.18 | 15.17 | 0.95 | 11.18 | 9.64 | 13.07 | 1.69 | 0.03 | 0.17 | 0.06 | 99.13 |
| st. dev. | 0.54 | 0.17 | 0.02 | 0.17 | 0.28 | 0.12 | 0.11 | 0.02 | 0.00 | 0.03 | 1.04 |
| ± % precision | 1.14 | 1.11 | 1.75 | 1.56 | 2.89 | 0.90 | 6.38 | 55.26 | 2.86 | 50.27 | 1.05 |
| ± % accuracy | 1.24 | 3.06 | 1.25 | 0.74 | 0.36 | 1.29 | 3.45 | 12.14 | 0.10 | 22.95 | 1.41 |

| USGS MAG-1 | | | | | | | | |
|---|---|---|---|---|---|---|---|---|
| element (ppm) | Rb | Ba | Nb* | Sr | Zr | Y | Cr† | Ni† |
| published value | 149 | 479 | 85 | 146 | 126 | 28 | 382 | 166 |
| no. | 24 | 25 | 6 | 20 | 20 | 24 | 8 | 4 |
| mean | 151.3 | 493.7 | 84.7 | 147.8 | 130.5 | 29.5 | 415.0 | 173.1 |
| st. dev. | 3.93 | 25.35 | 3.36 | 3.37 | 2.90 | 1.36 | 12.62 | 3.49 |
| ± % precision | 2.60 | 5.13 | 3.97 | 2.28 | 2.23 | 4.62 | 3.04 | 2.02 |
| ± % accuracy | 1.55 | 3.08 | 0.36 | 1.24 | 3.54 | 5.25 | 8.64 | 4.26 |

* - Sample used was CRPG standard GH; † - Sample used was USGS standard BIR-1.

Data precision and accuracy for geochemical standards used for INA analysis. Accepted values for the primary INAA standard (NIST1633a, fly-ash) are: Ba (1420 ppm), Th (24.7), Ta (2.00), Hf (7.40), La (84.0), Ce (175), Nd (74), Sm (17.0), Eu (3.70), Tb (2.50), Yb (7.40), Lu (1.12), Sc (39.0), Cr (196), Co (43.0), Ni (127) (Govindaraju, 1994).

| | USGS standard BVHO-1 (basalt) n=4 | | | | NIST* standard 278 (obsidian) n=8 | | | |
|---|---|---|---|---|---|---|---|---|
| | mean (ppm) | precision (% of mean) | accuracy | accept. (ppm) | mean (ppm) | precision (% of mean) | accuracy | accept. (ppm) |
| Ba | 140 | 11.5 | 0.7 | 139 | 968 | 9.0 | 15.1 | 1140 |
| Th | 1.13 | 16.3 | 4.6 | 1.08 | 12.6 | 1.7 | 1.7 | 12.4 |
| Ta | 1.24 | 7.6 | 0.8 | 1.23 | 1.33 | 6.6 | 11.1 | 1.2 |
| Hf | 4.68 | 1.7 | 6.8 | 4.38 | 8.70 | 2.5 | 3.6 | 8.4 |
| La | 15.7 | 2.8 | 0.6 | 15.8 | 32.5 | 1.7 | 1.6 | 32 |
| Ce | 39.4 | 11.4 | 1.0 | 39 | 66.7 | 1.6 | 7.2 | 62.2 |
| Nd | | | | | 30.2 | 33.3 | 0.8 | 30 |
| Sm | 6.47 | 2.3 | 4.4 | 6.2 | 5.95 | 2.1 | 4.4 | 5.7 |
| Eu | 1.97 | 5.9 | 4.4 | 2.06 | 0.821 | 5.7 | 2.8 | 0.84 |
| Tb | 0.91 | 12.3 | 5.2 | 0.96 | 1.02 | 9.0 | 2.0 | 1 |
| Yb | 1.81 | 3.8 | 10.4 | 2.02 | 4.54 | 2.3 | 0.8 | 4.5 |
| Lu | 0.28 | 19.8 | 30.0 | 0.4 | 0.68 | 7.0 | 6.4 | 0.73 |
| Sc | 30.9 | 1.2 | 2.8 | 31.8 | 5.07 | 3.3 | 0.6 | 5.1 |
| Cr | 293 | 2.5 | 1.4 | 289 | 7.28 | 17.7 | 19.4 | 6.1 |
| Co | 43.2 | 2.1 | 4.0 | 45 | 1.62 | 32.8 | 8.3 | 1.5 |
| Ni | | | | | | | | 3.6 |

| | NIST* standard 688 (basalt) n=8 | | | | CVTS† sample 78-218 (River Mtns. basalt), n=4 | |
|---|---|---|---|---|---|---|
| | mean (ppm) | precision (% of mean) | accuracy | accept. (ppm) | mean (ppm) | precision (% of mean) |
| Ba | 193 | 18.2 | 3.3 | 200 | 2347 | 4.0 |
| Th | 0.40 | 11.4 | 19.7 | 0.33 | 11.1 | 1.4 |
| Ta | 0.30 | 24.1 | 1.8 | 0.31 | 1.67 | 3.2 |
| Hf | 1.55 | 10.2 | 3.3 | 1.6 | 8.29 | 3.5 |
| La | 5.59 | 9.4 | 5.5 | 5.3 | 111 | 1.6 |
| Ce | 11.5 | 18.6 | 13.7 | 13.3 | 222 | 1.6 |
| Nd | 7.55 | 1.8 | 15.2 | 8.9 | 98.7 | 6.0 |
| Sm | 2.55 | 1.0 | 8.6 | 2.79 | 16.1 | 2.2 |
| Eu | 1.02 | 17.9 | 5.0 | 1.07 | 3.90 | 3.1 |
| Tb | 0.47 | 17.2 | 3.4 | 0.45 | 1.27 | 13.9 |
| Yb | 2.15 | 7.4 | 3.1 | 2.09 | 2.16 | 8.3 |
| Lu | 0.33 | 10.7 | 3.0 | 0.34 | 0.32 | 2.7 |
| Sc | 37.8 | 1.6 | 0.8 | 38.1 | 29.8 | 2.1 |
| Cr | 336 | 2.5 | 1.3 | 332 | 182 | 2.0 |
| Co | 47.5 | 3.0 | 4.4 | 49.7 | 33.1 | 2.4 |
| Ni | 158 | 17.5 | 5.3 | 150 | 60.7 | 2.5 |

* - National Institute of Science and Technology, USA (NIST) geochemical standard.

† - Center for Volcanic and Tectonic Studies (CVTS) internal geochemical standard.

# APPENDIX III

## GEOCHRONOLOGIC DATA

| Temp (°C) | $^{40}Ar^{*}$ | K derived $^{39}Ar$ | F value | Rad. yield | % $^{39}Ar$ total | Apparent age (Ma) | uncertainty (± 1 σ, Ma) |
|---|---|---|---|---|---|---|---|
| | | | sample 6-15 | | | | |
| 600 | .00759 | .00272 | 2.794 | 7.4 | 0.3 | 6.48 | 2.1 |
| 700 | .00154 | .03576 | 0.043 | 2.1 | 4.2 | 0.10 | 0.24 |
| 800 | .04041 | .16492 | 0.245 | 3.7 | 19.3 | 0.57 | 0.03 |
| 900 | .04587 | .28620 | 0.160 | 13.4 | 33.4 | 0.37 | 0.03 |
| 1000 | .03282 | .16157 | 0.203 | 11.2 | 18.9 | 0.47 | 0.05 |
| 1100 | .01581 | .07900 | 0.200 | 5.1 | 9.2 | 0.46 | 0.07 |
| 1200 | .02383 | .06682 | 0.357 | 7.5 | 7.8 | 0.83 | 0.08 |
| 1300 | .01402 | .02920 | 0.480 | 10.6 | 3.4 | 1.12 | 0.24 |
| 1400 | .02489 | .03030 | 0.821 | 21.1 | 3.5 | 1.91 | 0.16 |
| Total gas | | | 0.241 | | | 0.56 | 0.11 |
| | | | sample 7-21 | | | | |
| 600 | .02694 | .25967 | 0.104 | 1.3 | 6.9 | 0.23 | 0.08 |
| 700 | .04419 | .33442 | 0.132 | 8.5 | 8.9 | 0.30 | 0.04 |
| 800 | .06928 | .54795 | 0.126 | 3.1 | 14.5 | 0.28 | 0.01 |
| 900 | .07925 | .68967 | 0.115 | 7.0 | 18.3 | 0.26 | 0.02 |
| 1000 | .04957 | .48336 | 0.103 | 6.3 | 12.8 | 0.23 | 0.003 |
| 1100 | .03841 | .32351 | 0.119 | 3.5 | 8.6 | 0.27 | 0.01 |
| 1200 | .07957 | .63206 | 0.126 | 2.8 | 16.7 | 0.28 | 0.01 |
| 1300 | .06483 | .45723 | 0.142 | 4.3 | 12.1 | 0.32 | 0.01 |
| 1400 | .01473 | .04281 | 0.344 | 5.0 | 1.1 | 0.77 | 0.06 |
| Total gas | | | 0.124 | | | 0.28 | 0.02 |
| | | | sample 7-22 | | | | |
| 600 | .04272 | .02348 | 1.820 | 1.2 | 0.8 | 3.62 | 0.35 |
| 700 | .11234 | .19034 | 0.590 | 3.5 | 6.1 | 1.18 | 0.01 |
| 800 | .05964 | .31042 | 0.192 | 2.7 | 10.0 | 0.38 | 0.02 |
| 900 | .04842 | .35446 | 0.137 | 3.1 | 11.4 | 0.27 | 0.05 |
| 1000 | .04356 | .24916 | 0.175 | 3.3 | 8.0 | 0.35 | 0.03 |
| 1100 | .02822 | .10729 | 0.263 | 2.9 | 3.5 | 0.52 | 0.08 |
| 1200 | .48647 | 1.09748 | 0.443 | 1.9 | 35.3 | 0.88 | 0.01 |
| 1300 | .31837 | .69377 | 0.459 | 2.7 | 22.3 | 0.91 | 0.02 |
| 1400 | .08990 | .07907 | 1.137 | 6.5 | 2.5 | 2.26 | 0.03 |
| Total gas | | | 0.396 | | | 0.79 | 0.04 |

## APPENDIX IV

### DEFINITION OF GEOCHEMICAL INDICES

**Magnesium number (Mg#)**

$$Mg\# = [Mg/(Mg + Fe^{2+})]100;$$

calculated where total iron, $FeO^* = FeO + (0.8998)Fe_2O_3$

**Epsilon Nd ($\varepsilon_{Nd}$)**

$$\varepsilon_{Nd} = [(^{143}Nd/^{144}Nd_{(measured)}) / (^{143}Nd/^{144}Nd_{(CHUR)}) - 1]\ 10{,}000$$

where CHUR is the model chondritic reservoir and $^{143}Nd/^{144}Nd_{(CHUR)} = 0.512638$.

### DISTRIBUTION COEFFICIENTS

Trace element distribution coefficients are from Bradshaw (1991) except for Ni (Arth and Hanson, 1975) and Cr (Gill, 1981).

| | Ol | Opx | Cpx | Plag | Gt | Sp | Amph | IL | Ksp | Bio | phlog |
|---|---|---|---|---|---|---|---|---|---|---|---|
| **Rb** | 0.0001 | 0.001 | 0.05 | 0.1 | 0.01 | 0 | 0.25 | | 0.38 | 3.4 | 3.1 |
| **Ba** | 0.0001 | 0.001 | 0.05 | 0.23 | 0.01 | 0 | 0.31 | | 6.6 | 7 | 1.1 |
| **Th** | 0.001 | 0.01 | 0.01 | | 0.02 | 0 | 0.3 | | | 0.31 | 0.31 |
| **K2O** | 0.007 | 0.015 | 0.03 | 0.17 | 0 | 0 | 0.8 | | 1.4 | 3.5 | 2.7 |
| **Ta** | 0.001 | 0.15 | 0.07 | 0.01 | 0.1 | 0 | 1.3 | | | | 1 |
| **Nb** | 0.001 | 0.15 | 0.1 | 0.01 | 0.1 | 0 | 1.3 | 0.8 | | | 1 |
| **La** | 0.0002 | 0.002 | 0.069 | 0.14 | 0.01 | 0 | 0.27 | 0.01 | | 0.32 | 0.03 |
| **Ce** | 0.0005 | 0.003 | 0.098 | 0.14 | 0.021 | 0 | 0.34 | 0.01 | 0.04 | 0.1 | 0.03 |
| **Sr** | 0.001 | 0.01 | 0.1 | 1.8 | 0.01 | 0 | 0.57 | | 9.4 | 0.24 | 0.08 |
| **P2O5** | 0.001 | 0.008 | 0.14 | | 0.08 | 0 | 0.3 | | | | 0.05 |
| **Nd** | 0.001 | 0.0065 | 0.18 | 0.08 | 0.08 | 0 | 0.5 | 0.01 | 0.03 | 0.04 | 0.03 |
| **Hf** | 0.001 | 0.04 | 0.31 | 0.01 | 0.3 | 0 | 0.5 | | | 2.1 | 0.6 |
| **Zr** | 0.001 | 0.03 | 0.1 | 0.01 | 0.3 | 0 | 1.1 | 0.01 | | | 0.06 |
| **Sm** | 0.0013 | 0.013 | 0.26 | 0.08 | 0.217 | 0 | 0.91 | 0.01 | 0.02 | 0.2 | 0.03 |
| **TiO2** | 0.02 | 0.1 | 0.3 | 0 | 0.3 | 0 | 0.5 | 0.01 | | | 0.09 |
| **Y** | 0.001 | 0.04 | 0.3 | 0.03 | 2 | 0.02 | 0.89 | 0.01 | | | 0.03 |
| **Tb** | 0.0015 | 0.02 | 0.3 | 0.03 | 0.7 | 0.007 | 1.4 | 0.01 | | 0.39 | 0 |
| **Yb** | 0.0015 | 0.049 | 0.28 | 0.07 | 7 | 0.007 | 0.97 | 0.01 | 0.012 | 0.4 | 0.03 |
| **Lu** | 0.001 | 0.11 | 0.8 | 0.08 | 10 | 0 | 0.89 | | | 0.74 | 0.04 |
| **Ni** | 8.7 | 3.8 | 2 | 0.01 | 0.4 | 5 | 3 | | 0 | | |
| **Sc** | 0.17 | 1.1 | 2.7 | | 4 | 0 | 3.2 | | | 11.3 | 2.5 |
| **Cr** | 0.01 | 13 | 10 | 0.01 | 22 | | 30 | 32 | | | |

## REFERENCES CITED


Alibert, C., Michard, A., and Albarede, F., 1986, Isotope and trace element geochemistry of Colorado Plateau volcanics: Geochimica et Cosmochimica Acta, v. 50, p. 2735-2750.

Allmendinger, R. W., Hauge, T. A., Hauser, E. C., Potter, C. J., Klemperer, S. L., Nelson, K. D., Kneupfer, P., and Oliver, J., 1987, Overview of the COCORP 40°N transect, western United States: The fabric of an orogenic belt: Geological Society of America Bulletin, v. 98, p. 308-319.

Arculus, R. J., and Gust, D. A., 1995, Regional petrology of the San Francisco volcanic field, Arizona, USA: Journal of Petrology, v. 36, no. 3, p. 827-861.

Arth, J. G., and Hanson, G. N., 1975, Geochemistry and origin of the early Precambrian crust of northeastern Minnesota: Geochimica et Cosmochimica Acta, v. 39, p. 325-362.

Atwater, T., 1970, Implications of plate tectonics for the Cenozoic tectonic evolution of western North America: Geological Society of America Bulletin, v. 81, p. 3513-3536.

Anderson, R. E., 1988, Hazard implications of joint controlled basaltic volcanism in southwestern Utah: Geological Society of America Abstracts, v. 20, no. 7, p. A115.

Best, M.G., and Brimhall, W.H., 1970, Late Cenozoic basalt types in the western Grand Canyon region: Guidebook to the Geology of Utah, v. 23, p. 57-74.

Best, M.G., and Brimhall, W.H., 1974, Late Cenozoic alkalic basaltic magmas in the western Colorado Plateau and the Basin and Range Transition Zone, U.S.A., and their bearing on mantle dynamics: Geological Society of America Bulletin, v. 85, p. 1677-1690.

Best, M.G., McKee, E.H., and Damon, P.E., 1980, Space-time-composition patterns of Late Cenozoic mafic volcanism, southwestern Utah and adjoining areas: American Journal of Science, v. 280, p. 1035-1050.

Bradshaw, T. K., 1991, Tectonics and magmatism in the Basin and Range Province of the western United States [Ph. D. thesis]: Milton Keynes, Open University, 247 p.

Bradshaw, T. K., and Smith E. I., 1994, Polygenetic Quaternary volcanism at Crater Flat, Nevada: Journal of Volcanology and Geothermal Research, v. 63, p. 165-182.

Burchfiel, B. C., and Davis, G. A., 1975, Nature and controls of Cordilleran orogenesis, western United States: Extensions of an earlier synthesis: American Journal of Science, v. 275-A, p. 363-396.

Carr, M. J., 1994, IGPETWIN: Igpet for Windows petrology software: Somerset, Terra Softa, Inc.

Cole, E.C., 1989, Petrogenesis of Late Cenozoic alkalic basalt near the eastern boundary of the Basin-and-Range: Upper Grand Wash Trough, Arizona and Gold Butte, Nevada [M. S. thesis]: Las Vegas, University of Nevada, 68 p.

Condit, C. D., Crumpler, L. F., Aubele, J. C., and Elston, W. E., 1989, Patterns of volcanism along the southern margin of the Colorado Plateau-Springerville field: Journal of Geophysical Research, v. 94, p. 7975-7986.

Connor, C. B., 1990, Cinder cone clustering in the Trans-Mexican Volcanic Belt: Implications for structural and petrologic models: Journal of Geophysical Research, v. 95, no. B12, p. 19,395-19,405.

Conner C. B., and Condit, C. D., 1994, Estimating recurrence rate of volcanism in the Springerville volcanic field, Arizona: Geological Society of America Abstracts with Programs, v. 26, no. 7, p. A115.

Conrey, R. M., 1990, Olivine analcimite in the Cascade Range of Oregon: Journal of Geophysical Research, v. 95, no. B12, p. 19,639-19,649.

Cook, E. F., 1960, Geologic atlas of Utah - Washington County: Utah Geological and Mineral Survey, Bulletin 70, 124 p.

Crowe, B. M., Turrin, B., Wells, S. G., McFadden, L. D., Renault, C. E., Perry, F. V., Harrington, C., and Champion, D., 1989, Polycyclic volcanism: a common eruption mechanism of small volume basaltic volcanic centers of the southwestern Great Basin, USA (IAVCEI Abstracts): New Mexico Bureau of Mines and Mineral Resources Bulletin, v. 131, p. 63.

Delaney, P. T., Pollard, D. D., Ziony, J. I., and McKee, E. H., 1986, Field relations between dikes and joints: Emplacement processes and paleostress analysis: Journal of Geophysical Research, v. 91, no. B5, p. 4920-4938.

DePaolo, D. J., 1981, Trace element and isotopic effects of combined wall-rock assimilation and fractional crystallization: Earth and Planetary Science Letters, v. 53, p. 189-202.

Draper, G., Chen, Z., Conway, C., Conner, C. B., and Condit, C. D., 1994, Structural control of magma pathways in the upper crust: Insights from the San Francisco volcanic field, Arizona: Geological Society of America Abstracts with Programs, v. 26, no. 7, p. A115.

Farmer, G. L., Perry, F. V., Semken, S., Crowe, B., Curtis, D., and DePaolo, D. J., 1989, Isotopic evidence on the structure and origin of subcontinental lithospheric mantle in southern Nevada: Journal of Geophysical Research, v. 94, no. B6, p. 7885-7898.

Feuerbach, D. L., Smith, E. I., Walker, J. D., and Tangeman, J. A., 1993, The role of the mantle during crustal extension: Constraints from geochemistry of volcanic rocks in the Lake Mead area, Nevada and Arizona: Geological Society of America Bulletin, v. 105, p. 1561-1575.

Fisher, R. V., and Schmincke, H. -U., 1984, Pyroclastic Rocks: New York, Springer-Verlag, 471 p.

Fitton, J.G., James, D., Kempton, P.D., Ormerod, D.S., and Leeman, W.P., 1988, The role of lithospheric mantle in the generation of Late Cenozoic basic magmas in the western United States: Journal of Petrology, Special Lithospheric Issue, p. 331-349.

Fitton, J. G., James, D., and Leeman, W. P., 1991, Basic magmatism associated with Late Cenozoic extension in the western United States: Compositional variations in space and time: Journal of Geophysical Research, v. 96, no. B8, p. 13,693-13,712.

Foshag, W.F., and González-Reyna, J., 1956, Birth and development of Parícutin volcano: U. S. Geological Survey Bulletin 965-D, p. 355-489.

Gill, J. B., 1981, Orogenic andesites and plate tectonics: Berlin, Springer, 389 p.

Govindaraju, K., 1994, 1994 compilation of working values and sample description for 383 geostandards: Geostandards Newsletter, Special Issue, v. 18, 158 p.

Glazner, A. F., and Farmer, G. L, 1992, Production of isotopic variability in continental basalts by cryptic crustal contamination: Science, v. 255, p. 72-74.

Green, D. H., Edgan, H. D., Beasley, P., Kiss, E., and Ware, N. G., 1974, Upper mantle source for some hawaiites, mugaerites and benmorites: Contributions to Mineral Petrology, v. 48, p. 33-43.

Gregory, H. E., 1950, Geology and geography of the Zion Park region, Utah and Arizona: U. S. Geological Survey Professional Paper 220, 200 p.

Hamblin, W. K., 1970a, Structure of the western Grand Canyon region, *in* Hamblin, W. K. and Best, M. G., eds.,The western Grand Canyon district: Utah Geological Society Guidebook to the geology of Utah, v. 23, p. 3-20.

Hamblin, W.K., 1970b, Late Cenozoic basalt flows of the western Grand Canyon: *in* Hamblin, W. K. and Best, M. G., eds.,The western Grand Canyon district: Utah Geological Society Guidebook to the geology of Utah, v. 23, p. 21-37.

Hasenaka, T., and Carmichael, I. S. E., 1985, The cinder cones of Michoacán - Guanajuato, Central México: Their age, volume and distribution, and magma discharge rate: Journal of Volcanology and Geothermal Research, v. 25, p. 105-124.

Hausel, W.D., and Nash, W.P., 1977, Petrology of Tertiary and Quaternary volcanic rocks, Washington County, southwestern Utah: Geological Society of America Bulletin, v. 88, p. 1831-1842.

Hintze, L. F., compiler, 1963, Geologic map of southwestern Utah: Brigham Young University, scale 1:250,000.

Huntington, E., and Goldthwait, J.W., 1904, The Hurricane fault in the Toquerville district, Utah: Harvard College Museum Comp. Zoology Bulletin, v. 42, p. 199-259.

Hutchison, C. S., 1974, Laboratory handbook of petrographic techniques: New York, John Wiley and Sons, 527 p.

Keen, C. E., 1985, The dynamics of rifting: Deformation of the lithosphere by active and passive driving forces: Geophysical Journal of the Royal Astronomical Society of London, v. 80, p. 95-120.

Le Bas, M. J., Le Maitre, R. W., Streckeisen, A., and Zanettin, B., 1986, A chemical classificaton of volcanic rocks based on the total alkali-silica diagram: Journal of Petrology, v. 27, p. 745-750.

Leeman, W.P. and Rogers, 1970, Late Cenozoic alkali-olivine-basalts of the Basin and Range Province: Contributions to Mineral Petrology, v. 25, p. 1-24.

Lefebvre, R. H., 1961, Joint patterns in the central part of the Hurricane Fault zone, Washington County, Utah [M. S. thesis]: Lawrence, University of Kansas, 35 p.

McMillan, N. J., and Dugan, M. A., 1986, Magma mixing as a petrogenetic process in the development of the Taos Plateau Volcanic Field, New Mexico: Journal of Geophysical Research, v. 91, no. B6, p. 6029-6045.

Mills, J. G., 1991, The Timber Mountain Tuff, southwestern Nevada volcanic field: Geochemistry, mineralogy and petrogenesis [Ph.D. dissertation]: East Lansing, Michigan State University, 332 p.

Nealey, L. D., and Unruh, D. M., 1991, Geochemistry and isotopic characteristics of deep crustal xenoliths from Tule Tank, San Francisco volcanic field, northern Arizona: *in* Karlstrom, K. E., ed., Proterozoic geology and ore deposits of Arizona, Arizona Geological Society Digest 19, p. 153-163.

Nealey, L. D., Unruh, D. M., and Maldonado, F., 1993, Sr-Nd-Pb isotopic maps of the Panguitch 1:100,000 quadrangle: U. S. Geological Survey Open-File Report 93-691, scale 1:250,000.

Noorish, K., and Hutton, J. T., 1969, An accurate X-ray spectrographic method for the analysis of a wide range of geological samples: Geochimica et Cosmochimica Acta, v. 33, p. 431-453.

Perry, F. V., Baldridge, W. S., and DePaolo, D. J., 1987, Role of asthenosphere and lithosphere in the genesis of Late Cenozoic basaltic rocks from the Rio Grande rift and adjacent regions of the southwestern United States: Journal of Geophysical Research, v. 92, no. B9, p. 9193-9213.

Reid, M.R., and Ramos, F.C., 1993, $^{230}Th/^{232}Th$ evidence for asthenospheric and lithospheric components in intraplate volcanism of the western U.S.A.: Abstracts IAVCEI General Assembly, Canberra, Australia, p. 89.

Schramm, M.E., 1994, Structural analysis of the Hurricane fault in the transition zone between the Basin and Range province and the Colorado Plateau, Washington County, Utah [M. S. thesis]: Las Vegas, University of Nevada, 90 p.

Smith, E. I., Feuerbach, D. L., Naumann, T. L., and Faulds, J. E., 1990, The area of most recent volcanism near Yucca Mountain, Nevada: Implications for volcanic risk assessment: *in* Proceedings of the International Nuclear Waste Symposium, v. 1, American Nuclear Society and American Society of Civil Engineers, p. 90-97.

Snyder, W. S., Dickinson, W. R., and Silberman, M. L., 1976, Tectonic implicatons of space-time patterns of Cenozoic magmatism in the western United States: Earth and Planetary Science Letters, v. 32, p. 91-106.

Thompson, R. A., Dugan, M. A., and Lipman, P. W., 1986, Multiple differentiation processes in early-rift calc-alkalic volcanics, norhtern Rio Grande Rift, New Mexico: Journal of Geophysical Research, v. 91, no. B6, p. 6046-6058.

Threet, R., L., 1958, Crater Hill lava flow, Zion National Park, Utah: Geological Society of America Bulletin, v. 69, p. 1065-1070.

Unruh, D. M., Nealey, L. D., Maldonado, F., and Nusbaum, R., 1995, Sr-Nd-Pb isotopic maps of late Cenozoic volcanic rocks of the St. George 30' x 60' quadrangle, southwestern Utah: U. S. Geological Survey Open-File Report 94-11.

Watson, R. A., 1968, Structural development of the Toquerville-Pintura segment of the Hurricane Cliffs, Utah: Brigham Young University Geology Studies, v. 15, p. 67-76.

Wells, S. G., Crowe, B. M., and McFadden, L. D., 1992, Measuring the age of the Lathrop Wells volcanic center at Yucca Mountain, Science, v. 257, p. 555-556.

Wells, S. G., McFadden, L. D., Renault, C. E., and Crowe, B. M., 1990, Geomorphic assessment of late Quaternary volcanism in the Yucca Mountain area, southern Nevada: Implications for the proposed high-level radioactive waste repository: Geology, v. 18, p. 549-553.

Wenrich, K. J., Billingsley, G. H., and Blackerby, B. A., 1995, Spacial migration and compositional changes of Miocene-Quaternary magmatism in the Western Grand Canyon: Journal of Geophysical Research, v. 100, no. B7, p. 10,417-10,440.

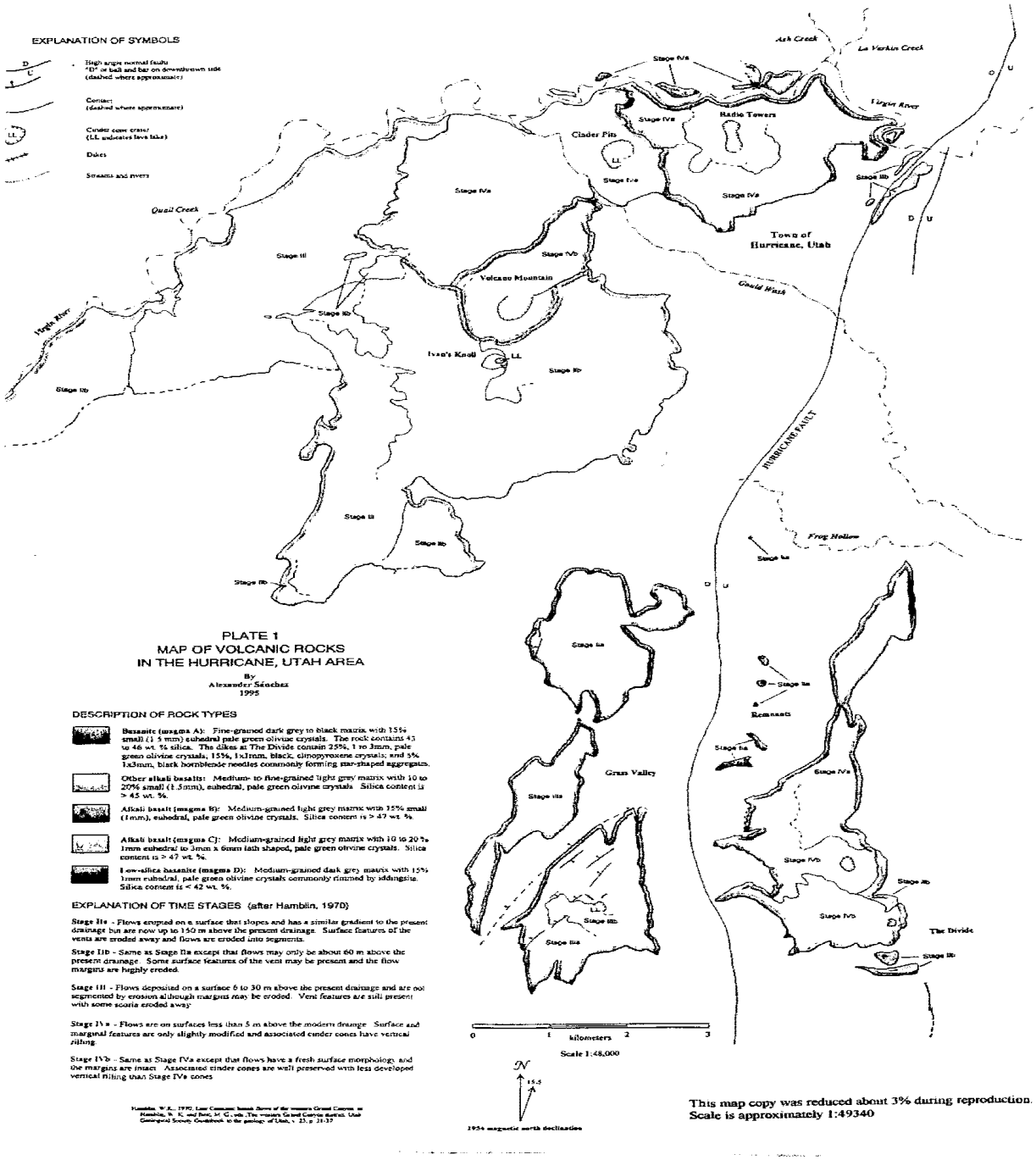


# PLATE 1
# MAP OF VOLCANIC ROCKS IN THE HURRICANE, UTAH AREA

By
Alexander Sánchez
1995

## DESCRIPTION OF ROCK TYPES

**Basanite (magma A):** Fine-grained dark grey to black matrix with 15% small (1.5 mm) euhedral pale green olivine crystals. The rock contains 45 to 46 wt. % silica. The dikes at The Divide contain 25%, 1 to 3mm, pale green olivine crystals, 15%, 1x1mm, black, clinopyroxene crystals, and 5%, 1x3mm, black hornblende needles commonly forming star-shaped aggregates.

**Other alkali basalts:** Medium- to fine-grained light grey matrix with 10 to 20% small (1.5mm), euhedral, pale green olivine crystals. Silica content is > 45 wt. %.

**Alkali basalt (magma B):** Medium-grained light grey matrix with 15% small (1mm), euhedral, pale green olivine crystals. Silica content is > 47 wt. %.

**Alkali basalt (magma C):** Medium-grained light grey matrix with 10 to 20 % 1mm euhedral to 3mm x 6mm lath shaped, pale green olivine crystals. Silica content is > 47 wt. %.

**Low-silica basanite (magma D):** Medium-grained dark grey matrix with 15% 1mm euhedral, pale green olivine crystals commonly rimmed by iddingsite. Silica content is < 42 wt. %.

## EXPLANATION OF TIME STAGES (after Hamblin, 1970)

**Stage IIa** - Flows erupted on a surface that slopes and has a similar gradient to the present drainage but are now up to 150 m above the present drainage. Surface features of the vents are eroded away and flows are eroded into segments.

**Stage IIb** - Same as Stage IIa except that flows may only be about 60 m above the present drainage. Some surface features of the vent may be present and the flow margins are highly eroded.

**Stage III** - Flows deposited on a surface 6 to 30 m above the present drainage and are not segmented by erosion although margins may be eroded. Vent features are still present with some scoria eroded away.

**Stage IVa** - Flows are on surfaces less than 5 m above the modern drainage. Surface and marginal features are only slightly modified and associated cinder cones have vertical rilling.

**Stage IVb** - Same as Stage IVa except that flows have a fresh surface morphology and the margins are intact. Associated cinder cones are well preserved with less developed vertical rilling than Stage IVa cones.

Hamblin, W.K., 1970, Lava Coverages Issued: Survey of the western Grand Canyon, in Hamblin, W. K., and Best, M. G., eds., The western Grand Canyon district: Utah Geological Society Guidebook to the geology of Utah, v. 23, p. 21-37.

This map copy was reduced about 3% during reproduction.
Scale is approximately 1:49340